COO-3435-19

OPTICALLY DETECTED MAGNETIC RESONANCE (ODMR) SPECTROSCOPY OF THE LOWEST TRIPLET STATES OF BENZOPHENONE AND HALOGENATED BENZOPHENONES

by

John Aaron Mucha

B.A., Washington and Jefferson College, 1965

A dissertation submitted to the Graduate Faculty of Arts and Sciences of the University of Pittsburgh in partial fulfillment of the requirements for the degree of

Doctor of Philosophy in Chemistry

December, 1974

DISCLAIMER

ABSTRACT

We report measurements of the complete angular dependence of the optically detected magnetic resonance (ODMR) spectra of 4,4'-disubstituted-benzophenones (4,4'-DXBP; X = H, F, Cl, Br) in 4,4'-dibromodiphenylether (DDE) and X-traps in neat 4,4'-dichlorobenzophenone at liquid helium temperatures. The results are used to calculate the principal values of the $\underset{\sim}{D}$ and $\underset{\sim}{g}$ tensors of the lowest triplet states. The temperature dependence of the ODMR spectra indicate the absolute zero-field (ZF) level ordering to be Z > O > Y > X. Carbon-13 hyperfine, fluorine hyperfine, and bromine hyperfine and quadrupole were observed and yield estimates of the π spin densities on the carbonyl carbon ($\rho^{\pi} \sim 0.2$) and the 4,4' ring positions of the benzene rings ($\rho^{\pi} \sim 0.1$). Experimental studies of level anticrossing and cross-relaxation effects on the phosphorescence and ODMR spectra of benzophenones in DDE are described and interpreted. A novel method of determining the magnitude of the perturbation giving rise to the level anticrossing is presented.

From this investigation, it is concluded that (1) the orbital symmetry of the lowest triplet state of benzophenones is A, (2) the ZF schemes are significantly perturbed by second-order spin-orbit coupling with higher triplet states, (3) ring conformations and substituents influence the ZF splittings, and (4) a significant amount of electron spin is delocalized throughout the molecule.

TABLE OF CONTENTS

Page

LIST OF FIGURES

LIST OF TABLES

Page

I. INTRODUCTION

A. The Triplet State

The mechanisms of the deactivation processes which a molecule undergoes following the formation of excited states have fascinated researchers for nearly a century. As early as the 1880's, Dewar[1] and others[2] observed an intense afterglow from many organic molecules after exposure to ultraviolet light. The suggestion that the phosphorescence of photo-excited aromatic molecules might be due to a radiative spin-forbidden transition from a triplet electronic state to the singlet ground state originated with G. N. Lewis[3,4] and subsequently the photo-induced paramagnetism associated with the metastable emitting state was measured.[5,6] At the end of the 1950's, the classic EPR experiments of Hutchison and Mangum[7] on naphthalene in a host single crystal of durene provided the decisive proof of the assignment of the long-lived emission to a triplet state. Since then the number of studies of triplets by EPR has increased enormously and a wealth of information concerning the properties of the triplet state has been obtained. There is not space here to dwell on the ramifications of triplet state studies, but very detailed surveys have been provided by the published proceedings of a conference held in Beirut,[8] recent books,[9] and review articles.[10]

The photophysical processes involving the electronic states of a molecular system can be represented by the common phenomenological model depicted in Fig. 1. By the absorption of light, the molecule is brought from its ground singlet state (S_o) into various excited singlet states (S_n) where rapid relaxation to the first excited singlet state (S_1) occurs by the non-radiative internal conversion (IC) process. The rate of IC is so rapid that radiative processes between singlets (fluorescence) and non-radiative intersystem crossing (ISC) to the triplet manifold (T_n) are most probable from S_1. Once T_n is populated by ISC, rapid IC occurs to the lowest excited triplet state (T_1). Excitation that finds its way into T_1 can be deactivated by radiative (phosphorescence) and non-radiative (ISC) means, thereby re-populating the ground state (S_o). As one can see, different nomenclature is used for distinguishing the various radiative and non-radiative processes. The differences, however, are more than in name only, and the distinctions can be made by examining the fundamental properties of singlet and triplet states.

If one considers a system with two electrons in two different orbitals, a total of four wavefunctions can be generated corresponding to different combinations of electron spin and orbital angular momenta. The two orbitals can be

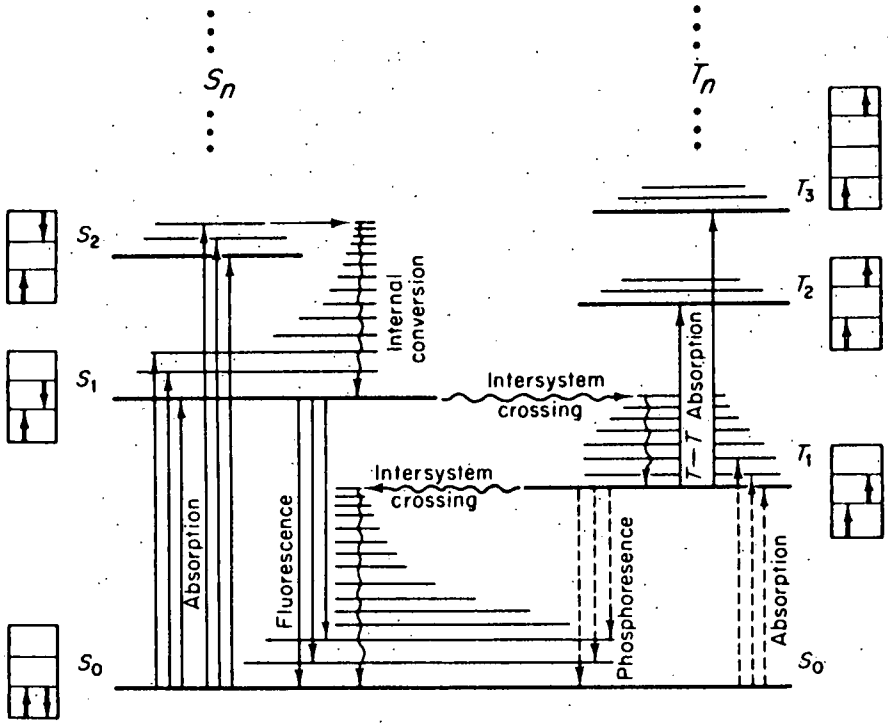

Figure 1. Primary photophysical processes in polyatomic molecules.[9] Allowed (forbidden) radiative processes are indicated by solid (dashed) straight lines, non-radiative processes by wavy lines.

considered to form symmetric and antisymmetric spatial wavefunctions while the electron spin functions can be combined to form one antisymmetric and three symmetric wavefunctions:

$$|+\rangle = |\alpha_1\alpha_2\rangle \qquad \text{(1a)}$$

$$|0\rangle = 1/\sqrt{2}\ |\alpha_1\beta_2+\beta_1\alpha_2\rangle \qquad \text{(1b)}$$

$$|-\rangle = |\beta_1\beta_2\rangle \qquad \text{(1c)}$$

Symmetric

and

$$|0'\rangle = 1/\sqrt{2}\ |\alpha_1\beta_2-\beta_1\alpha_2\rangle \qquad \text{Antisymmetric} \qquad (2)$$

The symmetric and antisymmetric spin functions are eigenvectors of the total spin angular momentum operator ($\underline{S}^2$) with eigenvalues $1\hbar$ and $0\hbar$, and form the basis for states of triplet and singlet multiplicity, respectively. By combining the orbital and spin wavefunctions the state functions of the system are obtained. Since the electrons are spin one-half particles, they must obey Fermi statistics. Therefore, states having symmetric spatial wavefunctions must have antisymmetric spin wavefunctions (singlets), and states having antisymmetric spatial wavefunctions must have symmetric spin wavefunctions (triplets). The differences in the two manifolds of electronic states - singlets (S_n) and triplets (T_n) - and photo-physical processes can now be characterized in terms of the difference in multiplicity associated with the difference in magnitude of the total electron spin angular momentum. For example,

the difference in energy between a given singlet state and its corresponding triplet state is readily explained. If one considers the four state functions (spin + orbital) and a Hamiltonian including a one-electron term and a two-electron term(electron repulsion), the energies of the singlet and triplet are modified. The matrix element associated with the two-electron term is found to consist of a coulomb and an exchange integral. The exchange integral leads to an increase in energy of the singlet and a decrease in energy of the triplet. Thus, triplet states lie lower in energy than the corresponding singlet states. Another consequence of the difference in multiplicity between singlet and triplet states is that the spin of one of the electrons must be altered or "flipped" if a transition occurs between a state in the singlet manifold and one in the triplet manifold. Such transitions are forbidden and serve to explain the distinction between the various radiative and non-radiative photophysical processes.

State multiplicities are important since the nature of the emission process depends on them. If the states involved are of the same multiplicity, the emission is called fluorescence and most commonly occurs between S_1 and S_o. Emission between states of different multiplicity is known as phosphorescence and generally occurs between T_1 and

S_o. Because the probability of transitions is much higher when $\Delta S=0$, phosphorescence lifetimes are longer (10^{-3} to 10 sec) than fluorescence lifetimes (10^{-7} to 10^{-10} sec). Similarly, the forbidden nature of altering the spin of one electron explains the low oscillator strengths of singlet-triplet absorption when compared to those for singlet-singlet absorption.

In addition to the radiative processes, the distinction between the non-radiative processes are best explained in terms of multiplicity. These processes are the result of conversion of electronic energy into vibrational energy and can occur, once again, between states of the same or different multiplicity. When a non-radiative process occurs between states of the same multiplicity, it is referred to as internal conversion (IC), while a non-radiative process between states of different multiplicity is called intersystem crossing (ISC). The approximate rates of the various non-radiative processes also reflect the multiplicity effects indicated previously for the radiative processes:

$$S_n \xrightarrow{10^{11}\text{-}10^{14}\ \text{sec}^{-1}} S_1 \qquad \text{(IC)}$$

$$S_1 \xrightarrow{10^{5}\text{-}10^{7}\ \text{sec}^{-1}} S_o \qquad \text{(IC)}$$

$$S_1 \xrightarrow{10^{8}\text{-}10^{11}\ \text{sec}^{-1}} T_n \qquad \text{(ISC)}$$

$$T_1 \xrightarrow{10 - 10^{3}\ \text{sec}^{-1}} S_o \qquad \text{(ISC)}$$

where $\rightsquigarrow$ represents a non-radiative path. Of course, the fact that the spin-forbidden processes (radiative and non-radiative) occur at all is due to the breakdown in the $\Delta S=0$ selection rule by the effects of spin-orbit coupling. The proceeding discussion of the photophysical processes involved when excitation of a molecule occurs is only qualitative in nature and is intended to provide a phenomenological description of an excited molecular system. More thorough accounts of all of the processes can be found elsewhere.[9,11]

In the case of organic molecules, the excited singlets and triplets involved in the aforementioned processes may be classified as (π,π^*) or (n,π^*) states depending on the nature of the ground state orbital of the "promoted" electron. In a molecule containing a heteroatom such as oxygen or nitrogen, the highest filled orbitals in the ground state are generally the non-bonding, essentially atomic n orbitals; the lowest unfilled orbitals are π^*. Hence the lowest excited states (S_1 and T_1) of carbonyl compounds, simple N-heterocyclics, and quinones are usually (n,π^*) in character.[12] Examples of molecules having (π,π^*)-type lowest excited states are naphthalene, benzene, and, in general, most unsubstituted aromatic hydrocarbons.

Based on extensive experimental and theoretical evidence, several generalizations about the properties of

these two classes of excited state can be made.[10,13] For example, (n,π^*) states have high quantum yields of phosphorescence and do not fluoresce significantly whereas (π,π^*) states generally show both fluorescence and phosphorescence. It has also been found that in most cases phosphorescence lifetimes, τ_p (determined by the combined radiative and non-radiative rates of depopulating the triplet state), are shorter for $^3(n,\pi^*)$ than those for the $^3(\pi,\pi^*)$ states of unsubstituted aromatic hydrocarbons. Furthermore, the phosphorescence from $^3(n,\pi^*)$ states is in-plane polarized while that from $^3(\pi,\pi^*)$ states is predominantly out-of-plane polarized. As a result, these criteria have been used by optical spectroscopists to ascertain the orbital nature of many triplet states.

B. Background

1. Applications of EPR to Triplet States

Since the triplet state is characterized by two unpaired electrons and is paramagnetic, the total spin of the electrons is unity (S=1) and the state consists of three distinct magnetic sublevels. If there were only exchange and electrostatic interactions between the unpaired electrons, the three sublevels of the triplet state would be degenerate in the

absence of a magnetic field. In the presence of a magnetic field the spin Hamiltonian ($\mathcal{H}_S$) would consist of a single term - the electron Zeeman interaction ($\mathcal{H}_Z$):

$$\mathcal{H}_z = g\,\beta\,\underline{H}\cdot\underline{S} \qquad (3)$$

where g is the spectroscopic splitting factor of the electron (here assumed isotropic) and β is the Bohr magneton. The three sublevels would then be distinguished by their spin angular momentum S_z about the field axis ($\underline{z}$) with eigenvalues +1, 0, and -1 $g\beta H$, and the EPR spectrum would consist of a single line at $H = h\nu/g\beta$ corresponding to the two (degenerate) "$\Delta m_S = \pm 1$" transitions $|-1\rangle \rightarrow |0\rangle$ and $|0\rangle \rightarrow |+1\rangle$. However, the classic experiments of Hutchison and Mangum[7] showed that the degeneracy of the three electron spin levels was lifted even in the absence of a magnetic field. This so-called zero-field splitting is due to the combined effects of non-cubic crystal fields and spin-orbit coupling in inorganic compounds.[14] However, in organic molecules, it is generally believed that the origin of the ZF splitting is the magnetic dipole-dipole interaction between the unpaired electrons.[15] The Hamiltonian for the dipolar interaction between two spins $\underline{s}_1$ and $\underline{s}_2$ is[16]

$$\mathcal{H}_{ZF} = g^2\beta^2\left\{\frac{\underline{s}_1\cdot\underline{s}_2}{r^3} - \frac{3(\underline{s}_1\cdot\underline{r})(\underline{s}_2\cdot\underline{r})}{r^5}\right\} \qquad (4)$$

where $\underline{r}$ is the vector joining the two electrons. When the dipolar interaction is averaged over all possible orientations of the spins and expressed in terms of the total spin $\underline{S} = \underline{s}_1 + \underline{s}_2$, it can be written in the form[16]

$$\mathcal{H}_{ZF} = \underline{S} \cdot \underset{\sim}{D} \cdot \underline{S} \tag{5}$$

where D is a symmetric second-rank tensor having elements (in Cartesian co-ordinates):

$$D_{ii} = \frac{1}{2} g^2\beta^2 \left\langle \frac{r^2-3i^2}{r^5} \right\rangle \qquad i = x, y, z \tag{6a}$$

$$D_{ij} = \frac{1}{2} g^2\beta^2 \left\langle \frac{-3ij}{r^5} \right\rangle \qquad i \neq j \tag{6b}$$

In terms of the principal axes $(\underline{x},\underline{y},\underline{z})$ which diagonalize $\underset{\sim}{D}$, the Hamiltonian becomes

$$\mathcal{H}_{ZF} = -XS_x^2 - YS_y^2 - ZS_z^2 \tag{7}$$

where X, Y, and Z are the principal values of $\underset{\sim}{D}$. These parameters are simply the energies of the three sublevels in the absence of a magnetic field and can be calculated from the spatial wavefunction of the triplet state using the expressions

$$X = \frac{1}{2} g^2\beta^2 \left\langle \psi_T \left| \frac{3x^2-r^2}{r^5} \right| \psi_T \right\rangle \tag{8a}$$

$$Y = \frac{1}{2} g^2\beta^2 \left\langle \psi_T \left| \frac{3y^2-r^2}{r^5} \right| \psi_T \right\rangle \tag{8b}$$

$$Z = \frac{1}{2} g^2\beta^2 \left\langle \psi_T \left| \frac{3z^2-r^2}{r^5} \right| \psi_T \right\rangle \tag{8c}$$

However, $\underset{\sim}{D}$ is traceless (i.e., X + Y + Z = 0), so $\mathcal{H}_{ZF}$ can be expressed in terms of just two independent parameters, D and E:

$$\mathcal{H}_{ZF} = D(S_z^2 - \frac{1}{3} S^2) + E(S_x^2 - S_y^2) \tag{9}$$

The new parameters D and E are given by

$$D = \frac{3}{4} g^2\beta^2 \left\langle \psi_T \left| \frac{r^2-3z^2}{r^5} \right| \psi_T \right\rangle \tag{10a}$$

$$E = \frac{3}{4} g^2\beta^2 \left\langle \psi_T \left| \frac{y^2-x^2}{r^5} \right| \psi_T \right\rangle \tag{10b}$$

and are related to X, Y, and Z by the expressions

$$D = 1/2(X + Y) - Z = -3/2\ Z \tag{11a}$$

$$E = -1/2(X - Y) \tag{11b}$$

From the form of the above expressions, it can be seen that the ZF parameters are extremely sensitive to the spatial distribution of the triplet electrons and reflect the symmetry and structure of the molecule in the triplet state. Thus, triplets possessing spherical, axial, and orthorhombic

symmetries should have ($D=E=0$), ($D\neq0$, $E=0$), and ($D\neq E\neq0$), respectively.

Clearly the magnitude of the ZF splitting parameters can also provide a great deal of information about the triplet state. For example, a comparison of the measured D values of the lowest triplet state of diphenylmethylene and naphthalene (0.41[17] and 0.10 cm^{-1},[7] respectively) indicates that in the former case, the unpaired electrons are essentially "localized" on the methylene carbon. Similarly, the fact that the E value of benzene was found to be non-zero for the lowest triplet state[18] suggested that the structure is not a regular hexagon although more recent experiments have shown that the molecule may not be intrinsically distorted.[19] Furthermore, the observed difference in ZF splitting parameters for different molecules is a useful tool for the study of energy transfer processes in molecular crystals. Triplet energy transfer in a biphenyl single crystal from guest phenanthrene to guest naphthalene molecules was first observed using EPR techniques.[20] Over the past decade the literature has become replete with similar studies on a wide variety of molecular triplet states.

2. Optical Detection of Magnetic Resonance (ODMR)

Despite the significant contributions EPR methods have made toward a more complete understanding of the triplet state,

experiments of this type are severely limited by signal-to-noise considerations. The sensitivity of the detection method in EPR depends only on the amount of microwave power absorbed by the sample, which in turn depends on the number of molecules in the triplet state. Molecules with triplet state lifetimes shorter than 100 msec are virtually impossible to study by EPR methods because of the low steady-state concentration of triplets that exist even under optimum conditions. Consequently, entire classes of important molecules such as the carbonyls and the (n,π^*) azines were not amenable for study. It therefore became necessary to develop modified EPR techniques for studying species with lifetimes of the order of a msec, and one such technique which found wide applicability in the last few years is that of optical detection of magnetic resonance (ODMR).

In 1949, Brossel and Kastler[21] were the first to propose that radiofrequency (rf) transitions in an excited state could probably be observed by monitoring changes in the intensity or polarization of the optical emission produced by rf saturation. This idea was first applied successfully by observing a transition between the sublevels of the $^3P_1$ excited state of Hg in the gas phase by Brossel and Bitter.[22] Within six years of the Brossel and Bitter experiment, the

analogous experiment was executed in the solid state. Geschwind et al.[23] succeeded in optically detecting magnetic resonance in the ^2E excited state of Cr^{3+} in a single crystal of ruby at 1.6°K. Meanwhile, McClure[24] and El-Sayed[25] had shown that both the populating and depopulating mechanisms involving the triplet state of aromatic molecules were spin-state selective, and this motivated de Groot et al.[26] to suggest that optical detection methods might also be used to observe transitions between the spin sublevels of excited triplet states. By 1967, such an experiment was carried out by Sharnoff,[27] who observed the "$\Delta m_s = \pm 2$" transition of naphthalene-$\underline{d}_8$ in a biphenyl host crystal by monitoring the intensity of the phosphorescence as the field was swept through resonance in the presence of microwaves. Both Kwiram[28] and van der Waals et al.,[29] working independently, succeeded shortly thereafter in doing similar experiments on aromatic molecules. It was soon discovered that the ODMR technique was well-suited for the study of triplet states with very short lifetimes.

The essential features of an ODMR experiment can be represented by the simple model shown in Fig. 2. Consider an excited state consisting of magnetic sublevels 1 and 2 which emit optical photons at a rate $k_i^r(v)$, where i refers to the spin sublevels and v designates the polarization or

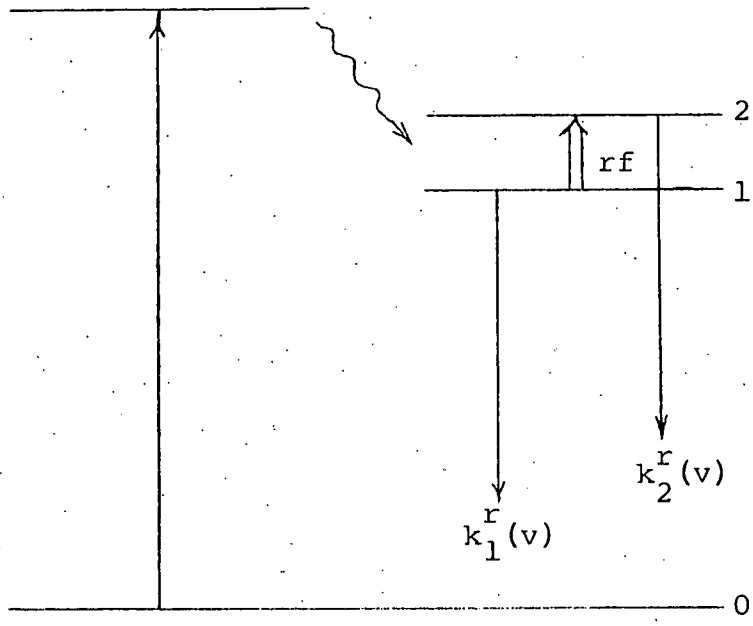

Figure 2 - An elementary model for the ODMR experiment

vibronic band of the optical emission. The excited state is populated through a mechanism such as outlined in Section A of this chapter. The observed emission intensity, I(v), is proportional to the number of photons emitted per unit time such that

$$I(v) = \sum_i k_i^r(v)\ N_i = k_1^r(v)\ N_1 + k_2^r(v)\ N_2 \qquad (12)$$

where N_i is the population of level i. If rf power is used to induce transitions between levels 1 and 2, the change

in emission intensity, $\Delta I(v)$, is given by

$$\Delta I(v) = k_1^r(v)\,\Delta N_1 + k_2^r(v)\,\Delta N_2 = [k_1^r(v) - k_2^r(v)]\,\Delta N \qquad (13)$$

where $\Delta N = \Delta N_1 = -\Delta N_2$. Thus, changes in the emission intensity (or polarization) in the presence of resonant rf will occur only if $k_1^r(v) \neq k_2^r(v)$ and $\Delta N \neq 0$.

It is reasonably easy to understand how the ODMR technique leads to a sensitivity enhancement of the EPR signal of short-lived triplets. In optical detection the signal-to-noise ratio (S/N) is proportional to the number of photons emitted from the excited state per unit time. For triplet states this would be of the order of N/τ_p, where N is the steady-state concentration of triplets and τ_p is the phosphorescence lifetime. But under steady-state conditions N is proportional to τ_p so that the S/N using optical detection is, to a first approximation, independent of τ_p. However, the S/N employing microwave detection in conventional EPR is proportional to N and, therefore, to τ_p.[30] Of course, in order to maximize the signal in either case it is advantageous to maximize the initial difference in the populations of the sublevels by cooling the sample to liquid helium temperatures. An important consequence of carrying out experiments at these temperatures is that the spin-lattice relaxation (SLR) processes which operate to maintain a Boltzmann equilibrium

among the spin sublevels become slow compared to the phosphorescence decay processes.[26] In fact, when SLR becomes very slow (i.e., $T_1 >> \tau_p$), the spin system is said to be in a state of spin polarization or spin alignment and the steady-state populations of the individual sublevels depend only on the competition between the separate populating and depopulating processes of each sublevel.

The experiments of Sharnoff, Kwiram, and van der Waals have stimulated a number of different groups to apply ODMR techniques to triplet states, and a virtual plethora of publications in this area have appeared in the past five years. These investigations have provided a wealth of information about the magnetic and optical properties of triplet states and have been reviewed recently by El-Sayed[30] and Kwiram.[31] Of particular importance were the findings of Schmidt and van der Waals[32] and Tinti et al.[33] that transitions between the electron spin sublevels of triplet states could be detected in zero-field by optical detection methods. The advantage of this technique is that polycrystalline samples and even glasses can be used to accurately measure the ZF parameters since the spectrum is free of the anisotropy introduced by the presence of a magnetic field. In addition, the ZF technique (called phosphorescence-microwave double resonance (PMDR) spectroscopy by some) avoids the mixing of the electron spin states which

is produced by application of a magnetic field. As a result PMDR is more suitable for determining the radiative and non-radiative decay constants, relative ISC rate constants, polarizations of ZF transitions, and coherent coupling of excitons in pure crystals.

C. ODMR and Its Application to Aromatic Carbonyls

The voracious hydrogen abstracting ability of photo-excited molecules containing the carbonyl moiety has been well known since Ciamician and Silber[34] first reported the photochemical reduction of ketones to pinacols or benzohydrols. There is now substantial agreement[35,36] that the first steps in the photopinacol reaction involve formation of the triplet state of the ketone which abstracts a proton from an alcohol to form a ketyl radical. Energy transfer from photo-excited benzophenone triplets has been reported in solids[37] and solutions,[38] and later found to be of utility in synthetic methods.[39] For example, irradiation of diazomethane in the presence of cis- and trans-2-butene results in stereospecific addition to form 1,2-dimethylcyclopropanes.[40]

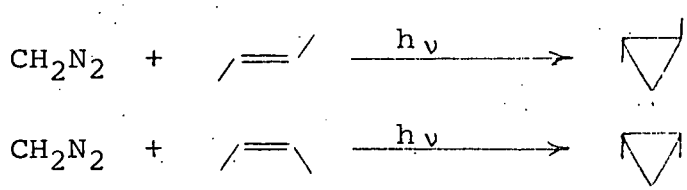

However, the same reaction carried out in the presence of benzophenone as a sensitizer results in non-stereospecific addition.[41] From these few examples,

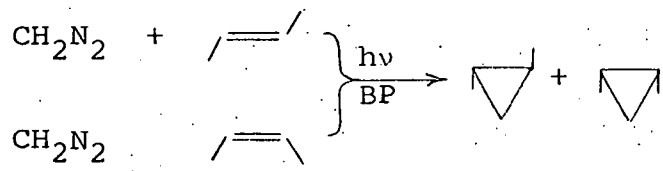

it is apparent that the triplet state of aromatic carbonyls plays a major role in chemistry and that studies of their properties are pertinent to a greater understanding of this role.

Extensive optical investigations of the properties of the lowest excited triplet state of benzophenone[42-45] led to its assignment as (n,π^*). As a rule assignments of the orbital symmetry of triplet states from polarization data are difficult and ambiguous. Measurement of the polarization of a transition leads only to the symmetry of perturbing singlet, and the consequent deduction of the triplet state symmetry requires an arbitrary choice of spin-state activity (i.e., spin-orbital activity) as well as a specific spin-orbit interaction mechanism. However, a most definitive series of investigations was carried out by Hochstrasser and co-workers[46-48] on the triplet state of benzophenones. By applying the Zeeman and Stark effects to

the polarized, high-resolution, singlet-triplet absorption spectrum of benzophenone, these authors showed the triplet state to be of C_2 symmetry, deduced the radiative activity of the triplet spin sublevels, and elucidated the mechanism of spin-orbit coupling in the population and depopulation of the benzophenone triplet. In addition, by optically resolving the absorption into each of the spin states of the triplet, the signs* and magnitudes of the ZF splittings were measured.

During the period when Hochstrasser's group was carrying out optical measurements on benzophenone crystals, ODMR was being applied to the triplet state of benzophenone. Sharnoff investigated the nature of triplet excitons in neat benzophenone crystals utilizing the high field ODMR technique. These studies provided measurements of the magnitudes and relative signs of the ZF splitting parameters of trapped[49] and nonlocalized[50] triplet excitations as well as yielding information about the exciton trapping mechanism[51] and decay.[52] Kinetic data (relative radiative rates, lifetimes, steady-state populations, and populating rates) were obtained by ZF ODMR

---

* The sign of E determined in this study was later shown to be in error.[49]

techniques (microwave-induced delayed phosphorescence[53] and magnetic resonance fast passage[54,55]). However, these measurements were made on traps in neat benzophenone crystals and only one ODMR study has been reported on essentially isolated benzophenone molecules in a well-defined crystal system.[56] Thus, it is apparent that further studies of isolated benzophenones are required in order to obtain a more complete understanding of the $^3(n,\pi^*)$ state of aromatic carbonyls.

Indeed, benzophenone is not the only aromatic carbonyl to come under the scrutiny of spectroscopists in the last few years. Extensive optical[51,58,59] and ODMR[60,61] studies of benzaldehydes and acetophenones have been carried out. These investigations have shown that the use of criteria such as short lifetimes, carbonyl progressions in the phosphorescence spectra, in-plane polarization of phosphorescence, and the absence of external heavy atom effects for distinguishing between $^3(n,\pi^*)$ and $^3(\pi,\pi^*)$ aromatic carbonyl molecules is questionable. Similarly, arguments based on the signs and magnitudes of the ZF splitting parameters for determining the orbital nature of the triplet state are equally inadequate. Models invoking second-order spin-orbit coupling effects on the energies of the triplet spin sublevels have appeared in the literature[62,63] in an effort to explain the ODMR data.

These models appear to be potentially fruitful, but require experimental measurement of the $\underset{\sim}{g}$ tensor in EPR experiments in order to establish a correlation. This type of information is extremely scarce.

This thesis is directed to the study of the high field ODMR spectra of benzophenone and substituted benzophenones. It is hoped that the data and discussions concerning ZF splittings, hyperfine structure, and g-value anisotropy contained herein will help provide some of the additional information necessary for answering the numerous unsolved questions concerning the nature of the triplet state of aromatic carbonyls.

II. EXPERIMENTAL

A. Sample Preparation

4,4'-Dichlorobenzophenone (4,4'-DCBP), 4,4'-dibromodiphenylether (DDE), and 4,4'-difluorobenzophenone (4,4'-DFBP) were purified by multiple recrystallization from hexane and ethanol, followed by zone refining under an atmosphere of nitrogen for 100 passes at 0.5 in/hr with continuous stirring of the molten zones. Princeton Organics PAR grade benzophenone (^{12}C-BP or BP) and Bio-Rad carbonyl ^{13}C-benzophenone (^{13}C-BP, assayed at 91.9 atom % ^{13}C) were used following vacuum sublimation. 4,4'-Dibromobenzophenone (4,4'-DBBP) was purified by five recrystallizations from hexane and ethanol followed by two vacuum sublimations. Neat crystals of 4,4'-DCBP and mixed crystals of guest in DDE (0.1-1 mole %) were grown <u>in vacuo</u> by the Bridgman technique. The crystal growing furnace was constructed by winding 24 gauge Nichrome wire around a Pyrex tube and insulating with asbestos. The temperature of the furnace was adjusted so that the liquid-solid interface was at the lower opening of the furnace. The crystal growing tube (8 mm ID), equipped with a capillary tip, was lowered through the furnace by a clock motor at a rate of 0.75 in/day. After a crystal was grown, it was often annealed in

a constant temperature environment (ca. 20° below the melting point) for one week.

B. Crystal Orientation

The molecular axes (x, y, and z) of DDE and 4,4'-DCBP (and other benzophenones) can be defined in terms of the local C_{2v} symmetry of the planar C_1-O-C_1' * and C_1-C(O)-C_1' atoms, respectively. The molecular z axis is defined as lying in the plane of these atoms, passing through the oxygen atom and corresponds to the molecular two-fold axis; x is normal to the plane of the atoms, and y completes the right-hand coordinate system. The orientation of these axes in DDE and 4,4'-DCBP crystals can be obtained by examining the crystal structure data.

Crystals of DDE are orthorhombic having four molecules per unit cell[64] and display ac cleavage as determined by X-ray crystallography. The crystallographic data are listed in Table I. Table II A gives the direction cosines of the molecular axes (x, y, and z) with respect to the crystallographic axes (a, b, and c). The direction cosines indicate there are two possible orientations of the molecules in the unit cell

---

* C_1 and C_1' refer to the carbons on the two phenyl rings which are bonded to the oxygen atom in DDE (the carbonyl group in benzophenones).

TABLE I: Crystal data for 4,4'-dichlorobenzophenone and 4,4'-dibromodiphenylether

	DDE[64]	4,4'-DCBP[65]
Space Group	C_{2v}^{13} (C_{cc})	C_{2h}^{6} (I2/a)
α	90°	90°
β	90°	95°20'
γ	90°	90°
a	7.70 Å	7.72 Å
b	26.50 Å	6.17 Å
c	5.85 Å	24.92 Å
Z	4	4
Cleavage Plane	{010}	{001}

TABLE II: Direction cosines of molecular axes with respect to crystallographic axes

A. 4,4'-Dibromodiphenylether

	a	b	c
x	±0.9996	±0.0291	0
y	∓0.0291	±0.9996	0
z	0	0	1

B. 4,4'-Dichlorobenzophenone[48]

	a	b	c	c'[a]
x	-0.986	0	-0.259	-0.168
y	-0.168	0	+0.966	+0.986
z	0	1	0	0

[a] c' axis is defined as being perpendicular to the ab-cleavage plane

which are distinguishable in the ab plane. The molecular two-fold axes (z) of both orientations are parallel to the crystallographic c axis. The xy molecular planes of both orientations lie in the ab plane, such that x and y make angles of 1°40' with a and b, respectively. The c axis of the crystal is a C_2 axis which relates the distinguishable molecular orientations in the ab plane.

Crystals of 4,4'-DCBP are monoclinic having four molecules per unit cell[65] and display a perfect ab cleavage. The crystallographic data are presented in Table I. The direction cosines of the molecular axes with respect to the crystallographic axes are given in Table II B. The direction cosines indicate that the x, y and z axes of the four molecules in the unit cell are coincident. The carbonyl axes (z) are parallel to the crystallographic b axis, and the xy molecular planes lie in the ac plane, such that x and y make angles of 9°36' with a and c' (normal to the ab plane), respectively. The interesting feature of the two crystal systems is that the planes of the two benzene rings make an acute angle of 29°± 2°[68,69] with the plane defined by the C_1-C(or O)-C_1' atoms in both crystal systems. Furthermore, the C_1-C-C_1' bond angle in 4,4'-DCBP is nearly the same as the C_1-O-C_1' bond angle in DDE, 127°± 1°[68] and 123°± 1°,[69] respectively.

After removing the crystal from the Bridgman tube, it was cleaved with a sharp razor blade. In initial experiments the crystallographic axes which lie in the cleavage plane were identified by X-ray crystallography for both crystal systems. In subsequent experiments it was found that the carbonyl bond axes in the crystals were, in general, parallel to the crystal growth axis. Thus, by examining the cleavage plane under a polarizing microscope the b and c crystallographic axes of 4,4'-DCBP and DDE crystals, respectively, were easily located. Once the carbonyl axis was identified, the crystal was mounted on a three-circle optical goniometer and oriented so that the reflection pattern from the cleavage face was distinct and the carbonyl axis was vertical. The crystal was then reoriented for mounting on the Hysol post (3 mm diam.) used as the axis of rotation in the ODMR experiments. In general, two mounts were made corresponding to a cleavage plane rotation and a rotation about the carbonyl bond axis (xy molecular plane rotation). These were found to be sufficient for determining the principal values of the fine-structure tensor. Other mounts corresponding to rotations in the principal axis system of the ZF tensor were made once these axes were located with respect to the crystallographic axes in an ODMR experiment.

The accuracy of each mount was checked during an ODMR experiment in the following manner. The crystal was rotated to a position in the orientational dependence of the ODMR spectrum where $\Delta H/\Delta\theta$ is a maximum, and a spectrum was recorded. In such a region of the orientational dependence, 1° of rotation produced a 50-200 G shift in line position, depending on the type of mount. The crystal was then rotated 180° and another spectrum was recorded. The deviation in line position was generally a factor of 10 less than that observed for 1° of rotation, indicating the mount was accurate to less than 0.3°.

C. Phosphorescence Spectra

Phosphorescence spectra at liquid helium temperatures were recorded with the crystals mounted in the ODMR apparatus prior to carrying out magnetic resonance experiments. A PEK high pressure Hg arc was used as an exciting source, and the light was filtered through a 10 cm path length cell containing an aqueous solution of either $NiSO_4$, $CuSO_4$, or $CoSO_4$ and through the appropriate glass filter(s)[13,65] to yield predominantly 3130, 3660, or both 3130 and 3660 Å wavelength excitation, respectively. A quartz lens was used to focus the light onto the sample through the quartz walls of the He cryostat. The emission was collected at 90° with a quartz

light pipe (0.25" diam x 3' length) placed ca. 1 cm from the sample and terminating outside of the cryostat at the entrance slit (100 μ) of a Jarrell-Ash ¼ m monochromator. The monochromator wavelength selector was driven by a variable speed motor. Following dispersion, the emission was detected using an EMI 6256S photomultiplier tube and a Keithley 417 picoammeter and displayed on a strip-chart recorder.

A composite of the phosphorescence spectra obtained in this manner for all the systems studied in this research is shown in Fig. 3. One notices the prominent carbonyl stretching progression as well as some lower frequency vibrational activity in each of the phosphorescence spectra. The origin and carbonyl stretching frequencies exhibited by each of the molecules are listed in Table III. One notices that the position of the (0,0)-band is, in general, unique except for the ^{12}C and ^{13}C benzophenones which have a common origin (4238 Å) within the resolution of the instrument. However, the presence of one or the other was readily distinguished by the magnitudes of the carbonyl stretching frequency which are in good agreement with those calculated from reduced-mass considerations for the C=O fragment ($\bar{\nu}_{^{12}CO}/\bar{\nu}_{^{13}CO} \approx [\mu_{^{13}CO}/\mu_{^{12}CO}]^{\frac{1}{2}}$).

Figure 3. Phosphorescence spectra of benzophenones at 1.6 °K.

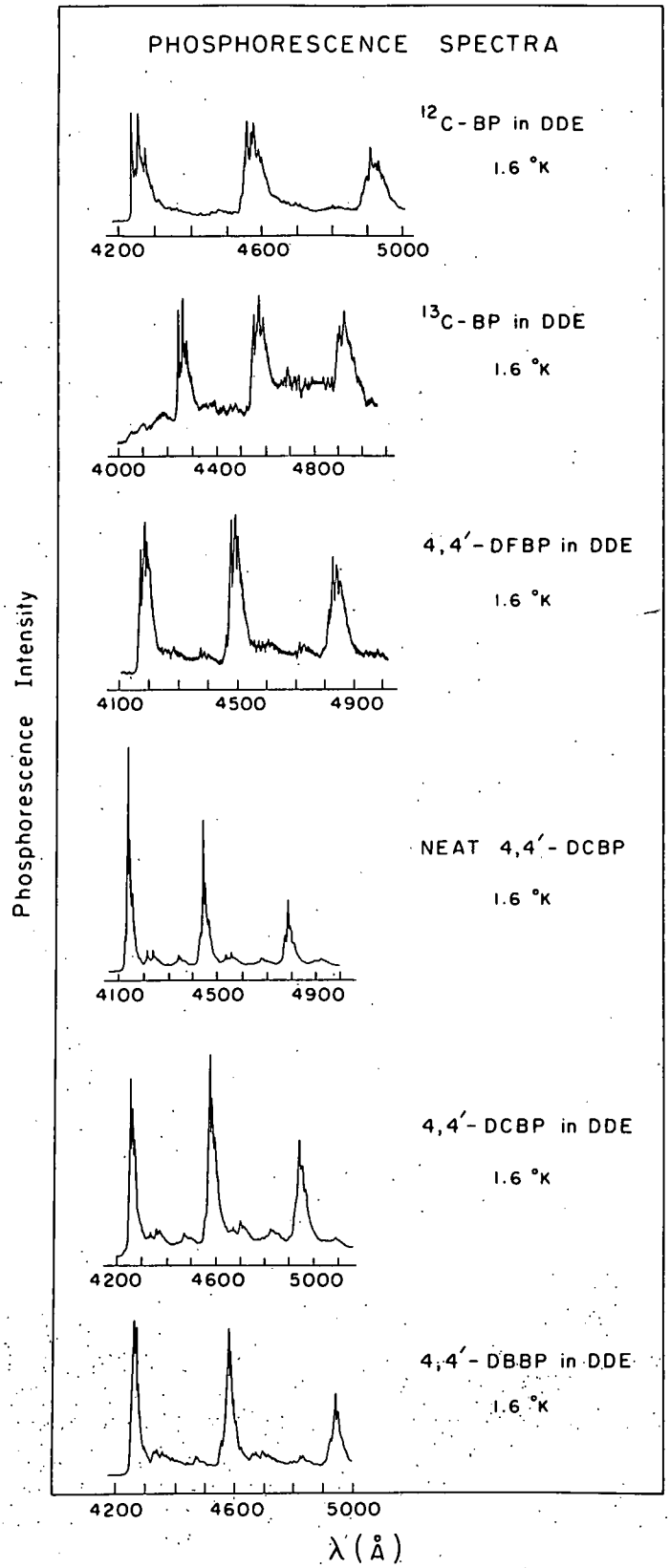
PHOSPHORESCENCE SPECTRA
^{12}C-BP in DDE
1.6 °K
4200
4600
5000
^{13}C-BP in DDE
1.6 °K
4000
4400
4800
4,4′-DFBP in DDE
1.6 °K
4100
4500
4900
NEAT 4,4′-DCBP
1.6 °K
4100
4500
4900
4,4′-DCBP in DDE
1.6 °K
4200
4600
5000
4,4′-DBBP in DDE
1.6 °K
4200
4600
5000
Phosphorescence Intensity
λ′(Å)

TABLE III: Phosphorescence data of benzophenones

Compound	Host	(0,0) band (A)	C=O stretch (cm^{-1})*
BP	DDE	4238	1666
^{13}C-BP	DDE	4238	1608
4,4'-DFBP	DDE	4165	1654
X-trap 4,4'-DCBP	neat	4133	1667
4,4'-DCBP	DDE	4252	1660
4,4'-DBBP	DDE	4250	1642

*Measured from (0,0)-(0,1) spacing in phosphorescence spectrum.

D. Optically-Detected Magnetic Resonance (ODMR) Spectra

The ODMR spectrometer consists of five basic parts -- optical source, cryostat, electromagnet, microwave source, and detection system. A block diagram of the spectrometer is shown in Fig. 4. The crystal and Hysol post (rotor) were mounted in a gear arrangement on the body of the TE_{102} rectangular cavity allowing rotation of the crystal in the cavity E-plane. The drive mechanism for the gear was coupled to a mechanical counting device (10 digits corresponding to 6° of rotation) and was found to be reproducible to $\pm 1°$. In addition, the magnet could be rotated (reproducible to $\pm 0.1°$) in a horizontal plane containing the axis of crystal rotation, thus providing the capability of aligning any desired axis within the crystal parallel to the magnetic field axis. As a result, the ODMR spectra could be studied in each of the principal magnetic planes of the emitting triplet state. A section of rectangular stainless waveguide was used to connect the cavity to a Bruker X-band microwave unit which is equipped with a variable 40dB attenuator. Microwave frequency measurements were made using a HP 5246 L electronic counter equipped with a HP 5257 A transfer oscillator operating in the APC mode and accurate to 1 part in 10^6.

Figure 4. Block diagram of the spectrometer used for optical detection of magnetic resonance (ODMR).

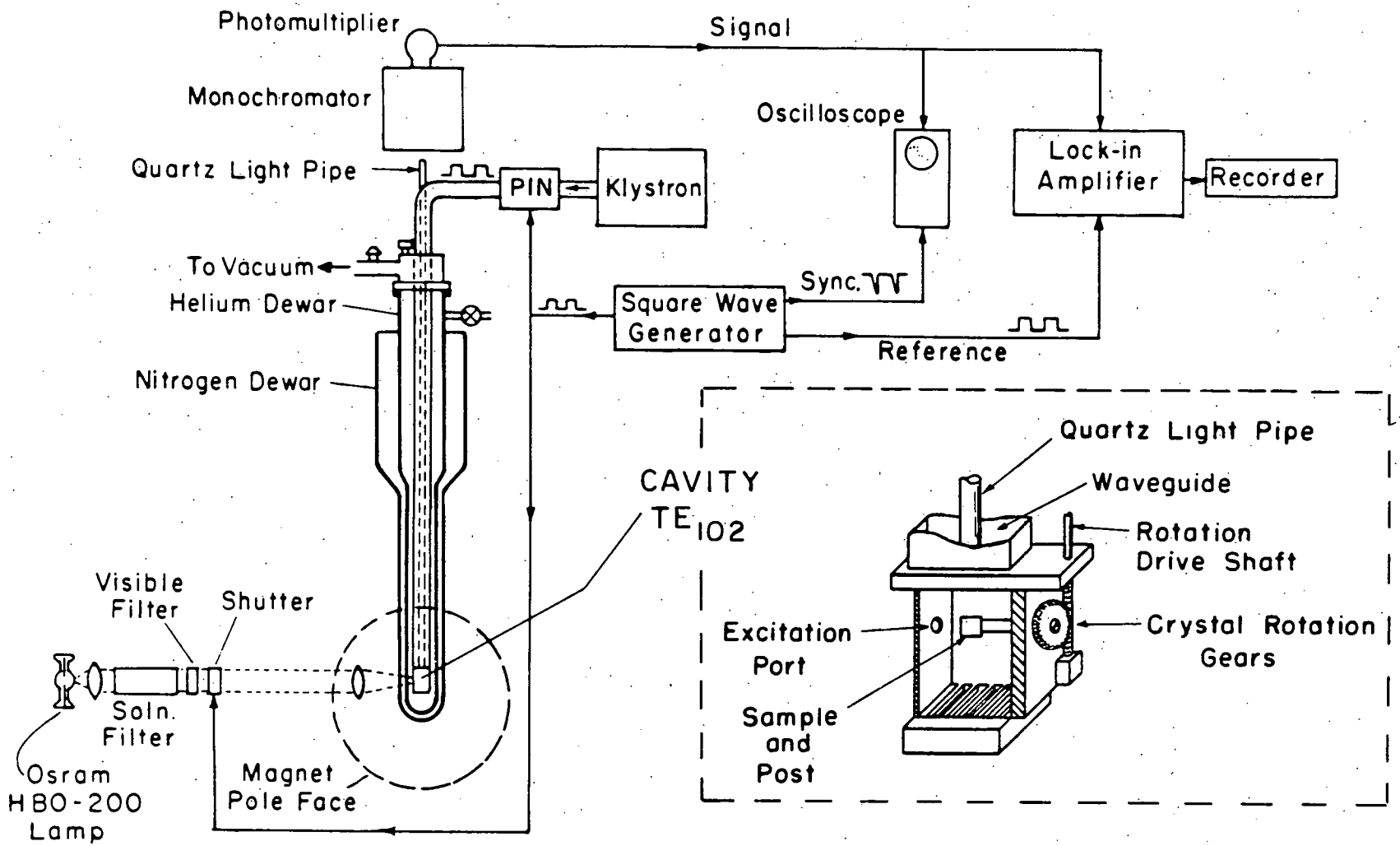

BLOCK DIAGRAM OF SYSTEM USED FOR OPTICAL DETECTION OF EXCITED STATE EPR

The cryostat was suspended between the pole pieces of a 10" Bruker electromagnet and consisted of a pair of concentric Pyrex dewars with quartz tail sections. The outer and inner dewars contained liquid nitrogen and liquid helium, respectively. Both dewars were completely silvered except for a 1 cm wide, vertical stripe which provided an optical path. The cavity and sample were immersed in liquid helium for experiments at or below 4.2°K. Temperatures above this were conveniently obtained by allowing the coolant level to drop below the sample. The use of a fixed frequency microwave cavity provided sufficient power during amplitude modulation (AM) (ave. peak power 100 mW) to saturate the ODMR transitions at temperatures above 4.2°K without extreme losses in signal-to-noise ratio (S/N). Allowing the coolant level to drop inside the cavity also provided a narrow range of cavity frequency tunability in experiments where different microwave frequencies were desired.

AM microwave power (modulation depth ~30dB) was obtained using a HP 8735 A PIN diode inserted in the cavity arm of the microwave bridge and driven with a HP 8403 A modulator which also provided a reference signal for the PAR Model HR-8 lock-in amplifier. The optical excitation and collection components were identical to those described in the preceding section except that during an ODMR experiment

the output of the photomultiplier was coupled to the impedance-matched input channel of the lock-in amplifier. ODMR spectra were detected by monitoring the intensity of either the (0,0) or (0,1) band of the phosphorescence. Modulation of the microwave power at 96 Hz (optimum) was employed and as the magnetic field was swept through a microwave resonance the AM component of the phosphorescence was detected at the lock-in amplifier and displayed on an XY recorder. The X axis of the recorder was driven by the output voltage of a Hall diode which also served to sweep the magnetic field. Magnetic field strengths were measured with a Hall probe attached to one of the pole pieces of the magnet or taken directly from a recorder tracing of the sweep, both of which were calibrated with a proton NMR probe. The measured fields are believed accurate to ± 5 G.

In experiments such as recording hyperfine structure in the ODMR spectra and level anticrossing spectra, sinusoidal field modulation was employed. Modulation coils were placed on the pole pieces of the magnet and driven by a HP 3310 B function generator which was used to reference the lock-in amplifier. The remaining detection components were identical to those used in the AM microwave experiment and the operation is completely analogous to that just described. In hyperfine measurements the microwave power was no longer amplitude

modulated, but was fixed so that a constant low level of microwave power was incident on the sample. The enhanced resolution owing to first derivative presentation of the spectra was extremely valuable for detecting small splittings. Level anticrossing spectra were obtained in the same way except no microwave power was incident on the sample. A modulation frequency of 173 Hz was found to be optimal in these experiments. Microwave power and modulation amplitude were adjusted for the best compromise between S/N and resolution.

E. Other Microwave-Optical Experiments

The versatility of the ODMR spectrometer can be demonstrated by the ability to perform other types of experiments employing resonant microwaves (pulsed or modulated). Action spectra (ODMR signal intensity vs. wavelength of emission) were obtained by setting the magnetic field at the position of an ODMR signal (with amplitude modulation of microwaves) and scanning the phosphorescence spectrum with the monochromator. Such a spectrum shows only those emission bands whose intensities are affected by microwave saturation. As a result impurity emission can be eliminated, and phosphorescence bands originating from different spin sublevels can often be identified. This type of experiment can be extremely valuable for obtaining

information about the various mechanisms which couple the triplet sublevels to the singlet manifold. In the case of benzophenones, the action spectra were identical to the normal phosphorescence spectra within experimental accuracy. This indicated that broad band emission collection - Corning CS 4-72 + CS 5-57 glass filters sans monochromator - could be used in situations where S/N became a problem. However, in general, 1 mm slits on the monochromator were sufficient.

Microwave-induced delayed phosphorescence (MIDP) experiments were carried out using an electronic shutter placed in the beam of the exciting light and triggered (together with the X axis of a Tektronix 547 oscilloscope) by the HP function generator. The function generator also served to synchronize the microwave modulation components which operated in the time-delayed pulse mode. The photomultiplier output was displayed on the Y axis of the oscilloscope, and the decay of, and microwave-induced change in the phosphorescence were photographed using a Polaroid camera with manual trigger. Fig. 5A shows the results of such a MIDP experiment on the low field "$\Delta m_S = \pm 1$" transition of 4,4'-DCBP in DDE with the field parallel to the z' axis of the fine-structure tensor. The horizontal scale corresponds to 5 msec/div. Application of the microwave pulse is seen to produce an increase in the phosphorescence intensity.

Figure 5. Pulsed microwave experiments on the low-field "$\Delta m_S = \pm 1$" transition of 4,4'-DCBP in DDE in the $\underline{H} \,||\, \underline{z}'$ orientation. (A) Microwave-induced delayed phosphorescence (MIDP) with exciting light shuttered. (B) Microwave-induced phosphorescence (MIP) with steady-state illumination of the sample.

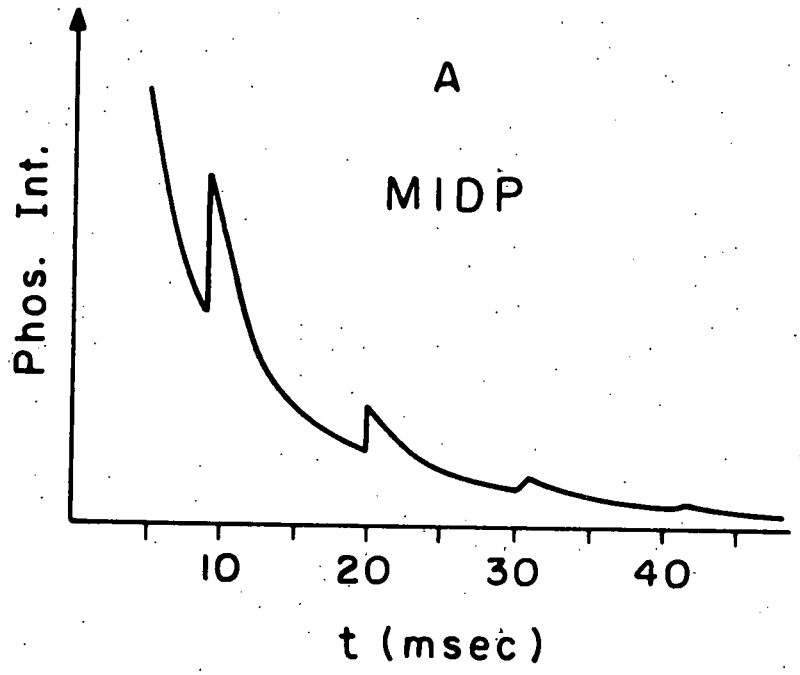
A
MIDP
Phos. Int.
10
20
30
40
t (msec)

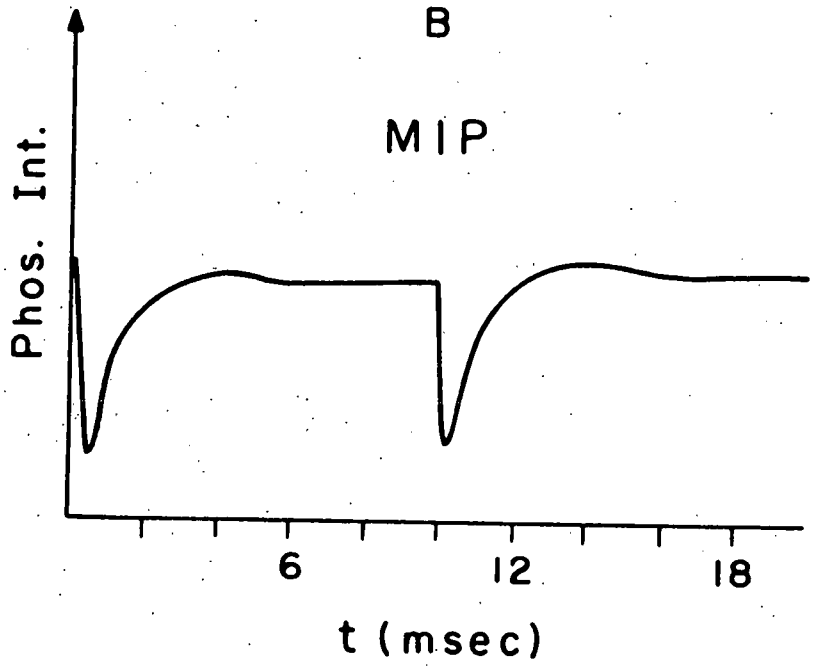
B
MIP
Phos. Int.
6
12
18
t (msec)

This type of experiment can be analyzed to obtain rate data of the two levels involved in the microwave transition as described in the literature;[66] however, the mixing of the sublevels caused by the presence of a magnetic field complicates the analysis somewhat. Of course, in the absence of microwaves the triplet state lifetimes can also be determined using this experimental arrangement by monitoring the decay of the phosphorescence. In all systems studied decay curves were non-exponential at 1.6°K and consisted of at least two lifetimes (1-2 msec and 15-25 msec). At 77°K the mixed crystal samples exhibited exponential decay with lifetimes ranging from 3-5 msec while the neat 4,4'-DCBP sample retained non-exponential behavior.

A second type of pulsed experiment called microwave-induced phosphorescence (MIP) was also carried out using the ODMR spectrometer. MIP is similar to MIDP except the exciting light is not shuttered when the resonant microwave pulse is applied and the HP modulator is used to trigger the oscilloscope. As a result, the pulse samples the steady-state populations of the two sublevels involved in the microwave transition. Fig. 5B shows the result of MIP on the same transition discussed in the preceding paragraph. In this case the horizontal scale corresponds to 2 msec/division. The microwave pulse produces a <u>decrease</u> in the phosphoresence

intensity indicating the transition occurs between a more radiative, more populated level and a less radiative, less populated level. Such experiments have been analyzed in zero-field[58,59] for rate data. In this work MIP was used to determine whether saturating the ODMR transitions produced an increase or decrease in the phosphorescence intensity.

III. ORIENTATIONAL DEPENDENCE OF THE ODMR SPECTRA AND THE DETERMINATION OF THE PRINCIPAL AXES OF THE FINE-STRUCTURE TENSOR

In the sections which follow, we use the coordinates $\underline{x}'$, $\underline{y}'$, $\underline{z}'$ to denote the principal axes of the fine-structure tensor ($\underset{\sim}{D}$) which is responsible for lifting the degeneracy of the two "$\Delta m_S = \pm 1$" transitions and for mixing the electron spin states $|+1\rangle$ and $|-1\rangle$ so that transitions of the type "$\Delta m_S = \pm 2$" become observable. In this coordinate system, $\underline{z}'$ is parallel to the C=O bond, $\underline{x}'$ is nearest the normal to the carbonyl plane, and $\underline{y}'$ completes the right-hand coordinate system. These axes may or may not be coincident with the molecular axes ($\underline{x}$, $\underline{y}$, $\underline{z}$) defined previously. However, if one assumes that the guest enters the host substitutionally, then the two coordinate systems can be related using the crystal structure data.

A. ODMR Spectra in DDE

1. ^{13}C-BP

ODMR spectra of ^{13}C-BP/DDE were obtained by monitoring the (0,1) band of the phosphorescence, and in all cases the observed signals correspond to increases in the intensity of this band. The magnetic orientation of each of the three

triplet electron spin sublevels (i.e., the assignment of the principal axes of the fine-structure tensor) was determined by studies of the orientational dependence of the ODMR spectrum of triplet ^{13}C-BP. Three studies of this type were carried out.

In the first set of experiments, the ^{13}C-BP/DDE crystal was mounted so that the axis of the post (rotation) was normal to the cleavage plane of the crystal. This mount permitted the study of the orientational dependence of the ODMR signals in the ac crystallographic plane. A plot of the magnetic fields at which resonances were observed in this plane is shown in Fig. 6A. Only three transitions are observed at any given orientation in this plane, and the angular dependence exhibits stationary behavior with the field parallel to the a and c axes. Subsequent rotation of the magnet at these two orientations indicated that only $\underline{H} \| \underline{c}$ is a true stationary field (i.e., an orientation in which the field is parallel to one of the three principal axes of $\underset{\sim}{D}$, which we denote by z'). However, magnet rotation away from the orientation $\underline{H} \| \underline{a}$ produces a splitting of each transition into a pair of lines, one moving to higher field and the second to lower field. In contrast, no such splitting is observed in the vicinity of $\underline{H} \| \underline{c}$, and the two "$\Delta m_S = \pm 1$" lines exhibit their maximum separation in this orientation.

Figure 6. Observed angular dependence of the "$\Delta m_S = \pm 1$" transitions in the ODMR spectrum of ^{13}C-BP in DDE at 1.6°K. (A) Rotation in the ac crystallographic plane; arrows indicate the positions of the "$\Delta m_S = \pm 1$" transitions in the $\underline{H} \,||\, \underline{c} \,||\, \underline{z}'$ orientation. (B) Rotation in the ab crystallographic plane; subscripts 1 and 2 refer to the two identical but inequivalent fine-structure patterns.

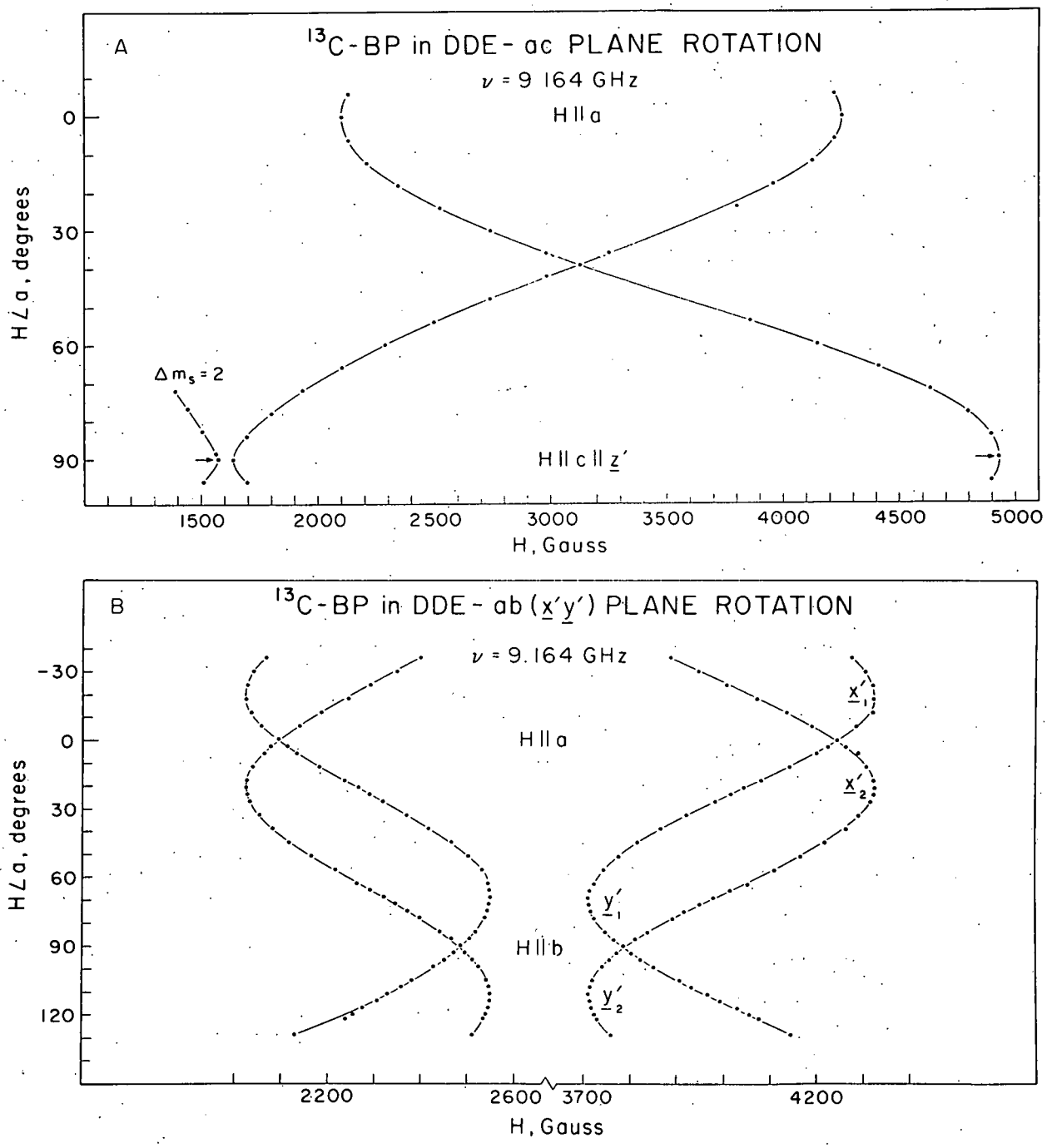
A
^{13}C-BP in DDE - ac PLANE ROTATION
ν = 9 164 GHz
H II a
H ∠ a, degrees
0
30
60
90
Δm$_s$ = 2
H II c II z′
1500
2000
2500
3000
3500
4000
4500
5000
H, Gauss
B
^{13}C-BP in DDE - ab (x′y′) PLANE ROTATION
ν = 9.164 GHz
H ∠ a, degrees
-30
0
30
60
90
120
H II a
H II b
x′$_1$
x′$_2$
y′$_1$
y′$_2$
2200
2600
3700
4200
H, Gauss

The field was also rotated in the bc crystallographic plane and similar results were obtained. Thus, only a single pair of "$\Delta m_S = \pm 1$" lines is observed with $\underline{H} || \underline{b}$, $\underline{c}$, but rotation of the magnet away from the orientation $\underline{H} || \underline{b}$ produces a splitting of the two transitions similar to that observed in the vicinity of $\underline{H} || \underline{a}$. From these experiments, it is obvious that there are two magnetically-inequivalent orientations of the fine structure tensor of triplet ^{13}C-BP in DDE, and that these two orientations are related by a rotation about the $\underline{c}$ ($\underline{z}'$) axis.

In order to determine the relationship between the two tensors, a third set of experiments was performed in which the field was rotated in the ab plane of the crystal. Fig. 6B shows the results obtained in this study. It is observed that the two triplet ^{13}C-BP molecules are magnetically-equivalent with $\underline{H} || \underline{a}, \underline{b}$, but that the $\underline{x}'$ and $\underline{y}'$ axes of their ZF tensors are rotated by $\pm 20° \pm 0.5°$ from the $\underline{a}$ and $\underline{b}$ axes, respectively. We denote these two sets of stationary orientations by $\underline{x}'_1$, $\underline{x}'_2$ and $\underline{y}'_1$, $\underline{y}'_2$, respectively, and list in Table IVA the values of the stationary fields in the three principal axis orientations of both molecules.

TABLE IV: Stationary fields and temperature dependence of the ODMR spectrum of ^{13}C-BP in DDE

A. Stationary Fields in Gauss

Orientation	"$\Delta m_S=2$"[a]	LF("$\Delta m_S=\pm 1$")[b]	HF("$\Delta m_S=\pm 1$")[b]	ν_o(GHz)[c]
$\underline{H} \parallel \underline{x}'$	1459	2026	4327	9.16470
$\underline{H} \parallel \underline{y}'$	1343	2549	3712	9.16328
$\underline{H} \parallel \underline{z}'$	1625	1576	4918	9.16230
$\underline{H} \parallel \underline{z}'$	1712	1780	5118	9.72310

[a] Field position of forbidden transition in Gauss.

[b] Field positions low field (LF) and high field (HF).

[c] Microwave frequency.

B. Ratio of intensity of the LF transition (I_L) to HF transition (I_H) at T = 1.6 °K and T > 4.2°K

Orientation	I_L/I_H (1.6 °K)	I_L/I_H (>4.2°K)
$\underline{H} \parallel \underline{x}'$	1.9	>3
$\underline{H} \parallel \underline{y}'$	2.5	>5
$\underline{H} \parallel \underline{z}'$	3.3	~12

The temperature dependence of the relative intensities of the two "$\Delta m_S = \pm 1$" transitions was also studied with $\underline{H} \| \underline{x}'$, $\underline{y}'$, and $\underline{z}'$. In all orientations, it was found that the intensity of the low-field line (I_L) increased relative to that of the high-field line (I_H) as the temperature increased from 1.6°K to 4.2°K and above. These results are summarized in Table IV B.

2. 4,4'-DCBP

The orientational dependence of the ODMR spectrum of 4,4'-DCBP in DDE was studied in three planes. MIP experiments showed that all signals detected corresponded to decreases in the intensity of all bands in the phosphorescence spectrum. An approximate $\underline{ac}$ plane study verified that the $\underline{z}'$ axis of the fine-structure tensor was in the $\underline{ac}$ plane parallel to the $\underline{c}$ axis. Subsequent to this experiment, two more-carefully oriented samples were studied in principal magnetic planes. Fig. 7A shows the results for the $\underline{x}'\underline{y}'$ fine-structure plane. A comparison of Fig. 7A with Fig. 6B shows that the angular dependence of the ODMR spectrum of 4,4'-DCBP is similar to that of ^{13}C-BP except that the angle of rotation of $\underline{x}'(\underline{y}')$ from $\underline{a}$ ($\underline{b}$) is slightly smaller in the former case ($\pm 18° \pm 0.5°$). Once this angle was determined, it was then possible to carry out a rotation about either $\underline{x}'$ or $\underline{y}'$ by suitable orientation

Figure 7. Observed angular dependence of the "$\Delta m_S = \pm 1$" transitions in the ODMR spectrum of 4,4'-DCBP in DDE at 1.6°K. (A) Rotation in the ab plane showing two (subscripts 1 and 2) identical but inequivalent sets of fine-structure axes. (B) Rotation in the x'z' fine-structure plane of one type of molecular orientation in the unit cell. The pattern indicated by * is due to the resonances from the other molecular orientation in the unit cell.

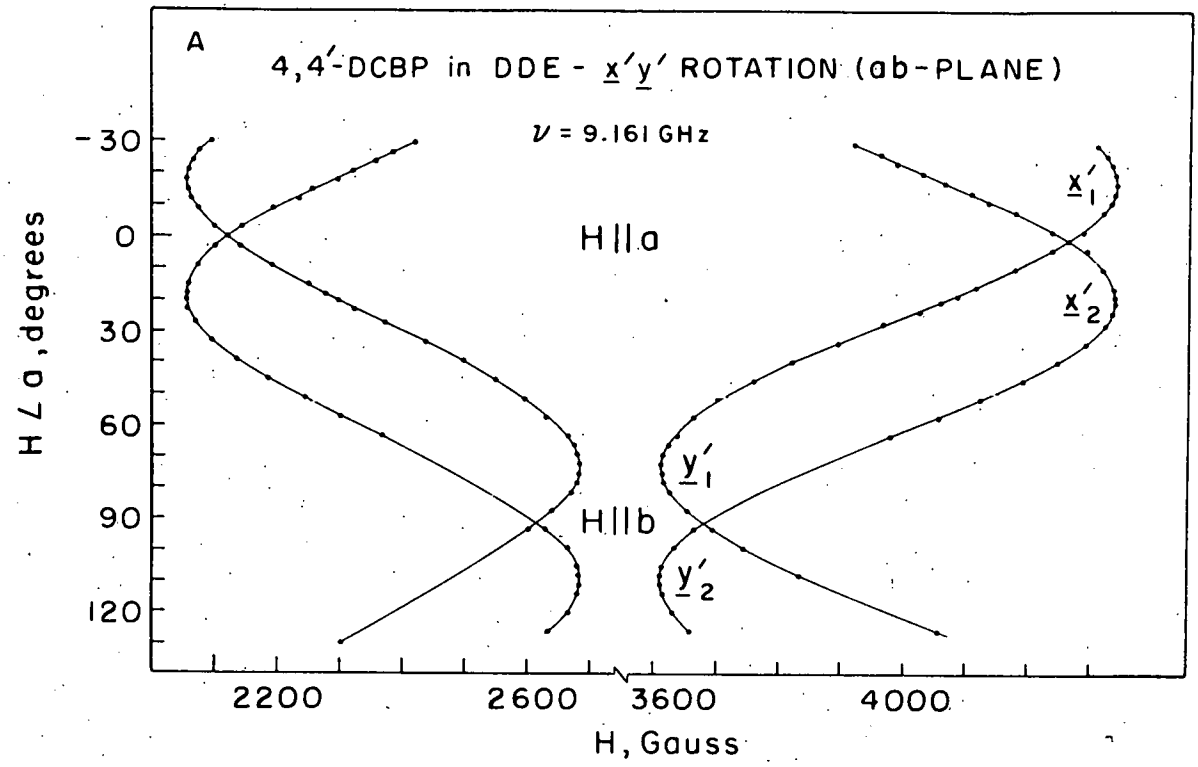
A
4,4′-DCBP in DDE - x′y′ ROTATION (ab-PLANE)
ν = 9.161 GHz
H∠a, degrees
-30
0
30
60
90
120
H||a
H||b
x′1
x′2
y′1
y′2
2200
2600
3600
4000
H, Gauss

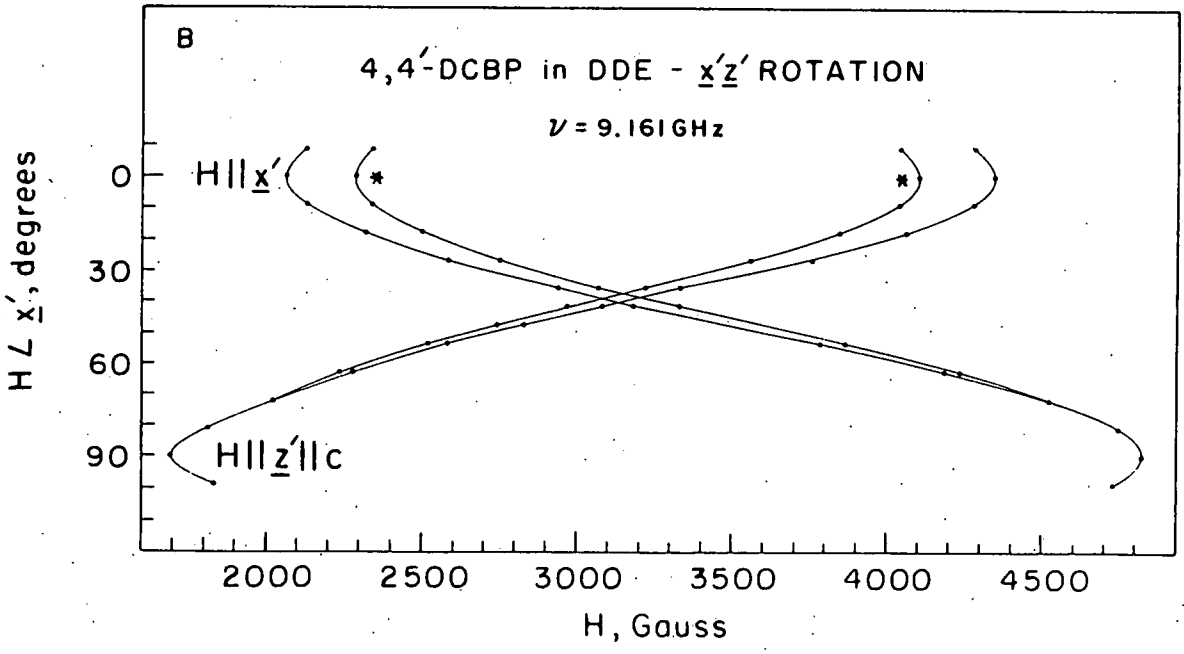
B
4,4′-DCBP in DDE - x′z′ ROTATION
ν = 9.161 GHz
H∠x′, degrees
0
30
60
90
H||x′
H||z′||c
2000
2500
3000
3500
4000
4500
H, Gauss

of the crystal. Fig. 7B shows the results of one study of this type. One set of curves illustrates the angular dependence in the $\underline{x}'\underline{z}'$ plane of one of the fine-structure pairs; the second set (marked by asterisks) shows the angular dependence of the second pair. It is observed that the two magnetically-inequivalent species become equivalent as the crystal is rotated to the $\underline{H} \| \underline{z}'$ ($\underline{c}$) orientation, as expected. The stationary fields observed in these experiments are listed in Table V A.

The relative intensities of the high-field and low-field "$\Delta m_S = \pm 1$" transitions of 4,4'-DCBP were also studied as a function of temperature. The results obtained for each canonical orientation are shown in Fig. 8. At 1.6°K, the low-field transition is observed to be the most intense line in each of the three orientations; however, an increase in temperature produces a dramatic decrease in the relative intensity of this transition in each case. The values of (I_L/I_H) are listed in Table V B.

3. ^{12}C-BP, 4,4'-DFBP, and 4,4'-DBBP

The orientational dependences of the ODMR spectra of several other benzophenones in the DDE host were studied using crystals mounted for $\underline{ac}$ and $\underline{ab}$ plane rotations. All showed the same basic behavior during rotation as that illustrated

TABLE V: Stationary fields and temperature dependence of the ODMR spectrum of 4,4'-DCBP in DDE

A. Stationary Fields in Gauss

Orientation	"$\Delta m_S=2$"	LF("$\Delta m_S=\pm 1$")	HF("$\Delta m_S=\pm 1$")	ν_o(GHz)
$\underline{H} \| \underline{x}'$	1494	2057	4335	9.16170
$\underline{H} \| \underline{y}'$	1375	2682	3612	9.16174
$\underline{H} \| \underline{z}'$	1612	1690	4804	9.16122

B. Ratio of intensity of the LF transition to HF transition at T = 1.6 °K and T > 4.2 °K

Orientation	I_L/I_H (1.6°K)	I_L/I_H(>4.2°K)
$\underline{H} \| \underline{x}'$	1.5	<0.2
$\underline{H} \| \underline{y}'$	1.5	$\ll$0.1
$\underline{H} \| \underline{z}'$	1.7	1.0

Figure 8. Observed temperature dependence of the "$\Delta m_s = \pm 1$" ODMR transitions for each principal axis orientation of 4,4'-DCBP in DDE. All transitions correspond to decreases in phosphorescence intensit

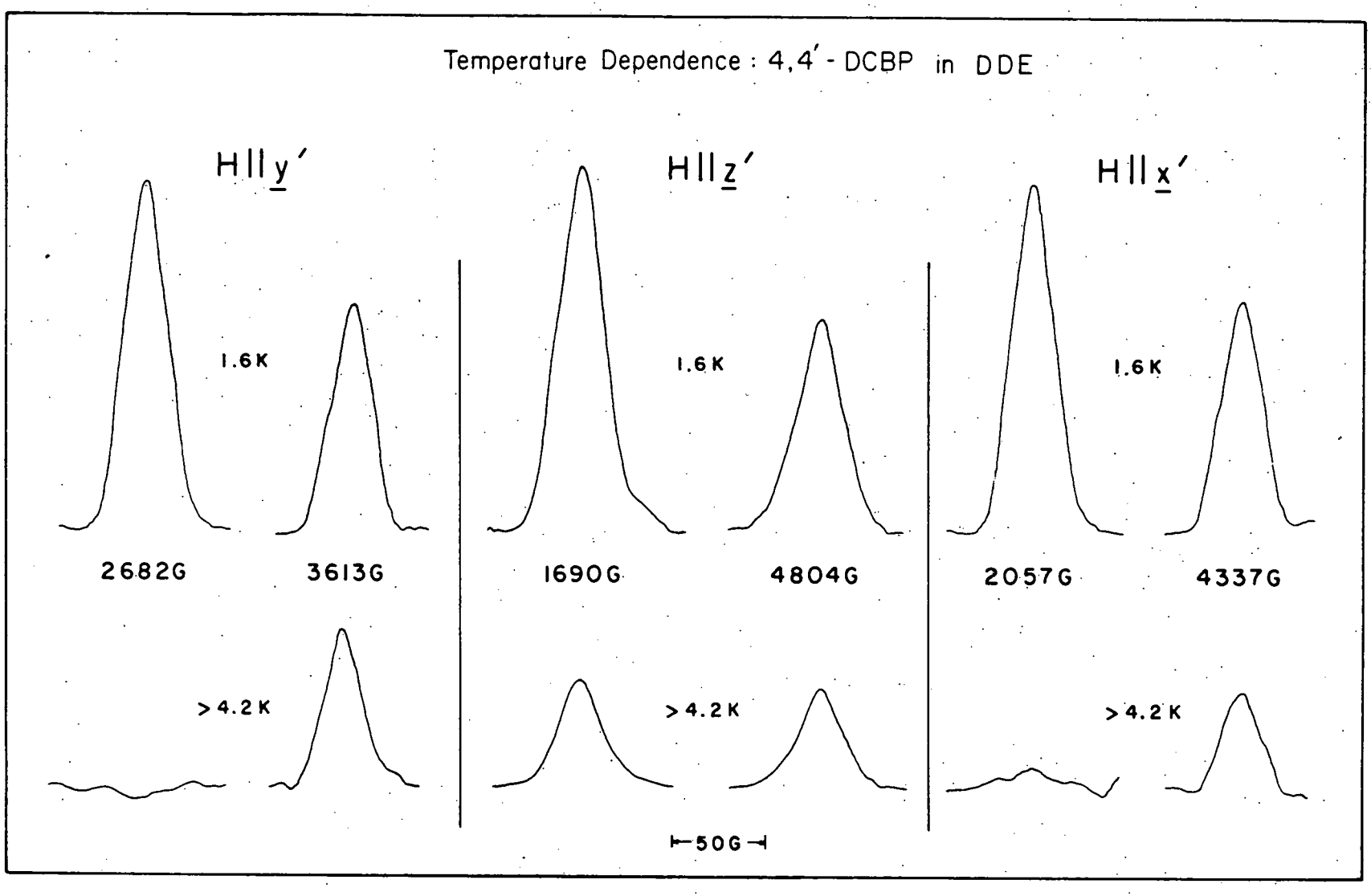
Temperature Dependence : 4,4′ - DCBP in DDE
H||y′
H||z′
H||x′
1.6K
1.6K
1.6K
2682G
3613G
1690G
4804G
2057G
4337G
>4.2K
>4.2K
>4.2K
50G

in Fig. 6; however, the relative orientations of the two sets of fine-structure axes that are observed in the ab plane are different for different molecules. The x'(y') fine-structure axes of ^{12}C-BP, 4,4'-DFBP, and 4,4'-DBBP were found at angles of 20° ± 0.5°, 19° ± 0.5°, and 9° ± 0.5° from the a(b) crystal axis, respectively. The field positions of the ODMR signals observed in the canonical orientations for each of these systems are listed in Table VI. All transitions in 4,4'-DFBP and ^{12}C-BP corresponded to increases in phosphorescence intensity, and no differences were observed in the relative intensities of the low-field and high-field "$\Delta m_S = \pm 1$" transitions at the two temperatures studied (1.6°K and 4.2°K) in either case. At 4.2°K, the ODMR transitions of 4,4'-DBBP in the canonical orientations were detected as decreases in phosphorescence intensity. Cooling the sample to 1.6°K produces no change in the relative intensities of the two "$\Delta m_S = \pm 1$" transitions in the $H \| z'$ and $H \| y'$ orientations. However, in the $H \| x'$ orientation of 4,4'-DBBP, cooling led to a complete reversal in phase of the high-field "$\Delta m_S = \pm 1$" transition so that at 1.6°K an increase in phosphorescence intensity was observed on microwave saturation.

TABLE VI: Stationary fields (in Gauss) in the ODMR Spectra of 4,4'-DFBP, BP, and 4,4'-DBBP in DDE

Guest	Orientation	"$\Delta m_S=2$"	LF("$\Delta m_S=\pm1$")	HF("$\Delta m_S=\pm1$")	ν_o(GHz)
4,4'-DFBP	$\underline{H}\|\|\underline{x}'$	1429	1929	4382	9.16166
	$\underline{H}\|\|\underline{y}'$	1303	2483	3744	9.16127
	$\underline{H}\|\|\underline{z}'$	1627	1466	5024	9.16851
BP	$\underline{H}\|\|\underline{x}'$	1456	2022	4327	9.16557
	$\underline{H}\|\|\underline{y}'$	1341	2547	3715	9.16538
	$\underline{H}\|\|\underline{z}'$	1709	1776	5121	9.72255
4,4'-DBBP	$\underline{H}\|\|\underline{x}'$	1535	2146	4287	9.16803
	$\underline{H}\|\|\underline{y}'$	1423	2810	3509	9.16713
	$\underline{H}\|\|\underline{z}'$		2073	4836	9.7648

B. ODMR Spectra in Neat 4,4'-DCBP

ODMR spectra of neat 4,4'-DCBP were obtained by monitoring the (0,0) band of the phosphorescence emission, and the study of the orientational dependence in two crystallographic planes was sufficient to assign the orientation of each of the three principal axes of the fine-structure tensor to specific axes of the 4,4'-DCBP crystal. In one set of experiments, the crystal was mounted for rotation in the cleavage (ab) plane and oriented in the cavity so that the b axis was parallel to the magnetic field. The ODMR spectrum obtained in this orientation at 1.6°K is shown in Fig. 9. Slight adjustments of the orientation of the field relative to the crystal verified this to be a canonical orientation corresponding to an alignment of the field along the C=O bond (z'). Closer inspection of Fig. 9 shows there are, in fact, two pairs of transitions which exhibit slightly different ZF splittings. The more intense features in this orientation are excitonic in origin whereas the weaker transitions, which are just resolved in the low-field resonance and produce an asymmetry in the high-field resonance, are assigned as traps in the neat 4,4'-DCBP cyrstal (vide infra.).

Figure 10 A illustrates the orientational dependence of the exciton and trap transitions in the ab plane of 4,4'-DCBP.

Figure 9. Observed "$\Delta m_S = \pm 1$" transitions in the ODMR spectrum of neat 4,4'-DCBP at 1.6°K in the orientation $\underline{H} \| \underline{b} \| \underline{z}'$. All transitions correspond to decreases in phosphorescence intensity. The most prominent signals are excitonic in origin, while X-trap resonances are just resolved in the low-field region and produce a slight asymmetry in the high-field region.

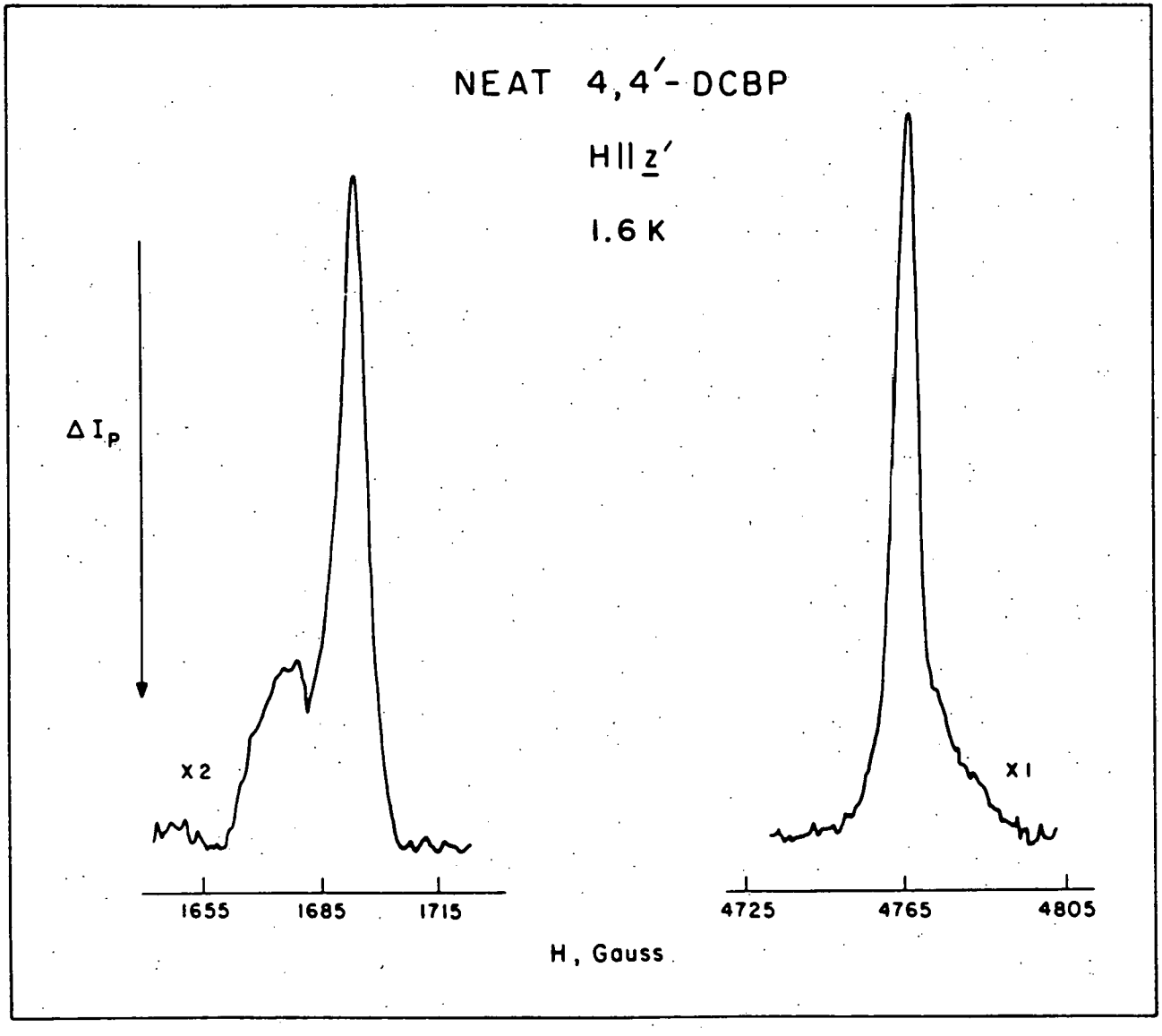
NEAT 4,4′-DCBP
H ∥ z′
1.6 K
ΔI_P
X2
X1
1655
1685
1715
4725
4765
4805
H, Gauss

Figure 10. Observed angular dependence of the "$\Delta m_s = \pm 1$" transitions in the ODMR spectrum of neat 4,4'-DCBP at 1.6°K. (A) Rotation in the ab crystallographic plane; x(·) indicates resonances due to excitons (X-traps). (B) Rotation in the x'y' fine-structure plane of X-traps in neat 4,4'-DCBP. Arrows locate the angular positions of the a and c' crystallographic axes. No exciton resonances were observed in this plane.

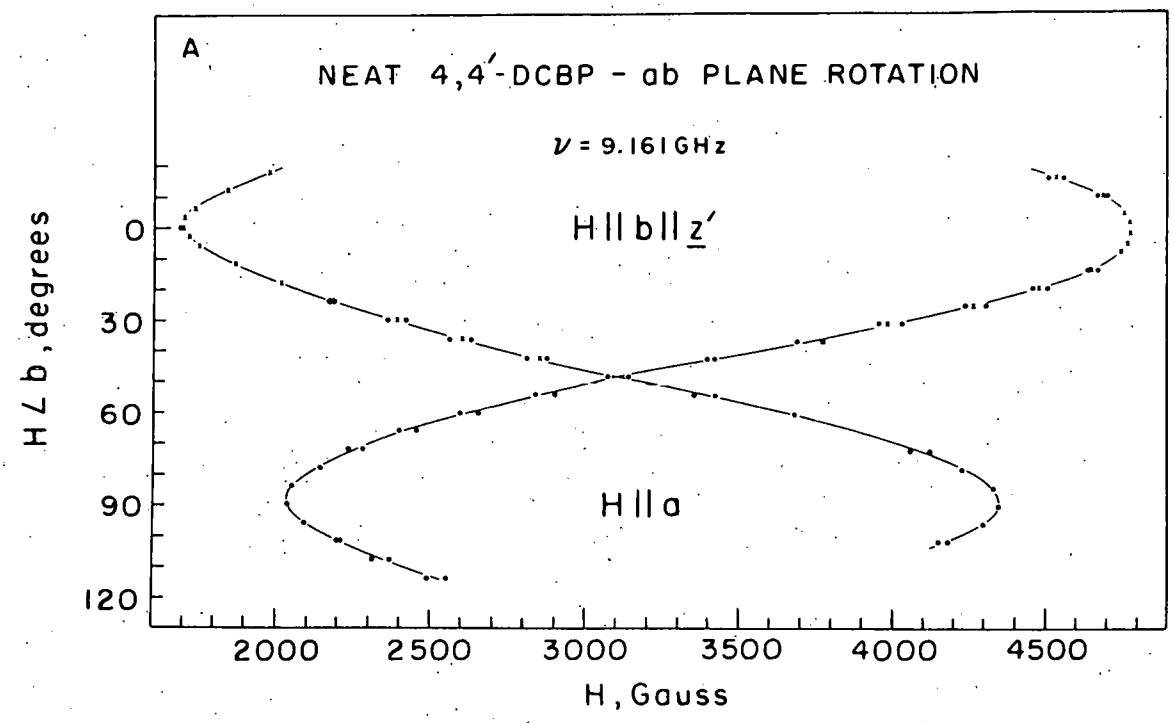
A
NEAT 4,4′-DCBP - ab PLANE ROTATION
ν = 9.161 GHz
H∥b∥z′
H∥a
H ∠ b, degrees
0
30
60
90
120
2000
2500
3000
3500
4000
4500
H, Gauss

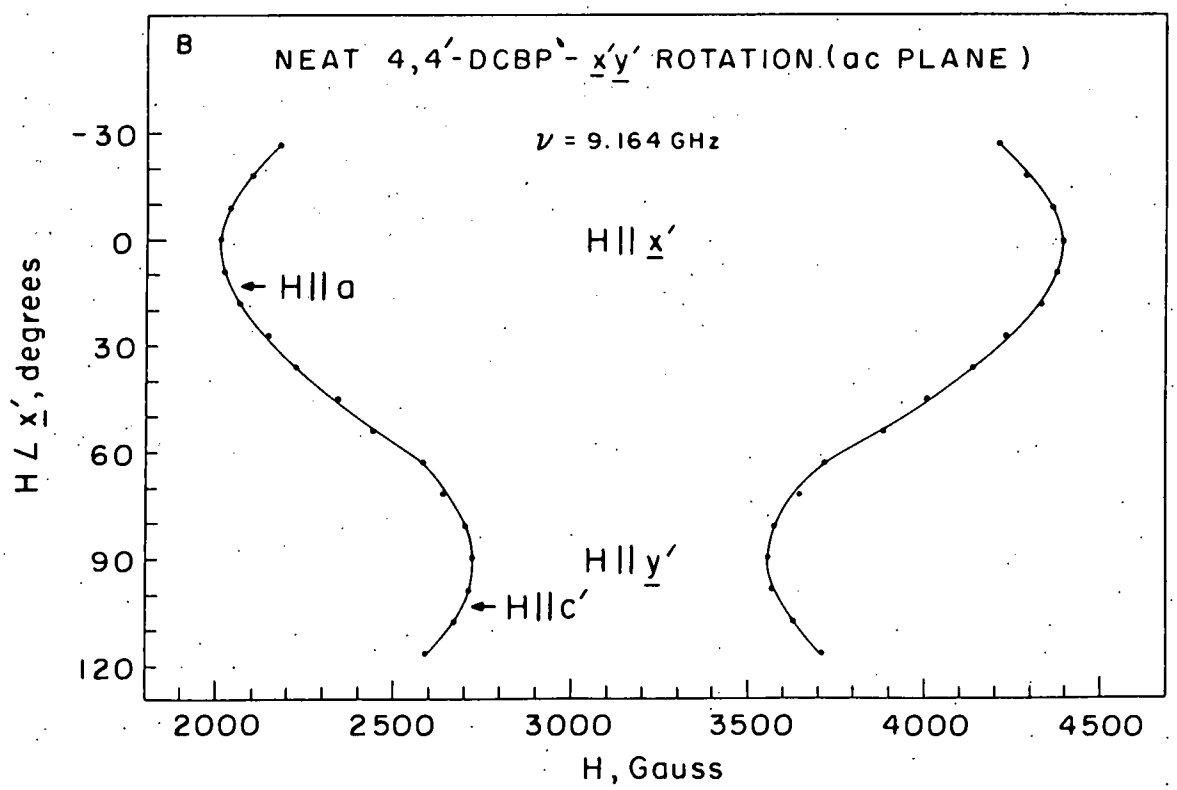
B
NEAT 4,4′-DCBP - x′y′ ROTATION (ac PLANE)
ν = 9.164 GHz
H∥x′
H∥a
H∥y′
H∥c′
H ∠ x′, degrees
-30
0
30
60
90
120
2000
2500
3000
3500
4000
4500
H, Gauss

Rotation of the crystal away from the b axis ($\underline{H} \| \underline{z}'$) causes a continuous decrease in the intensity of exciton signals (x in Fig. 10A), and they are unobservable after 40° of rotation. Both the low-field and high-field trap transitions (• in Fig. 10 A) are observed to invert and split into two pairs of lines as the crystal is rotated away from $\underline{H} \| \underline{b}$. The four "$\Delta m_S = \pm 1$" transitions, which now correspond to increases in the phosphorescence intensity, again converge into a single pair of lines as H approaches the a axis. This behavior suggests that, as in the case of the DDE crystal, there are two magnetically-inequivalent orientations of the fine-structure tensor of the triplet traps in the ab plane of neat 4,4'-DCBP. However, since the maximum splitting of each of the "$\Delta m_S = \pm 1$" lines in only 86 G, the relative orientation of the two sites cannot differ by more than 1°. Thus, at positions where stationary behavior was observed, the two sets of axes appear to be equivalent within the resolution of our experiments.

This interpretation was confirmed by a second set of experiments which were carried out in order to determine the orientation of the two remaining fine-structure axes (x', y') of the trap triplet state in the ac' plane. The results of this study are shown in Fig. 10 B. Stationary behavior of the angular dependence is observed at angles of 15°± 1° from the a and c' axes, and these orientations are assigned as

$\underline{H} \parallel \underline{x}'$ and $\underline{y}'$, respectively, by examination of the 4,4'-DCBP crystal structure data. Although no splitting of the ODMR signals was observed in the $\underline{ac}'$ plane, considerable line broadening was evident at orientations intermediate to the $\underline{x}'$ and $\underline{y}'$ stationary field positions, and is most likely due to the second set of fine-structure axes. The stationary field positions observed for the $\underline{x}'$, $\underline{y}'$, and $\underline{z}'$ principal orientations of the trap triplet state are listed in Table VII. No exciton transitions were observed in the $\underline{ac}'$ plane.

The temperature dependence of the ODMR signals in principal axis orientations was studied as described previously and the results are summarized in Fig. 11. In both the $\underline{H} \parallel \underline{x}'$ and $\underline{H} \parallel \underline{y}'$ orientations, the low-field and high-field transitions were observed as increases in phosphorescence intensity at 1.6°K. As the crystal was allowed to warm up, the high-field transition decreases in intensity and was observed to invert at the highest temperature studied in each case. In the $\underline{H} \parallel \underline{z}'$ orientation the asymmetry observed in the exciton transitions at 1.6°K caused by the overlapping trap transitions was observed to disappear at temperatures greater than 4.2°K. The exciton transitions were still observed as decreases in phosphorescence intensity and maintain a 2:1 relative intensity ratio throughout the warmup experiment.

TABLE VII: Stationary fields (in Gauss) in the ODMR spectrum of X-traps in neat 4,4'-DCBP

Orientation	"$\Delta m_S=2$"	LF("$\Delta m_S=\pm 1$")	HF("$\Delta m_S=\pm 1$")	ν_o(GHz)
$\underline{H} \| \underline{x}'$	1493	2004	4368	9.164097
$\underline{H} \| \underline{y}'$	1355	2714	3544	9.16375
$\underline{H} \| \underline{z}'$	1596	1676(1695)	4771(4766)	9.15354

Field positions in parentheses are those observed for excitons.

Figure 11. Observed temperature dependence of the "$\Delta m_S = \pm 1$" ODMR transitions for each principal axis orientation of X-traps and excitons in neat 4,4'-DCBP. The $\underline{H} \| \underline{x}'$ and $\underline{y}'$ spectra are X-trap resonances. The $\underline{H} \| \underline{z}'$ spectrum is predominantly excitonic in origin with the X-trap resonances producing an asymmetry in the line shape at 1.6°K. Signals deflecting towards the bottom of the figure correspond to increases in phosphorescence intensity.

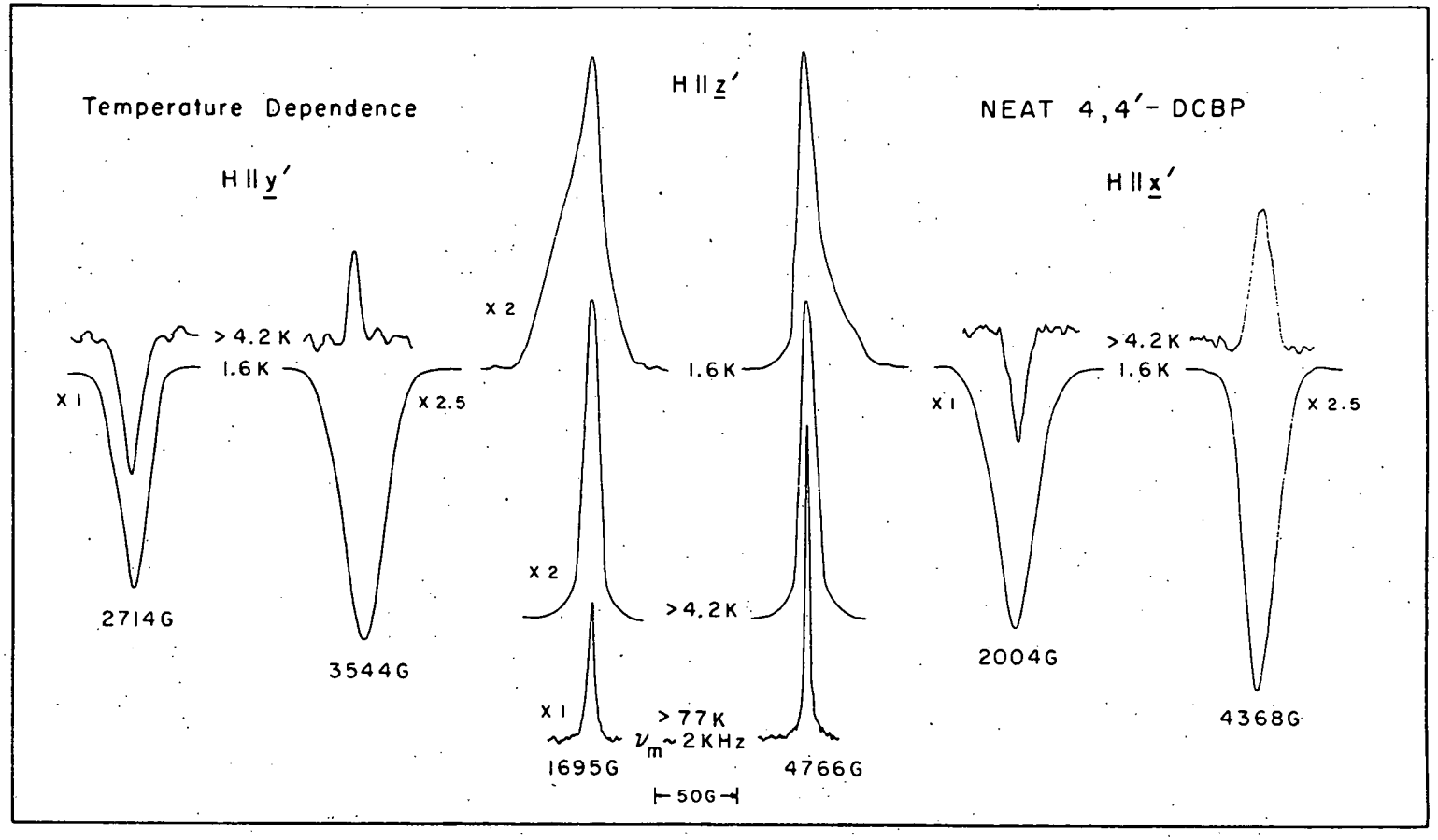
Temperature Dependence
H ∥ y′
H ∥ z′
NEAT 4,4′- DCBP
H ∥ x′
> 4.2 K
1.6 K
X 1
X 2.5
2714G
3544G
X 2
1.6K
X 2
> 4.2K
X 1
> 77K
ν_m ~ 2KHz
1695G
4766G
50G
> 4.2K
1.6K
X 1
X 2.5
2004G
4368G

Subsequently, the experiment was continued at a temperature near 77°K by putting liquid nitrogen into the cryostat. As can be seen, the phasing and relative intensities of the two exciton transitions remained the same as those observed at much lower temperatures. However, the linewidth (full width at half maximum) of the exciton transitions was observed to decrease from 9 G at 1.6°K to 4 G at 77°K.

C. Interpretation

1. The $\underset{\sim}{g}$ and $\underset{\sim}{D}$ Tensors

The total spin Hamiltonian which describes the relative energies of the electron and nuclear spin levels of the lowest triplet state of a molecule is given by[16]

$$\mathcal{H}_S = \mathcal{H}_{ZF} + \mathcal{H}_Z + \mathcal{H}_Q + \mathcal{H}_{HF} + \mathcal{H}'_Z \qquad (14)$$

where $\mathcal{H}_{ZF}$ represents the ZF splitting of the electron spin sublevels due to magnetic dipole-dipole and spin-orbit interactions between the two unpaired electrons [cf., Eq. (7)], $\mathcal{H}_Z$ the electron Zeeman interaction [cf., Eq. (3)], $\mathcal{H}_Q$ the nuclear quadrupole interaction (for $I \geq 1$), $\mathcal{H}_{HF}$ the electron-nuclear hyperfine interaction, and $\mathcal{H}'_Z$ the nuclear Zeeman interaction. The ODMR results presented thus far can be analyzed almost entirely by considering only the first two

terms of (14), thus we take

$$\mathcal{H}_S^o = \mathcal{H}_{ZF} + \mathcal{H}_Z \tag{15}$$

where $\mathcal{H}_{ZF}$ is given by Eq. (7) and

$$\mathcal{H}_Z = \beta \underline{H} \cdot \underset{\sim}{g} \cdot \underline{S} \tag{16}$$

for the general case (*i.e.*, anisotropic $\underset{\sim}{g}$ tensor), where $\underline{S}$ is the resultant electron spin of the triplet state (*i.e.*, $\underline{S} = \underline{s}_1 + \underline{s}_2$).

The choice of a basis set for the spin wavefunctions is somewhat arbitrary. The $|+1\rangle$, $|0\rangle$, and $|-1\rangle$ basis set [*cf.*, Eqs. (1)] diagonalizes $\mathcal{H}_Z$ in the limit of infinite magnetic field, while the basis set

$$|\tau_x\rangle = \frac{1}{\sqrt{2}} |\beta_1\beta_2 - \alpha_1\alpha_2\rangle = \frac{1}{\sqrt{2}} \left(|-1\rangle - |+1\rangle\right) \tag{17a}$$

$$|\tau_y\rangle = \frac{i}{\sqrt{2}} |\beta_1\beta_2 + \alpha_1\alpha_2\rangle = \frac{i}{\sqrt{2}} \left(|-1\rangle + |+1\rangle\right) \tag{17b}$$

$$|\tau_z\rangle = \frac{1}{\sqrt{2}} |\alpha_1\beta_2 + \beta_1\alpha_2\rangle = |0\rangle \tag{17c}$$

diagonalizes $\mathcal{H}_{ZF}$ and can be written as linear combinations of the "high-field" spin wavefunctions. For an ODMR experiment in high field, neither basis set diagonalizes $\mathcal{H}_S^o$, but both are equally sufficient for describing the experimental results.

Choosing the basis set $|\tau_x\rangle$, $|\tau_y\rangle$, and $|\tau_z\rangle$, the resulting Hamiltonian matrix of $\mathcal{H}_S^\circ$ becomes

$$\mathcal{H}_S^\circ = \begin{array}{c} \begin{matrix} |\tau_x\rangle & |\tau_y\rangle & |\tau_z\rangle \end{matrix} \\ \begin{bmatrix} X & -ig_{zz}\beta Hn & ig_{yy}\beta Hm \\ ig_{zz}\beta Hn & Y & -ig_{xx}\beta H\ell \\ -ig_{yy}\beta Hm & ig_{xx}\beta H\ell & Z \end{bmatrix} \end{array} \qquad (18)$$

where X, Y, Z and g_{xx}, g_{yy}, g_{zz} are the principal values of the fine-structure tensor ($\underset{\sim}{D}$) and the $\underset{\sim}{g}$ tensor; ℓ, m, and n are the direction cosines of the magnetic field axis with respect to the $\underline{x}'$, $\underline{y}'$, and $\underline{z}'$ axes, respectively. In this form, the assumption is made that the principal axes of $\underset{\sim}{D}$ and $\underset{\sim}{g}$ are coincident. Since $\mathcal{H}_S^\circ$ is not diagonal and both the diagonal and off-diagonal terms are the same order of magnitude, perturbation theory cannot be applied and the Hamiltonian must be diagonalized for each orientation of the external field. This calculation is simplified considerably in any one of the three principal axis orientations. For example, with $\underline{H} \,||\, \underline{z}'$ ($\ell = m = 0$), the Hamiltonian becomes

$$\mathcal{H}_S^o = \begin{bmatrix} X & -ig_{zz}\beta H & 0 \\ ig_{zz}\beta H & Y & 0 \\ 0 & 0 & Z \end{bmatrix} \tag{19}$$

Thus, $|\tau_z\rangle$ is an eigenfunction of $\mathcal{H}_S^o$ with eigenvalue $W_o = Z$ but $|\tau_x\rangle$ and $|\tau_y\rangle$ are mixed by the off-diagonal element $\pm ig_{zz}\beta H$. The remaining eigenvalues and eigenfunctions can then be obtained by solving the 2 x 2 secular determinant

$$\begin{vmatrix} X-W & -ig_{zz}\beta H \\ ig_{zz}\beta H & Y-W \end{vmatrix} = 0 \tag{20}$$

which yields

$$W_{\pm} = 1/2(X+Y) \pm \alpha_z/2 \tag{21a}$$

where

$$\alpha_z = 2\left[\tfrac{1}{4}(Y-X)^2 + (g_{zz}\beta H)^2\right]^{\frac{1}{2}} \tag{21b}$$

Since $\underset{\sim}{D}$ is a traceless tensor, X + Y + Z = 0, and the energy levels and wavefunctions of the triplet electron spin states with $\underline{H} \| \underline{z}'$ may be written as

$$W_+ = -Z/2 + \alpha_z/2 \tag{22a}$$

$$W_o = Z \tag{22b}$$

$$W_{-} = -Z/2 - \alpha_z/2 \tag{22c}$$

$$|+\rangle = \left|i\, c_1 |\tau_x\rangle + c_2 |\tau_y\rangle\right\rangle \tag{23a}$$

$$|0\rangle = |\tau_z\rangle \tag{23b}$$

$$|-\rangle = \left|c_2 |\tau_x\rangle - i\, c_1 |\tau_y\rangle\right\rangle \tag{23c}$$

where

$$c_1 = 1/\sqrt{2}\left[1 - \frac{(Y-X)}{\alpha_z}\right]^{\frac{1}{2}} \tag{24a}$$

$$c_2 = 1/\sqrt{2}\left[1 + \frac{(Y-X)}{\alpha_z}\right]^{\frac{1}{2}} \tag{24b}$$

In the absence of a magnetic field, $c_1 = 0$ and $c_2 = 1$, so that the states $|+\rangle$, $|0\rangle$, and $|-\rangle$ go smoothly into τ_x, τ_z, and τ_y, respectively. On the other hand, in the "high-field" limit, $|+\rangle$ and $|-\rangle$ approach $|\alpha_1\alpha_2\rangle$ and $|\beta_1\beta_2\rangle$, respectively; i.e., the field decouples the electron spins completely from the molecular framework. Similar calculations with $\underline{H} \| \underline{x}'$ and $\underline{y}'$ lead to expressions analogous to (22) and (23) and are summarized in Table VIII. Note that these expressions can be obtained by simply permuting X, Y, and Z.

The energy of the three spin sublevels can be plotted as a function of the magnetic field for each of the three principal axis orientations using the energy expressions in

TABLE VIII: Energies, wavefunctions, and resonance fields for a lowest triplet state with $Z > 0 > Y > X$

Orientation	Energy	$\|\tau_x\rangle$	$\|\tau_y\rangle$	$\|\tau_z\rangle$	"$\Delta m_S = \pm 1$"	"$\Delta m_S = 2$"
$\underline{H}\|\|\underline{x}'$	$W_+ = -\frac{X}{2} + \frac{a_x}{2}$	0	$\frac{i}{\sqrt{2}}[1-(Z-Y)/a_x]^{\frac{1}{2}}$	$\frac{1}{\sqrt{2}}[1+(Z-Y)/a_x]^{\frac{1}{2}}$	$(1/g_{xx}\beta)\{(h\nu \pm 3X/2)^2 - [(Z-Y)/2]^2\}^{\frac{1}{2}}$	$(1/2g_{xx}\beta)\{(h\nu)^2 - (Z-Y)^2\}^{\frac{1}{2}}$
	$W_o = X$	1	0	0		
	$W_- = -\frac{X}{2} - \frac{a_x}{2}$	0	$\frac{1}{\sqrt{2}}[1+(Z-Y)/a_x]^{\frac{1}{2}}$	$\frac{-i}{\sqrt{2}}[1-(Z-Y)/a_x]^{\frac{1}{2}}$		
			$a_x = 2[\frac{1}{4}(Z-Y)^2 + (g_{xx}\beta H)^2]^{\frac{1}{2}}$			
$\underline{H}\|\|\underline{y}'$	$W_+ = -\frac{Y}{2} + \frac{a_y}{2}$	$\frac{i}{\sqrt{2}}[1-(Z-X)/a_y]^{\frac{1}{2}}$	0	$\frac{1}{\sqrt{2}}[1+(Z-X)/a_y]^{\frac{1}{2}}$	$(1/g_{yy}\beta)\{(h\nu \pm 3Y/2) - [(Z-X)/2]^2\}^{\frac{1}{2}}$	$(1/2g_{yy}\beta)\{(h\nu)^2 - (Z-X)^2\}^{\frac{1}{2}}$
	$W_o = Y$	0	1	0		
	$W_- = -\frac{Y}{2} - \frac{a_y}{2}$	$\frac{1}{\sqrt{2}}[1+(Z-X)/a_y]^{\frac{1}{2}}$	0	$\frac{i}{\sqrt{2}}[1-(Z-X)/a_y]^{\frac{1}{2}}$		
			$a_y = 2[\frac{1}{4}(Z-X)^2 + (g_{yy}\beta H)^2]^{\frac{1}{2}}$			
$\underline{H}\|\|\underline{z}'$	$W_+ = -\frac{Z}{2} + \frac{a_z}{2}$	$\frac{i}{\sqrt{2}}[1-(Y-X)/a_z]^{\frac{1}{2}}$	$\frac{1}{\sqrt{2}}[1+(Y-X)/a_z]^{\frac{1}{2}}$	0	$(1/g_{zz}\beta)\{(h\nu \pm 3Z/2) - [(Y-X)/Z]^2\}^{\frac{1}{2}}$	$(1/2g_{zz}\beta)\{(h\nu)^2 - (Y-X)^2\}^{\frac{1}{2}}$
	$W_o = Z$	0	0	1		
	$W_- = -\frac{Z}{2} - \frac{a_z}{2}$	$\frac{1}{\sqrt{2}}[1+(Y-X)/a_z]^{\frac{1}{2}}$	$\frac{-i}{\sqrt{2}}[1-(Y-X)/a_z]^{\frac{1}{2}}$	0		
			$a_z = 2[\frac{1}{4}(Y-X)^2 + (g_{zz}\beta H)^2]^{\frac{1}{2}}$			

Table VIII, and a schematic representation is shown in Fig. 12 together with the possible microwave transitions. Labeling the states by their "high-field" functions $|+1\rangle$, $|0\rangle$, and $|-1\rangle$, the transitions A and B are classified as "$\Delta m_S = \pm 1$" transitions and C as a "$\Delta m_S = 2$" transition. The former are allowed in both ZF and high field, whereas the latter is allowed in ZF but forbidden in the "high-field" limit ($H \to \infty$). Since the ODMR experiments are carried out in a magnetic field intermediate to the two extremes, the "$\Delta m_S = 2$" transition is not rigorously forbidden and can frequently be detected.

Referring to Fig. 12 and Eqs.(21) and (22) for the $\underline{H} \| \underline{z}'$ case, the following are the resonance expressions for the transitions A, B and C at constant microwave frequency (ν):

$$h\nu = W_o - W_- = 3Z/2 + [\tfrac{1}{4}(Y-X)^2 + (g_{zz}\beta H_A)^2]^{\frac{1}{2}} \qquad (25a)$$

$$h\nu = W_+ - W_o = -3Z/2 + [\tfrac{1}{4}(Y-X)^2 + (g_{zz}\beta H_B)^2]^{\frac{1}{2}} \qquad (25b)$$

$$h\nu = W_+ - W_- = 2[\tfrac{1}{4}(Y-X)^2 + (g_{zz}\beta H_C)^2]^{\frac{1}{2}} \qquad (25c)$$

where $h\nu$ is the microwave energy and the ZF ordering scheme $Z > O > Y > X$ is assumed. The magnetic fields at which resonances are observed are easily found to be

Figure 12. Triplet energy levels of benzophenones. Transitions are shown for a frequency of 9.6 GHz when the magnetic field is in the x', y', and z' directions, respectively. The ZF ordering scheme Z > O > Y > X is assumed.

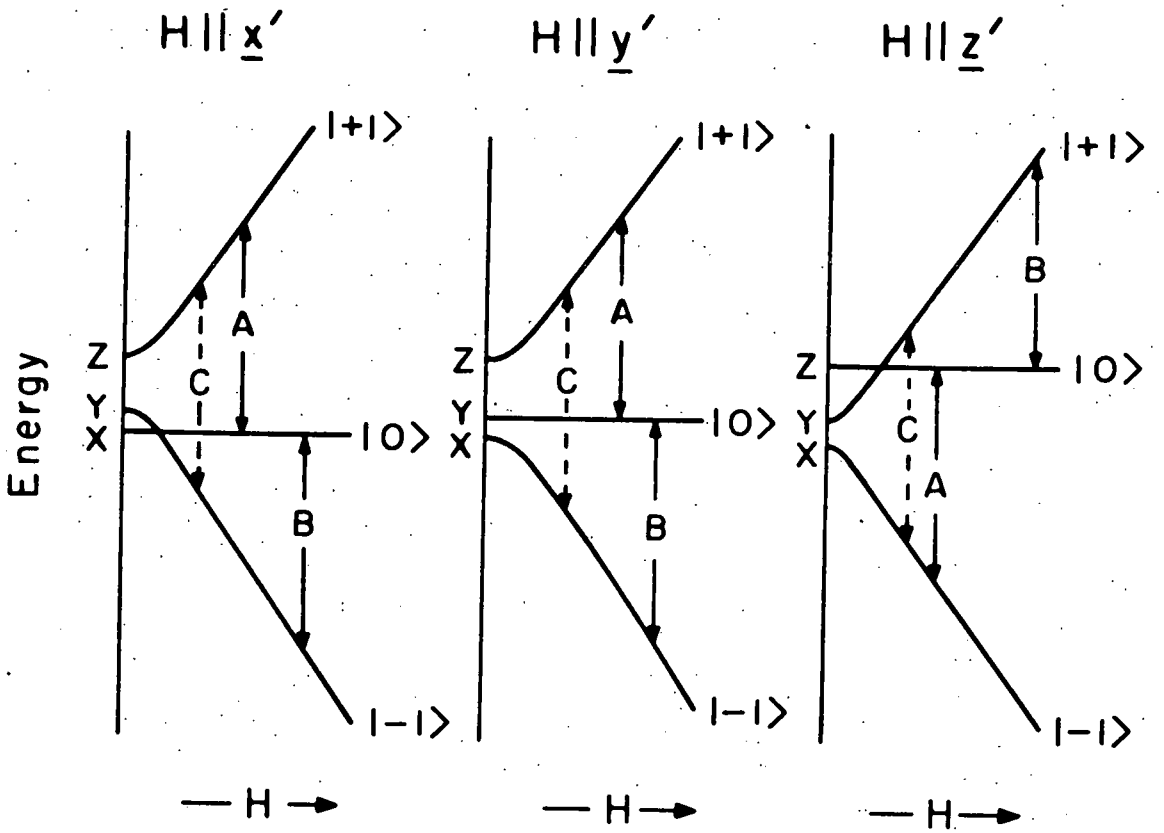
H || x′
H || y′
H || z′
Energy
|+1>
|0>
|−1>
A
B
C
Z
Y
X
— H →

$$H_A = (1/g_{zz}\beta)\ \{(h\nu-3Z/2)^2-[(Y-X)/2]^2\}^{\frac{1}{2}} \qquad (26a)$$

$$H_B = (1/g_{zz}\beta)\ \{(h\nu+3Z/2)^2-[(Y-X)/2]^2\}^{\frac{1}{2}} \qquad (26b)$$

$$H_C = (1/2g_{zz}\beta)\ \{(h\nu)^2-(Y-X)^2\}^{\frac{1}{2}} \qquad (26c)$$

The resonance field positions for the other principal axis orientations are listed in Table VIII. Note that if the level ordering X > Y > O > Z had been assumed, analogous, but slightly different, expressions for the eigenvalues would be obtained. However, by examining the expressions for the resonance fields (the experimental observables), one sees that the transitions would be observed at the same field positions in both ordering schemes. Thus, a given set of experimental field positions can only give the magnitude and relative signs of the ZF parameters.

By combining the expressions for the "$\Delta m_S = \pm 1$" transitions [cf., Eqs. (26a,b)] in each of the principal axis orientations, expressions for each of the six magnetic parameters (X, Y, Z and g_{xx}, g_{yy}, g_{zz}) can be derived. For example, in the $\underline{H}||\underline{z}'$ orientation, one finds

$$g_{zz} = \left[\frac{(h\nu+3Z/2)^2+(h\nu-3Z/2)^2-\frac{1}{2}(Y-X)^2}{\beta^2(H_A^2 + H_B^2)}\right]^{\frac{1}{2}} \qquad (27a)$$

$$Z = 1/3\left[\left\{\tfrac{1}{4}(Y-X)^2+(g_{zz}\beta H_B)^2\right\}^{\frac{1}{2}} - \left\{\tfrac{1}{4}(Y-X)^2+(g_{zz}\beta H_A)^2\right\}^{\frac{1}{2}}\right] \quad (27b)$$

Similar expressions can be derived from the two remaining principal axis orientations; hence, there are a total of six equations and six unknowns. Self-consistent values for the principal elements of $\underset{\sim}{D}$ and $\underset{\sim}{g}$ can be determined by initially estimating the values of the magnetic parameters and iterating the six equations until convergence is achieved (see Appendix I). This method is exactly analogous to that described by Hutchison and Mangum[7] except that the quadratic terms are included explicitly and not expanded in terms of a power series. For the systems studied in this laboratory, there has been no difficulty in achieving convergence, and usually no more than ten iterations were required to reach a convergence tolerance of 10^{-6}. As a check for a false convergence limit, the self-consistent magnetic parameters were used to calculate the resonance fields of the "$\Delta m_S = \pm 1$" and "$\Delta m_S = 2$" transitions in the principal axis orientations as well as the positions of level anticrossing signals (Chapter V). The calculated field positions were found to be in excellent agreement with those observed experimentally in all systems studied. In cases where the resonance field positions along one principal axis are in doubt (e.g., the X-trap high-field

transition in the $\underline{H} \| \underline{z}'$ orientation of neat 4,4'-DCBP), one can use the condition

$$X + Y + Z = 0 \qquad (28)$$

in the iterative process to obtain the energy and g-value for that principal axis.

The principal values of $\underset{\sim}{D}$ and $\underset{\sim}{g}$ obtained in this manner for the systems studied in this work are summarized in Table IX. It is seen that X + Y + Z = 0 within experimental error. Further, the agreement between our results for the fine-structure tensor and those obtained in zero-field[56] and level anticrossing[67] studies is excellent. Table IX also shows that the $\underset{\sim}{g}$ tensors are anisotropic with $g_{zz} \gg g_{xx}, g_{yy}$. These parameters cannot, of course, be obtained by ODMR spectroscopy in zero field.

The observed orientational dependence of the ODMR transitions can be explained by employing a more explicit form of the Hamiltonian for the electron Zeeman interaction [cf., Eq. (16)];

$$\mathcal{H}_Z = (\ell H,\ mH,\ nH) \begin{pmatrix} g_{xx} & g_{xy} & g_{xz} \\ g_{yx} & g_{yy} & g_{yz} \\ g_{zx} & g_{zy} & g_{zz} \end{pmatrix} \begin{pmatrix} S_x \\ S_y \\ S_z \end{pmatrix} \qquad (29)$$

TABLE IX: Principal values of the $\underset{\sim}{g}$ and $\underset{\sim}{D}$ tensors of the lowest triplet state of benzophenones[a]

System	Z(cm^{-1})	Y(cm^{-1})	X(cm^{-1})	|X+Y+Z|	D(cm^{-1})[b]	E(cm^{-1})[b]	g_{zz}	g_{yy}	g_{xx}
^{12}C-BP/DDE	+0.10447	-0.03484	-0.06962	0.00001	-0.15670	+0.01739	2.0106	2.0021	2.0009
^{13}C-BP/DDE	+0.10425	-0.03470	-0.06947	0.00008	-0.15638	+0.01738	2.0105	2.0023	1.9998
4,4'-DFBP/DDE	+0.11122	-0.03733	-0.07375	0.00013	-0.16683	+0.01821	2.0136	1.9999	2.0019
4,4'-DCBP/DDE	+0.09713	-0.02783	-0.06917	0.00013	-0.14569	+0.02067	2.0102	1.9996	1.9990
neat 4,4'-DCBP X-traps	+0.09705	-0.02492	-0.07215	0.00007	-0.14558	+0.02362	2.0207	2.0094	2.0075
4,4'-DBBP/DDE	+0.08649	-0.02114	-0.06550	0.00015	-0.12982	+0.02218	2.0163	2.0073	2.0009

[a] All values accurate to ±10 in the last two digits.

[b] Obtained from the values of X, Y, and Z using Eqs. (11a,b).
The assignment of the absolute sign of these parameters is based on arguments that follow.

Using this form of $\mathcal{H}_Z$ in the spin Hamiltonian (15), one can obtain the orientational dependence of the energy levels (and therefore, the transitions) in any plane. For example, assuming $\underset{\sim}{g}$ and $\underset{\sim}{D}$ are diagonal in the same coordinate system, the Hamiltonian for a rotation in the $\underline{x}'\underline{z}'$ plane is found to be

$$\mathcal{H}_S^o = \beta H(g_{xx}S_x \sin\theta + g_{zz}S_z \cos\theta) - XS_x^2 - YS_y^2 - ZS_z^2 \qquad (30)$$

where θ is the angle the magnetic field makes with $\underline{z}'$. In the representation of the $|\tau_x\rangle$, $|\tau_y\rangle$, $|\tau_z\rangle$ basis set, the matrix of this Hamiltonian is

$$\begin{bmatrix} X & -ig_{zz}\beta H \cos\theta & 0 \\ ig_{zz}\beta H \cos\theta & Y & -ig_{xx}\beta H \sin\theta \\ 0 & ig_{xx}\beta H \sin\theta & Z \end{bmatrix} = \mathcal{H}_S^o \qquad (31)$$

The eigenvalues and eigenvectors can be found in exactly the same manner as done for the principal axis orientations. Thus, given the principal elements of $\underset{\sim}{g}$ and $\underset{\sim}{D}$, the positions of ODMR signals can be calculated as a function of θ. Since such calculations require the diagonalization of $\mathcal{H}_S^o$ at each value of θ, it is a time consuming process and necessitates the use of a computer. Once such calculation was carried out

for the x'y' plane of X-traps in neat 4,4'-DCBP using the values given in Table IX, and the results were found to be in good agreement with experiment.

2. Temperature Dependence of the ODMR Spectra and the Absolute Signs of the ZF Parameters

In the preceding section it was mentioned that the two level ordering schemes Z > O > Y > X and X > Y > O > Z are equally sufficient for explaining the observed field positions of the "$\Delta m_S = \pm 1$" transitions. However, it is possible to determine the correct scheme by monitoring the relative intensity of the low- and high-field lines as a function of temperature in a manner similar to that employed by Hornig and Hyde,[69] except that in our experiments the non-exponential phosphorescence decays observed at the lowest temperatures clearly indicate that the levels are not in thermal equilibrium. Thus, it is clear that the absolute ordering of the levels can be determined by allowing the system to thermalize by increasing the temperature to a point where SLR becomes faster than the decay rate of the triplet sublevels. Similar methods have been employed in this laboratory to determine the absolute signs of the ZF parameters of s-tetrachlorobenzene in durene.[70]

a) X-Traps in neat 4,4'-DCBP. Consider the H||y' orientation for X-traps in neat 4,4'-DCBP and the corresponding energy level diagrams for each of the two possible

ordering schemes shown in Fig. 13. The relative steady-state populations of the levels in a magnetic field $n_i (i=+,0,-)$, in the absence of microwaves and rapid SLR, are determined by the relative rates of intersystem crossing (K_i) and decay (k_i) processes, i.e., $n_i = K_i/k_i$.[30,71] These rates may in turn be calculated from kinetic data obtained in zero field using simple field-induced mixing considerations.[72] For example, for the $|+\rangle$ level in Fig. 13 A,

$$K_+ = \tfrac{1}{2}[1-(Z-X)/\alpha_y]K_x+\tfrac{1}{2}[1+(Z-X)/\alpha_y]K_z \qquad (32a)$$

$$k_+ = \tfrac{1}{2}[1-(Z-X)/\alpha_y]k_x+\tfrac{1}{2}[1+(Z-X)/\alpha_y]k_z \qquad (32b)$$

where K_j and k_j (j=x,y,z) are the corresponding ZF rate constants and the terms in brackets are the squares of the coefficients of $|T_j\rangle$ in the "in-field" eigenvector (See Table VIII). Similarly the radiative rate constants for each level in the presence of a magnetic field can be determined from simple mixing considerations and is found to be

$$k_+^r = \tfrac{1}{2}[1-(Z-X)/\alpha_y]k_x^r+\tfrac{1}{2}[1-(Z-X)/\alpha_y]k_z^r \qquad (32c)$$

for the $|+\rangle$ level in Fig. 13 A. Thus, relative values of n_i and k_i^r can be determined for each resonant field position and orientation from zero-field rate data using this method. Furthermore, the relative intensity and phasing of the two

Figure 13. Energy levels for the two possible ZF schemes of neat 4,4'-DCBP in DDE with the magnetic field parallel to the y' axis of the fine-structure tensor. Solid arrows indicate the "$\Delta m_S = \pm 1$" transitions and whether they are emissive (↓) or absorptive (↑) in the absence of SLR; dashed arrows indicate the same in the presence of rapid SLR. Arrows designated by $k^r_{+,-}$ refer to the dominant radiative levels. (A) For the ZF scheme Z > O > Y > X (D < O). (B) For the ZF scheme X > Y > O > Z (D > O).

H || y′ 4,4′ DCBP

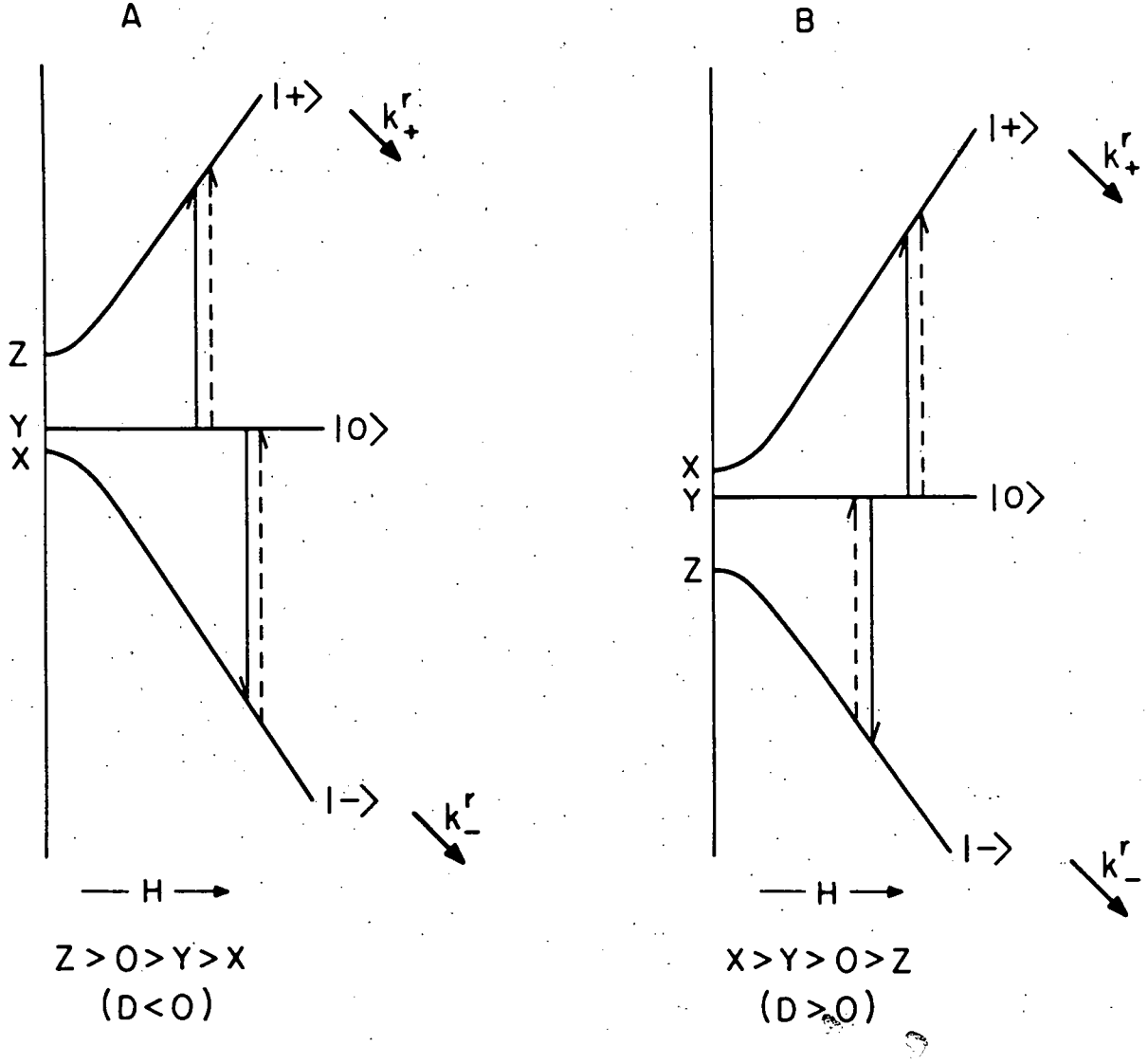

transitions indicated in Fig. 13 can be calculated using Eq. (13). Unfortunately, these data are not available for X-traps in neat 4,4'-DCBP; however, Dym and Hochstrasser[48] have shown that the radiative spin activity for the $^3(n,\pi^*) \leftarrow {}^1A$ transition in neat 4,4'-DCBP is 61% $|\tau_z\rangle$, 32% $|\tau_x\rangle$, and 7% $|\tau_y\rangle$. These data alone are sufficient for analyzing the temperature dependence of the ODMR spectra of 4,4'-DCBP.

Figure 11 shows that the two "$\Delta m_S = \pm 1$" transitions in the $\underline{H} \,||\, \underline{y}'$ orientation of neat 4,4'-DCBP correspond to increases in phosphorescence intensity at 1.6°K. This indicates that either $n_o > n_+$, n_- and $k_+^r, k_-^r > k_o^r$, or $n_o < n_+$, n_- and $k_+^r, k_-^r < k_o^r$ at both resonant fields. Since $k_z^r, k_x^r > k_y^r$ in zero-field[48] and the properties of $|\tau_x\rangle$ and $|\tau_z\rangle$ are the only ones mixed in the presence of a magnetic field, the former is true at both resonant fields. From these considerations, the ODMR transitions at 1.6°K are as indicated by the solid lines in Fig. 13. In Scheme A, the high-field transition is therefore microwave emissive while in scheme B the low-field transition is microwave emissive. Although the microwave transition probabilities for the two transitions in each scheme are slightly different,[73] the ratio of these is the same for either scheme,[69] and thus a comparison of the relative intensities of the two transitions at different temperatures can be used to determine the correct ordering scheme.

Changes in the relative intensity of the two "$\Delta m_S = \pm 1$" transitions on warmup will depend primarily on the effect of SLR on the population differences of the levels being saturated. As T_1 becomes short and Boltzmann equilibrium is established, $n_- > n_o > n_+$ obtains for both scheme A and scheme B. Thus, one expects the high-field transition to decrease in intensity relative to the low-field transition if scheme A applies; while the opposite should occur if scheme B applies. Experimentally, it is observed (Fig. 11) that the high-field transition decreases in relative intensity as the temperature increases and is observed to invert at the highest temperature studied (consistent with microwave emission at 1.6°K). Thus, scheme A ($Z > O > Y > X$; $D < O$, $E > O$) appears to be the correct level ordering for X-traps in 4,4'-DCBP. A similar analysis for the $\underline{H} || \underline{x}'$ orientation is consistent with this result. The exciton lines (*vide infra*) which dominate the ODMR spectrum in the $\underline{H} || \underline{z}'$ orientation precluded such an analysis.

Two effects might invalidate this determination of the absolute level ordering. A field dependence of T_1 might explain a more rapid decrease in the relative intensity of the high-field transition; however, such an effect cannot account for the inversion of the high-field transition as the temperature is increased. Hochstrasser and Michaluk,[74] in their

optical studies of neat 4,4'-DCBP crystals, found the origin of singlet-triplet absorption at 4124.6 Å while the crystal phosphorescence originated mainly from a triplet X-trap (a 4,4'-DCBP molecule near a crystal imperfection or impurity) with an origin at 4135.4 Å (in agreement with this work). From the origins of absorption and emission a trap depth of 63 cm^{-1} can be estimated. In such shallow traps, detrapping effects might be expected to be spin-state selective and highly temperature dependent.[75] This could affect the relative steady-state populations of the sublevels and result in a change of the relative ODMR signal intensities with temperature. An analysis of the temperature dependence in a deep trap system (i.e., 4,4'-DCBP in DDE) should eliminate effects due to detrapping.

b) 4,4'-DCBP in DDE. The absorption spectrum of neat DDE shows no bands above 2600 Å indicating that excitation with 3660 Å light should excite a guest ketone directly. Thus, the populations of the guest triplet sublevels are governed predominantly by mechanisms inherent to the guest molecule and not by energy transfer processes involving crystal exciton states. This is exemplified by the decreases in phosphorescence intensity observed on microwave saturation of all transitions in the principal axis orientations of 4,4'-DCBP in DDE at 1.6°K. In contrast, it is observed that the ODMR transitions in neat

4,4'-DCBP in the $\underline{H}||\underline{x}'$ and $\underline{y}'$ orientations correspond to increases in the phosphorescence intensity. Thus, the populating mechanisms in the two systems are substantially different.

Considering the $\underline{H}||\underline{y}'$ orientation of 4,4'-DCBP in DDE, the analysis of the temperature dependence of the ODMR spectrum can be made in the same manner as just discussed for neat 4,4'-DCBP. Fig. 13 can be used with a few minor, but nonetheless important, changes. Since $k_z^r, k_x^r > k_y^r$, the observed decreases in phosphorescence intensity at 1.6°K indicate $n_+, n_- > n_o$ obtains for this orientation of 4,4'-DCBP in DDE. Thus, the solid arrows of Fig. 13 should be reversed in direction, so that the low-field (high-field) transition in scheme A (B) is microwave emissive. The dashed arrows which indicate the direction of transitions (in a microwave sense) at Boltzmann equilibrium remain the same. If scheme A is correct the low-field transition should decrease in relative intensity more rapidly than the high-field transition as SLR becomes effective. This is what is observed experimentally (Fig. 8 and Table V B). Similar analyses in the other two principal orientations are consistent with this result since $|\tau_z\rangle$ is predominantly radiative.[48] A field dependence of T_1 might invalidate these results; however, SLR should be

more rapid for the high-field transition and thus decrease the relative intensity of this line during warmup. Clearly this is not observed experimentally, and it is concluded that the correct ZF ordering of states in the lowest triplet state of 4,4'-DCBP is Z > O > Y > X (D < O, E > O). Since the analysis of the doped and neat 4,4'-DCBP temperature dependences lead to similar conclusions, it appears that temperature dependent detrapping effects in the neat 4,4'-DCBP crystal do not become significant before SLR becomes rapid. Although this may be true for neat 4,4'-DCBP, it is probably not true in general and caution should be exercised in the interpretation of the temperature dependence of ODMR spectra in shallow-trap systems.

c) Other Benzophenones. The temperature dependence of the ODMR spectra of ^{12}C-BP and ^{13}C-BP in DDE (Table IV B) was analyzed in a similar manner. Assuming $|T_z\rangle$ is the dominant radiative level,[53-55] the experimental results in all three principal axis orientations are readily explained by the same absolute level ordering; i.e., Z > O > Y > X.

The ODMR spectrum of 4,4'-DBBP in the $\underline{H} \| \underline{x}'$ orientation showed that at 1.6°K the two "$\Delta m_S = \pm 1$" transitions are of opposite phase. In addition, the high-field transition was observed to be microwave emissive since it inverts when

the temperature is raised from 1.6°K to 4.2°K. Thus, if $|\tau_z\rangle$ is the dominant radiative level, the absolute level ordering Z > O > Y > X is obtained using the aforementioned analysis. On the other hand, if $|\tau_x\rangle$ is the principal radiative level, one obtains the opposite level ordering; i.e., X > Y > O > Z. However, in both cases the analysis suggests that both "$\Delta m_s = \pm 1$" transitions should be microwave emissive at 1.6°K. In neither level ordering scheme can the assignment be made in terms of a single microwave emissive transition. Attempts to experimentally verify the emissive nature of the low-field transition at temperatures above 4.2°K were precluded by the severe overlap of these transitions with resonances due to the other molecules in the unit cell. The fact that the high-field transition inverts at a lower temperature than the low-field transition, even though both are believed to be emissive at 1.6°K, could very well be due to a field dependence of T_1. On the basis of the smooth decrease in D values observed in this and other benzophenones, it is tentatively concluded that the level ordering in 4,4'-DBBP remains Z > O > Y > X. This implies that the radiative character of $|\tau_z\rangle$ still dominates after bromination, which was found to be true in 3,3'-dibromobenzophenone.[48] The determination of the relative radiative rate constants in ZF would definitely lend support to one of the two arguments. The absolute signs of all of

the benzophenones given in Table IX were determined from the observed temperature dependence and are consistent with the high field Zeeman results of Hochstrasser and Lin[47] on benzophenone itself.

3. Excitons and X-Traps in Neat 4,4'-DCBP

Thus far, the interpretation of the ODMR results in neat 4,4'-DCBP has rested on the unproven assignment of X-trap and exciton transitions. The two pairs of ODMR transitions observed with the magnetic field parallel to the b (z') axis could also be explained by multiple sites or inclusion of some impurity. The fact that the action spectra of the two features in the low-field region are identical to the normal phosphorescence spectrum, as well as the extensive purification of the material, suggests that impurities are not responsible. The difference in linewidths of the two lower field transitions suggests that multiple sites are also not present. The more intense feature has a linewidth (full width at half maximum) of 9 G whereas the linewidth of the less intense feature is ~20 G. Comparison of these results with those of Sharnoff et al.[54,55] on neat BP indicates that the more prominent features observed in this orientation are excitonic in origin, while the less intense transitions -- just resolved in the low-field region and producing a slight asymmetry in the high field region -- are due to an X-trap in

the neat 4,4'-DCBP crystal. With a trap depth of 63 cm^{-1},[74] it is not surprising that both traps and excitons are observed in the ODMR spectrum.

Attempts were made to characterize the exciton and trap transitions by varying microwave power, modulation frequency, and temperature. The effect of microwave power on the peak signal intensities of the low-field trap and exciton transitions is shown in Fig. 14. The nearly linear dependence (with slope 1/2) of the log-log plot exhibited by the trap signal is indicative of an inhomogeneously broadened line (e.g., by hyperfine interactions) of a localized excitation.[54] The nonlinear behavior observed for the exciton transition is indicative of homogeneous broadening. Homogeneous broadening is generally caused by exposing a spin system to local magnetic fields which fluctuate severely. Since a nonlocalized excitation, such as a triplet exciton, experiences local fields whose fluctuations are larger and more rapid than those due to molecular reorientation at 1.6°K, it is probable that the most prominent features in the $\underline{H} \| \underline{z}'$ ODMR spectrum of neat 4,4'-DCBP are excitonic in origin.

When the modulation frequency was increased from 93 Hz (used to obtain the spectra in Fig. 9) to 1 kHz, the trap transition decreases in intensity relative to the exciton transition. This suggests that the lifetime of the exciton

Figure 14. Microwave power dependence of the low-field "$\Delta m_S = \pm 1$" ODMR transitions of neat 4,4'-DCBP in the orientation $\underline{H} \,||\, \underline{z}'$. The peak signal intensities of the exciton (x) and X-trap (·) resonances are plotted as a function of microwave power attenuation; 0dB corresponds to a maximum of ∿100 mW.

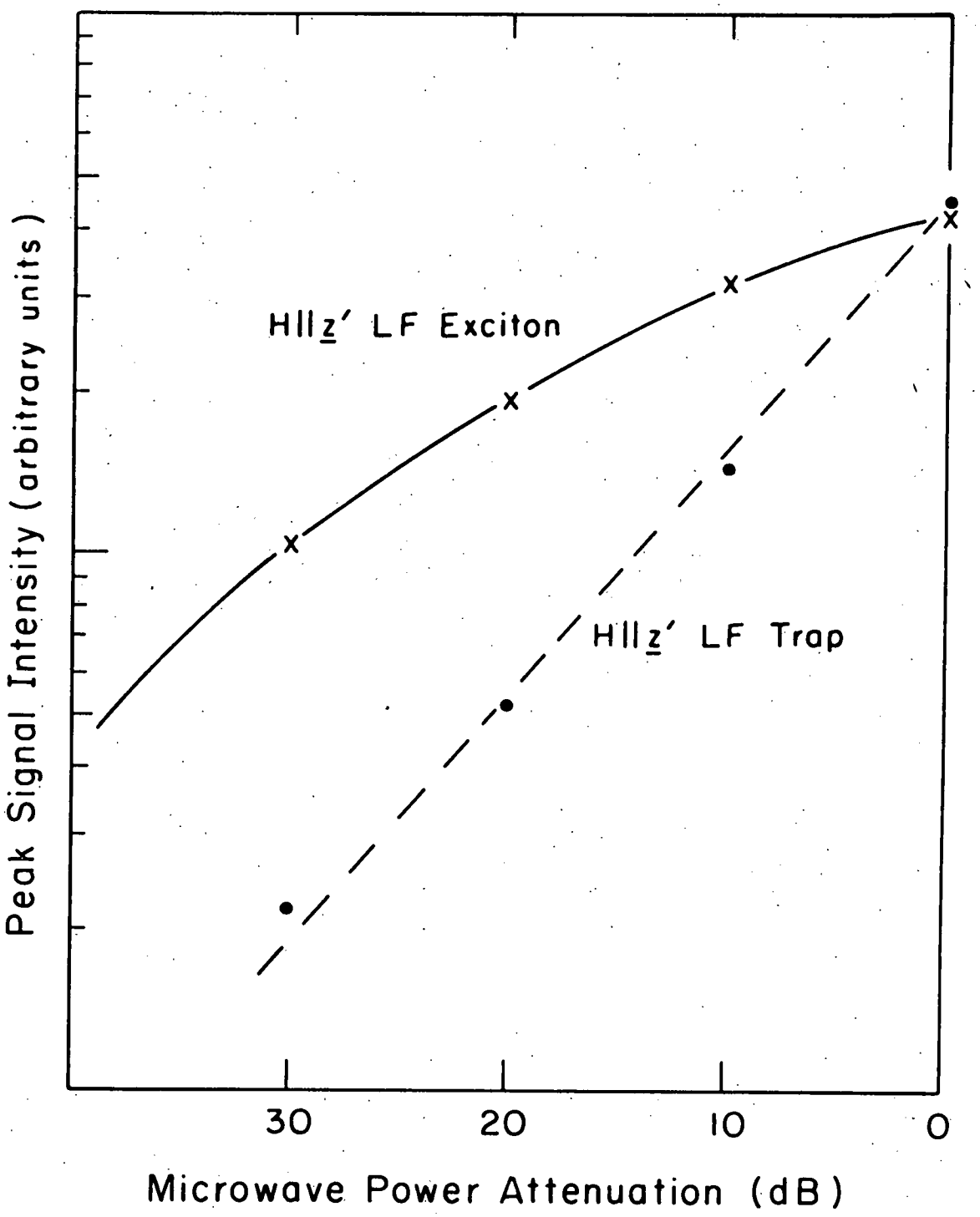
H||z' LF Exciton
H||z' LF Trap
Peak Signal Intensity (arbitrary units)
30
20
10
0
Microwave Power Attenuation (dB)

is considerably shorter than that of the trap. MIP experiments carried out on both transitions support this result. Thus, application of a microwave pulse to the trap transition produces a small but detectable decrease in the steady-state phosphorescence intensity, while no effect could be detected by pulsing the exciton transition even though it is the most intense feature in the ODMR spectrum in this orientation. The fact that application of a microwave pulse produces no detectable changes indicated that the exciton lifetime is considerably shorter than the pulse width (10 μsec). It also suggests that the exciton ODMR signal is observed by directly monitoring triplet exciton emission. If the population changes in the exciton levels were being monitored by the changes in trap population caused by energy transfer, the MIP behavior should be qualitatively the same as that observed for the trap.

The temperature dependence of the $\underline{H} \| \underline{z}'$ resonances is shown in the center portion of Fig. 11. One notices the asymmetry observed in the signals at 1.6°K, which are manifestations of the X-trap, disappears as the sample is allowed to warm above 4.2°K, and no change in relative intensity of the exciton signals is observed. Repeating the experiment with liquid nitrogen in the cryostat allowed observation of the exciton signals at a temperature near 77°K. As can be

seen, the ratio of the intensities of the high-field to low-field "$\Delta m_s = \pm 1$" exciton transitions (2:1) is nearly the same as that observed at 1.6 °K, and both transitions still correspond to decreases in phosphorescence intensity. The observed temperature dependence again confirms the exciton and trap assignments. The inability to detect the trap ODMR signals at temperatures considerably greater than 4.2 °K can be explained in two ways, either by the onset of rapid SLR and/or thermally-induced detrapping. At 1.6 °K, SLR is slow compared to the lifetime of the trap and some degree of spin polarization develops in the triplet sublevels of the trap. As the temperature is raised, SLR becomes rapid the populations of the sublevels tend to equalize and the trap signals disappear. The observations at 77 °K can be explained equally well by noting that kT is comparable to the trap depth. Thus, any nonlocalized excitation in the crystal never really "sees" the trap and no trap signals would be observable. The exciton signals observed at 77 °K are also seen to be sharper than those observed at 1.6 °K; the linewidths being 4 G and 9 G, respectively. This is consistent with the increased rate of propagation of the nonlocalized excitations in the crystal as temperature increases. The local fields experienced by the exciton spin system are fluctuating even more rapidly and the line becomes sharper.

Since the exciton transitions are not observable in the other principal orientations of the crystal, little can be said about their magnetic properties. However, by comparing the results for the $\underline{H} || \underline{z}'$ orientation in neat 4,4'-DCBP with those obtained by Sharnoff and Iturbe[55] for the same orientation in neat BP, some information can be obtained about the energy transfer processes in this system. Both exciton lines in neat 4,4'-DCBP showed the same phasing (i.e., both were detected as decreases in phosphorescence intensity), while opposite phasing was observed in neat BP. This suggests that SLR is rapid for excitons in BP; saturation studies indicate T_1 to be of the order of 10^{-7} sec at 4.2°K.[50] Since $|\tau_z\rangle$ is the dominant radiative level in 4,4'-DCBP (as in BP itself), the same phasing of the exciton transitions and the observed non-exponential decay at 77°K indicates that the exciton states in 4,4'-DCBP are spin polarized even at 77°K. This implies that the correlation time (τ_c) for exciton migration in the neat 4,4'-DCBP crystal is several orders of magnitude less than T_1 for the exciton at all temperatures studied in this work. If one assumes that an exchange interaction is responsible for energy transfer,[76] then the trapping mechanism is spin conservative. When this is the case, the relative populations of the spin sublevels of the trap will be

similar to the relative populations of the corresponding exciton levels. Indeed, both trap resonances observed at 1.6°K in the $\underline{H}||\underline{z}'$ orientation correspond to decreases in intensity even though $|\tau_z\rangle$ possesses most of the radiative activity. Thus, the exchange model appears to qualitatively describe the energy transfer from exciton to traps.

D. Discussion

1. Effect of Spin-Orbit Coupling on the Principal Values of $\underset{\sim}{g}$ and $\underset{\sim}{D}$.

It is well known that the first-order effect of spin-orbit (SO) coupling leads to a breakdown in the $\Delta S=0$ selection rule but produces no shift in the energies of an orbitally non-degenerate state. Hameka[77] was the first to examine theoretically the second-order effects of the SO interaction on the ZF parameters of triplet aromatic hydrocarbons. In a now classic paper on benzene,[78] he showed that the SO contribution to D was of the order of 10^{-5} cm^{-1}, a value which is clearly negligible compared to the observed D value (0.158 cm^{-1}). However, he was careful to state that this conclusion was not necessarily valid for all molecules, expecially those containing atoms with large SO coupling constants and/or spin densities. Indeed, Hameka has recently

shown that the SO contributions to the ZF parameters of CH_2[79] and NH[80] are 11 and 25%, respectively, of the observed D values. Similarly, calulations on triplet formaldehyde indicate that up to 30% of the observed D value may be caused by SO interactions.[81] Thus, there is ample precedent for considering the effect of second-order SO coupling on the $\underset{\sim}{g}$ and $\underset{\sim}{D}$ tensors of triplet benzophenones.

Using the McClure[42] central field approximation, the SO Hamiltonian may be written as[9]

$$\mathcal{H}_{SO} = \frac{1}{2m^2c^2} \sum_{k=1}^{N} \sum_{i=1}^{n} r_{ik}^{-1} \frac{\partial V(r_{ik})}{\partial (r_{ik})} (L_{x_i} S_{x_i} + L_{y_i} S_{y_i} + L_{z_i} S_{z_i}) \quad (33)$$

where N is the number of nuclei and n is the number of electrons. The operators for the x components of the orbital and spin angular momenta of the ith electron are denoted by L_{x_i} and S_{x_i}, respectively. Defining

$$A_i = \frac{1}{2m^2c^2} \sum_{k=1}^{N} r_{ik}^{-1} \frac{\partial V(r_{ik})}{\partial (r_{ik})} \quad (34)$$

we have, for two electrons

$$\begin{aligned} \mathcal{H}_{SO} = {} & A_1 (L_{x_1} S_{x_1} + L_{y_1} S_{y_1} + L_{z_1} S_{z_1}) \\ & + A_2 (L_{x_2} S_{x_2} + L_{y_2} S_{y_2} + L_{z_2} S_{z_2}) \end{aligned} \quad (35)$$

Eq. (35) may be separated into sums whose orbital and spin factors are separately symmetric or antisymmetric with respect to electron interchange:

$$\mathcal{H}_{SO} = \tfrac{1}{2} \sum_{p=x,y,z} [(A_1 L_{1p} + A_2 L_{2p})(S_{1p}+S_{2p}) + (A_1 L_{1p} - A_2 L_{2p})(S_{1p} - S_{2p})] \qquad (36)$$

Using perturbation theory, the contributions of $\mathcal{H}_{SO}$ to the energies of the spin sublevels $|\tau_u\rangle$ are given by

$$\Delta E_u^{SO} = \sum_u \langle {}^3\psi_1^o, \tau_u | \mathcal{H}_{SO} | {}^3\psi_1^o, \tau_u \rangle - \sum_{u,j} \frac{\langle {}^3\psi_1^o, \tau_u | \mathcal{H}_{SO} | {}^3\psi_j^o, \sigma \rangle \langle {}^1\psi_j^o, \sigma | \mathcal{H}_{SO} | {}^3\psi_1^o, \tau_u \rangle}{E({}^1\psi_j^o) - E({}^3\psi_1^o)} - \sum_{u,v,k} \frac{\langle {}^3\psi_1^o, \tau_u | \mathcal{H}_{SO} | {}^3\psi_k^o, \tau_v \rangle \langle {}^3\psi_k^o, \tau_v | \mathcal{H}_{SO} | {}^3\psi_1^o, \tau_u \rangle}{E({}^3\psi_k^o) - E({}^3\psi_1^o)} \qquad (37)$$

Here, $|{}^3\psi_1^o, \tau_u\rangle$ are the zeroth-order wavefunctions of the lowest triplet state sublevels; $|{}^1\psi_j^o, \sigma\rangle$ are the zeroth-order singlet state wavefunctions, and $|{}^3\psi_k^o, \tau_v\rangle$ are the zeroth-order wavefunctions of the sublevels $|\tau_v\rangle$ of higher triplet states. Thus, the three terms in Eq. (37) represent the effect of first-order SO coupling in the triplet manifold, the effect of second-order SO coupling of the lowest triplet state with excited <u>singlet</u> states, and the effect of second-order SO coupling of the lowest triplet state with higher <u>triplet</u> states, respectively.

It can be shown that $\mathcal{H}_{SO}$ may be transformed to yield the same form as Eq. (7), <u>i.e.</u>

$$\mathcal{H}_{SO} = -(XS_x^2 + YS_y^2 + ZS_z^2). \qquad (38)$$

Hence, it is clear that when second-order SO coupling contributions are important, there is no change in the appearance of the ODMR spectrum. Thus, $\mathcal{H}_{ZF}$ [Eq. (7)] is really of the form

$$\mathcal{H}_{ZF} = \mathcal{H}_{SS} + \mathcal{H}_{SO} \qquad (39)$$

where $\mathcal{H}_{SS}$ and $\mathcal{H}_{SO}$ are the contributions to the ZF splittings from the magnetic dipole-dipole and spin-orbit interactions between the two electrons, respectively. This does not alter the interpretation of the preceding sections, but the parameters X, Y, and Z (or D and E) obtained include the net effect of both interactions.

Two models have been developed which rely on different experimental observables in order to quantify the effects of the SO interactions on the energies of the triplet sublevels. The first, proposed independently by Jones et al.[82] and Hayashi and Nagakura,[63] requires knowledge of the ZF splittings and energy differences between the two lowest excited triplets in order to determine the SO contribution to the ZF splitting. The Batley and Bramley model[62] requires knowledge of the ZF splittings and $\underset{\sim}{g}$ tensor to determine this contribution. Since the ODMR studies of this work give the principal values of the fine-structure and $\underset{\sim}{g}$ tensors, the Batley and Bramley model seemed more appropriate, and a brief description of their approach follows.

The second-order contributions of SO coupling to the energies of the spin substates of a $^3(n,\pi^*)$ state, such as the lowest triplet state of benzophenone, are given by

$$\Delta E_u^{SO} = - \frac{\sum_p \langle n,\pi^*;\tau_u | \mathcal{H}_{SO} | p \rangle \langle p | \mathcal{H}_{SO} | n,\pi^*;\tau_u \rangle}{E_p - E_u^o} \quad (40)$$

in accord with Eq. (37). Here, E_u^o is the zeroth-order energy of the lowest triplet sublevel $|n,\pi^*;\tau_u\rangle$ and p refers to the singlets and triplets to which this state is coupled. Of the possible interacting states, $|p\rangle$, only $|\pi,\pi^*\rangle$ will give one-center terms and only the $\underline{z}$ component of $\mathcal{H}_{SO}$ will be effective. It may be shown using group theory that[72]

(1) $\mathcal{H}_{SO}(\underline{z})$ mixes the $|\tau_x\rangle$ sublevel of the lowest triplet state with the $|\tau_y\rangle$ sublevel of higher $|\pi,\pi^*\rangle$ <u>triplet</u> states,

(2) $\mathcal{H}_{SO}(\underline{z})$ mixes the $|\tau_y\rangle$ sublevel of the lowest triplet state with the τ_x sublevel of higher $|\pi,\pi^*\rangle$ <u>triplet</u> states, and

(3) $\mathcal{H}_{SO}(\underline{z})$ mixes the $|\tau_z\rangle$ sublevel of the lowest triplet state with excited $|\pi,\pi^*\rangle$ states in the <u>singlet</u> manifold.

Since the energy denominators $(E_p - E_u^o)$ will be larger for the singlet-triplet interactions than for the triplet-triplet interactions, we can neglect, to a first approximation, the

shift in the energy of $|\tau_z\rangle$. With this assumption, any change in the value of Z due to second-order SO coupling is a result of changes in the energies of $|\tau_x\rangle$ and $|\tau_y\rangle$. Since ΔE_z^{SO} is -2/3 of the shift in the absolute energies of $|\tau_x\rangle$ and $|\tau_y\rangle$ (assuming $\Delta E_x^{SO} = \Delta E_y^{SO}$), then

$$\Delta E_Z^{SO} = \frac{\frac{2}{3}\,\frac{1}{4}\langle {}^3n,\pi^* | \sum_i \mathcal{H}_{SO_i}(\underline{Z}) | {}^3\pi,\pi^*\rangle \langle {}^3\pi,\pi^* | \sum_i \mathcal{H}_{SO_i}(\underline{Z}) | {}^3n,\pi^*\rangle}{E({}^3\pi,\pi^*) - E({}^3n,\pi^*)} \tag{41}$$

Also note that, since D = -3/2 Z,

$$\Delta D^{SO} = \frac{-\frac{1}{4}\langle {}^3n,\pi^* | \sum_i \mathcal{H}_{SO_i}(\underline{Z}) | {}^3\pi,\pi^*\rangle \langle {}^3\pi,\pi^* | \sum_i \mathcal{H}_{SO_i}(\underline{Z}) | {}^3n,\pi^*\rangle}{E({}^3\pi,\pi^*) - E({}^3n,\pi^*)} \tag{42}$$

The Zeeman Hamiltonian [cf. Eq. (16)], which was written previously in terms of spin operators only, can also be expressed as

$$\mathcal{H}_Z = \beta\, \underline{H} \cdot (\underline{L} + 2\underline{S}) \tag{43}$$

in order to account for the fact that the orbital angular momentum is no longer zero. This again creates no difficulty in the previous interpretation, since the g values determined earlier include the effects of both spin and orbital angular momenta, that is

$$\underline{S}_{eff} = \underline{L} + 2\underline{S} \tag{44}$$

and

$$(g_{ii})_{eff} = g_e + \Delta g_{ii} \tag{45}$$

where g_e is the free electron value (2.0023) and Δg_{ii} represents the contribution to the principal g-values, g_{ii}, from orbital angular momentum introduced by the SO interaction. For $\mathcal{H}_{SO}(\underline{z})$, Batley and Bramley show

$$\Delta g_{zz} = g_{zz} - g_e$$

$$= \frac{\langle {}^3n,\pi^* | \sum_i L_{Z_i} | {}^3\pi,\pi^* \rangle \langle {}^3\pi,\pi^* | \sum_i \mathcal{H}_{SO_i}(\underline{z}) | {}^3n,\pi^* \rangle}{E({}^3\pi,\pi^*) - E({}^3n,\pi^*)} \qquad (46)$$

By taking a simple ratio of Eqs. (42) and (46) one finds

$$\frac{\Delta D^{SO}}{\Delta g_{zz}} = -\tfrac{1}{4} \frac{\langle {}^3n,\pi^* | \sum_i \mathcal{H}_{SO_i}(\underline{z}) | {}^3\pi,\pi^* \rangle}{\langle {}^3n,\pi^* | \sum_i L_{Z_i} | {}^3\pi,\pi^* \rangle} \qquad (47)$$

If one assumes that for carbonyl compounds, one-center terms on the oxygen atom dominate $\mathcal{H}_{SO}$, then

$$\Delta D^{SO} = -(\zeta_o/4)\Delta g_{zz} \qquad (48)$$

where ζ_o is the SO coupling constant for oxygen (152 cm^{-1}). Eq. (48) can be used directly to calculate the SO contribution to D.

An examination of Table IX shows that, for ^{12}C-BP and ^{13}C-BP, g_{zz} deviates from the free spin value (2.0023) to a far greater extent than g_{xx} and g_{yy}. This indicates that the important component of the SO Hamiltonian is $\mathcal{H}_{SO}(\underline{z})$ and that it does mix the $|\tau_x\rangle$ and $|\tau_y\rangle$ spin sublevels of the lowest triplet state with those of higher triplet states, principally (π,π^*) in character. Moreover, it is also clear

from the magnitude of Δg_{zz} that second-order SO coupling does contribute significantly to the observed ZF parameters of $^3(n,\pi^*)$ benzophenone. Thus from Eq. (48) and the data in Table IX, we calculate $\Delta D^{SO} = -0.315\ cm^{-1}$ for ^{12}C-BP in DDE. The dipolar contribution to D is therefore $D^{SS} = D_{obs} - \Delta D^{SO} = +0.158\ cm^{-1}$, and in the absence of SO coupling effects, the ZF level ordering would be $Z \ll X < Y$ (i.e., $D > 0$, $E < 0$). This is in qualitative accord with the ZF scheme expected on the basis of dipolar arguments.[84] However, it should also be noted that the magnitude of D^{SS} is considerably less than expected if all of the triplet excitation were localized on the carbonyl group.[81]

On the basis of the above results, it can be concluded that the magnetic resonance parameters of $^3(n,\pi^*)$ benzophenone are affected by second-order SO coupling and that the Batley-Bramley model accounts for these effects in at least a qualitative way. However, there are some difficulties. For example, the D value of triplet 4,4'-DCBP is essentially the same in DDE and the neat crystal, but g_{zz} differs considerably in the two hosts. This suggests that interactions with the host can also effect the g-values. Furthermore, 4,4'-DBBP exhibits the smallest D value of all benzophenones studied and yet shows a significantly larger value of g_{zz}. Since the model for the SO contributions to D is based on the simple

picture of spin density localized on the carbonyl group, the discrepancies indicate there is some delocalization of the unpaired spins onto the phenyl rings. Although these discrepancies are small compared to the SO contributions from one-center terms on oxygen, their characterization should enable a more complete understanding of the $^3(n,\pi^*)$ state of carbonyl molecules.

2. Substituent and Ring Effects on the Principal Values of $\underset{\sim}{D}$

If the triplet excitation were truly localized on the carbonyl group, halogen substitution in the 4 and 4' positions of the two rings should produce little, if any, effect on the ZF splittings of benzophenone. However, the orientational dependences of the dihalobenzophenones in DDE show that the $\underline{x}'$ and $\underline{y}'$ axes of $\underset{\sim}{D}$ are rotated by an amount which depends on the substituent. Furthermore, the ZF parameters obtained from the orientational dependence show that D decreases in the order F > H > Cl > Br while E decreases in the order Br > Cl > F > H (Fig. 15A). Moreover, these effects are not small, with the overall changes in D and E being 22 and 28%, respectively. Thus, we are led to conclude that the triplet excitation in $^3(n,\pi^*)$ benzophenone is not confined to the carbonyl group.

Figure 15. Comparison of the ZF level ordering schemes of benzophenones in DDE. (A) Plot of data given in Table IX. (B) The energy of the $|\tau_y\rangle$ sublevel is used as a reference.

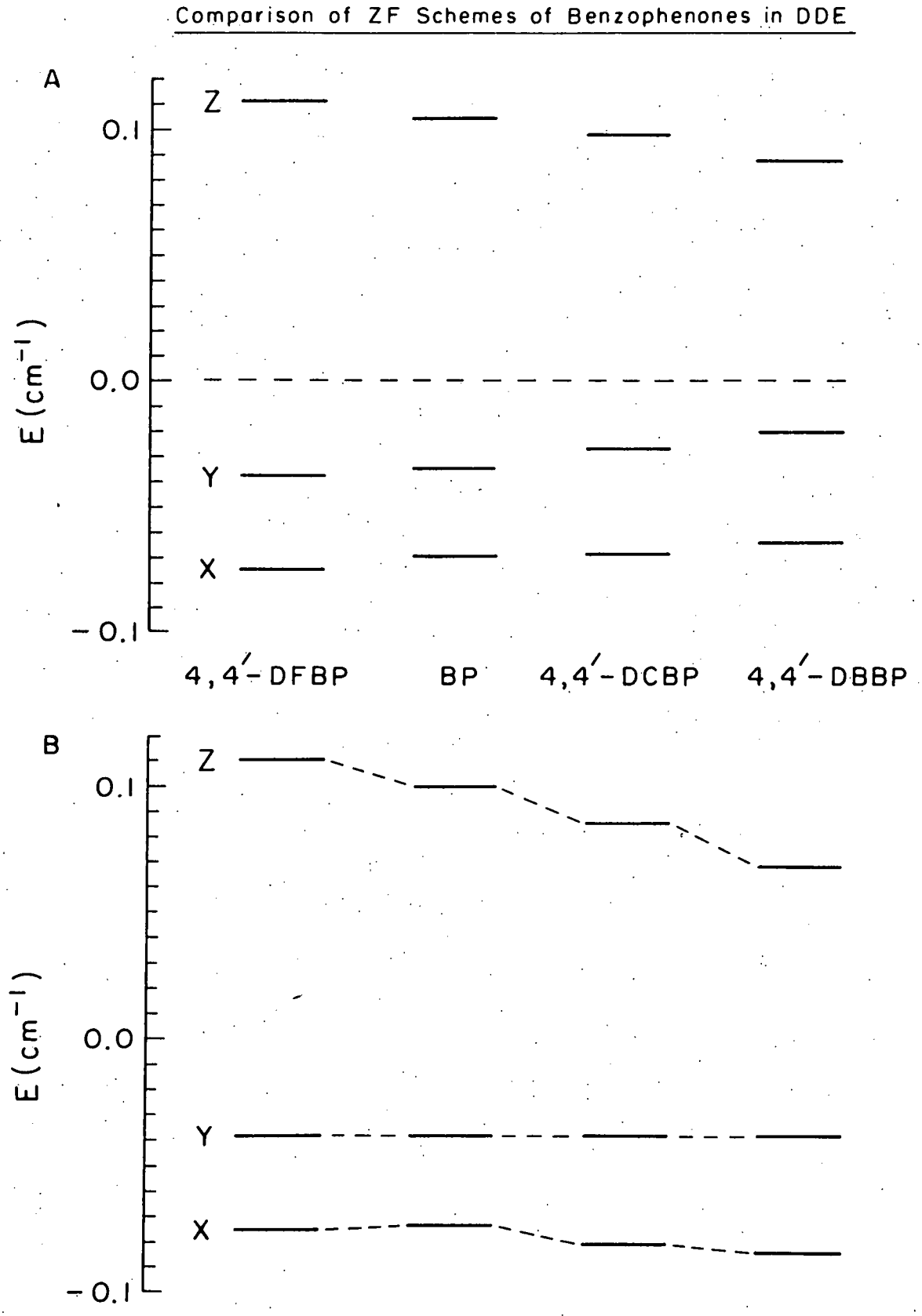
Comparison of ZF Schemes of Benzophenones in DDE
A
Z
Y
X
0.1
0.0
-0.1
E (cm⁻¹)
4,4′-DFBP
BP
4,4′-DCBP
4,4′-DBBP
B
Z
Y
X
0.1
0.0
-0.1
E (cm⁻¹)

Shown in Fig. 15 B is a comparison of the ZF schemes of the benzophenones studied in this work. Fig. 15 B is the same as Fig. 15 A but plotted in a slightly different way for illustrative purposes. It is clear from this plot that the $|\tau_z\rangle$ and $|\tau_x\rangle$ sublevels are increasingly stabilized with respect to $|\tau_y\rangle$ as heavier atoms are attached to the 4,4' positions. We believe that this effect can also be explained by second-order SO coupling, but in this case the coupling occurs because of a finite spin density at carbons 4 and 4' rather than the oxygen atom. In support of this, it is noted that the halogen substituents lie closest to the y' axis of the ZF tensor, and that coupling with higher excited states derived mainly from the phenyl rings (e.g., (π,π^*)) via $\mathcal{H}_{SO}(y)$ will depress $|\tau_x\rangle$ and $|\tau_z\rangle$ with respect to $|\tau_y\rangle$. Similar effects have also been observed in the $^3(\pi,\pi^*)$ states of halogenated benzenes and naphthalenes studied by Kothandaraman et al. in this laboratory.[85]

In the preceding discussion, little has been said about the structure of benzophenones in the lowest triplet state. The orientation of the phenyl rings in the crystal were described in Chapter II where it was noted that they were tilted by 29° with respect to the carbonyl plane. Hoffmann and Swenson[86] used extended Huckel and CNDO/2 methods to determine the equilibrium geometries of benzophenone

(Fig. 16) in the ground and $^1(n,\pi^*)$ excited states. Their

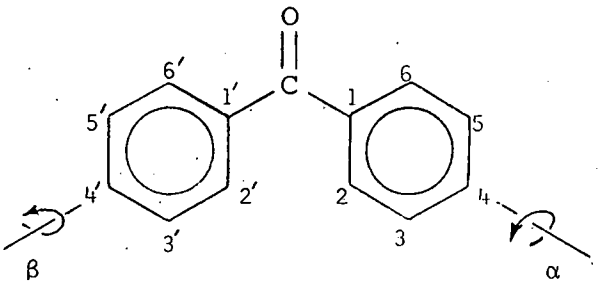

Figure 16. Equilibrium geometry of benzophenone. In the ground state, $\alpha = \beta = 38^\circ$. In the $^1(n,\pi^*)$ state, $\alpha = \beta = 32^\circ$.[86]

results indicate that in both states the phenyl rings were twisted out of plane in a conrotatory fashion to a C_2 geometry by 38° and 32°, respectively. Thus, excitation leads to a more nearly planar form of benzophenone. Although these calculations were carried out in the excited singlet state, the ODMR results on triplet state suggest similar conclusions. If the phenyl rings were coplanar with the carbonyl group (C_{2v} molecular symmetry), the principal axes of the fine-structure tensor ($\underline{x}'$, $\underline{y}'$, and $\underline{z}'$) would be colinear with the $\underline{x}$, $\underline{y}$, and $\underline{z}$ axes defined earlier for the carbonyl group itself. Similarly, a disrotatory twisting of the phenyl rings by the same amount should also lead to both sets of axes remaining colinear. Recalling that in the crystal the $\underline{x}$ ($\underline{y}$) axes defined for the two orientations of

the carbonyl group make an angle of $+1^{\circ}40'$ and $-1^{\circ}40'$, respectively, with the a (b) axis of the crystal, one would expect to see two sets of fine-structure patterns in the ab plane orientational dependence of the ODMR spectra. For the the two geometries just mentioned, the two patterns would be identical, but displaced from each other by only $3^{\circ}20'$. The experimental orientational dependences in this plane show a displacement of the patterns by angles considerably greater than $3^{\circ}20'$. The x' and y' principal axes of the fine-structure tensor are rotated away from the x and y axes defined for the carbonyl group by an angle which depends on the substituent in the 4 and 4' ring positions. This rotation of the fine-structure axes in the ab plane is evidence of the conrotatory twisting of the phenyl rings in the $^3(n,\pi^*)$ state of benzophenones, and indicates the molecular symmetry to be C_2 in the $^3(n,\pi^*)$ state. Thus, the orbital symmetry of the triplet state of benzophenone is ^3A, and the total symmetries (spin + orbital) of the triplet sublevels $|\tau_x\rangle$, $|\tau_y\rangle$ and $|\tau_z\rangle$ are ^3B, ^3B, and ^3A, respectively.

The angle by which the ZF tensor is rotated varies with substituent. This implies that the angle of conrotatory twist of the phenyl rings is also varying. This effect is also evidenced by the observed trend in the E values shown

in Table X. The value of E is seen to increase as the angle by which the spin tensor is rotated decreases. This suggests that in the limit of C_{2v} molecular symmetry for the triplet state an E value of approximately +0.025 cm^{-1} should be observed. Although this interpretation is only tentative, theoretical calculations of this effect would seem to be warranted. The effects of ring twisting and the similarities between the halonaphthalenes and benzophenones are convincing enough to suggest that the simple picture of a localized carbonyl triplet state should be modified.

TABLE X: Correlation between angle of spin tensor rotation and E value

System	θ[a] (deg)	E(cm^{-1})
neat 4,4'-DCBP	$6° \pm 1°$	+0.02362
4,4'-DBBP/DDE	$9° \pm 2°$[b]	+0.02218
4,4'-DCBP/DDE	$18° \pm 2°$[b]	+0.02067
4,4'-DFBP/DDE	$19° \pm 2°$[b]	+0.01821
^{12}C-BP/DDE	$20° \pm 2°$[b]	+0.01739

[a] θ is defined as the angle between the y' axis of the ZF tensor and the plane of the carbonyl group. θ = 0 corresponds to coplanarity of the phenyl rings and the carbonyl group.

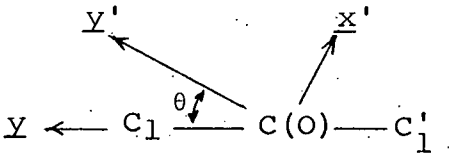

[b] The possible error of $\pm 2°$ results from the inability to distinguish the carbonyl y axis (+ or - 1°40') corresponding to the ZF tensor y' axis whose angle was measured.

IV. HYPERFINE AND QUADRUPOLE INTERACTIONS IN THE ODMR SPECTRA OF BENZOPHENONES

A. ^{13}C-BP in DDE

At low microwave power (0.15 mW), the electron spin transitions in the ODMR spectra of ^{13}C-BP exhibit a doublet structure for most orientations of the crystal in the magnetic field. For example, Fig. 17 shows some first-derivative spectra taken in the three principal axis orientations of the $\underline{D}$ tensor using field modulation techniques. Similar structure was observed in ^{12}C-BP; however, it differed from the ^{13}C-BP observations in two respects. First, an approximately 1:2:1 triplet structure was observed in ^{12}C-BP corresponding to a 10-12 G splitting which remained fairly constant as a function of crystal orientation. Second, this structure was only observed using maximum microwave power (~150 mW). As the power was decreased, the two wing lines of the 1:2:1 pattern rapidly lost intensity relative to the center line, and only a single line was observed at power levels comparable to those used to obtain the spectra in Fig. 17. In addition, at intermediate power levels (~5-10 mW), a second triplet structure was observed in the ^{12}C-BP ODMR lines with a splitting of 5-6 G. The wing

Figure 17. Observed ^{13}C-BP hyperfine splittings in the principal axis orientations of the fine-structure tensor. In the $\underline{H} \| \underline{x}'$ and $\underline{y}'$ orientations the observed ^{13}C coupling constants are 14.5 and 6.4 G, respectively. In the $\underline{H} \| \underline{z}'$ orientation, a ^{13}C coupling constant of 6.0 G was estimated from the linewidth.

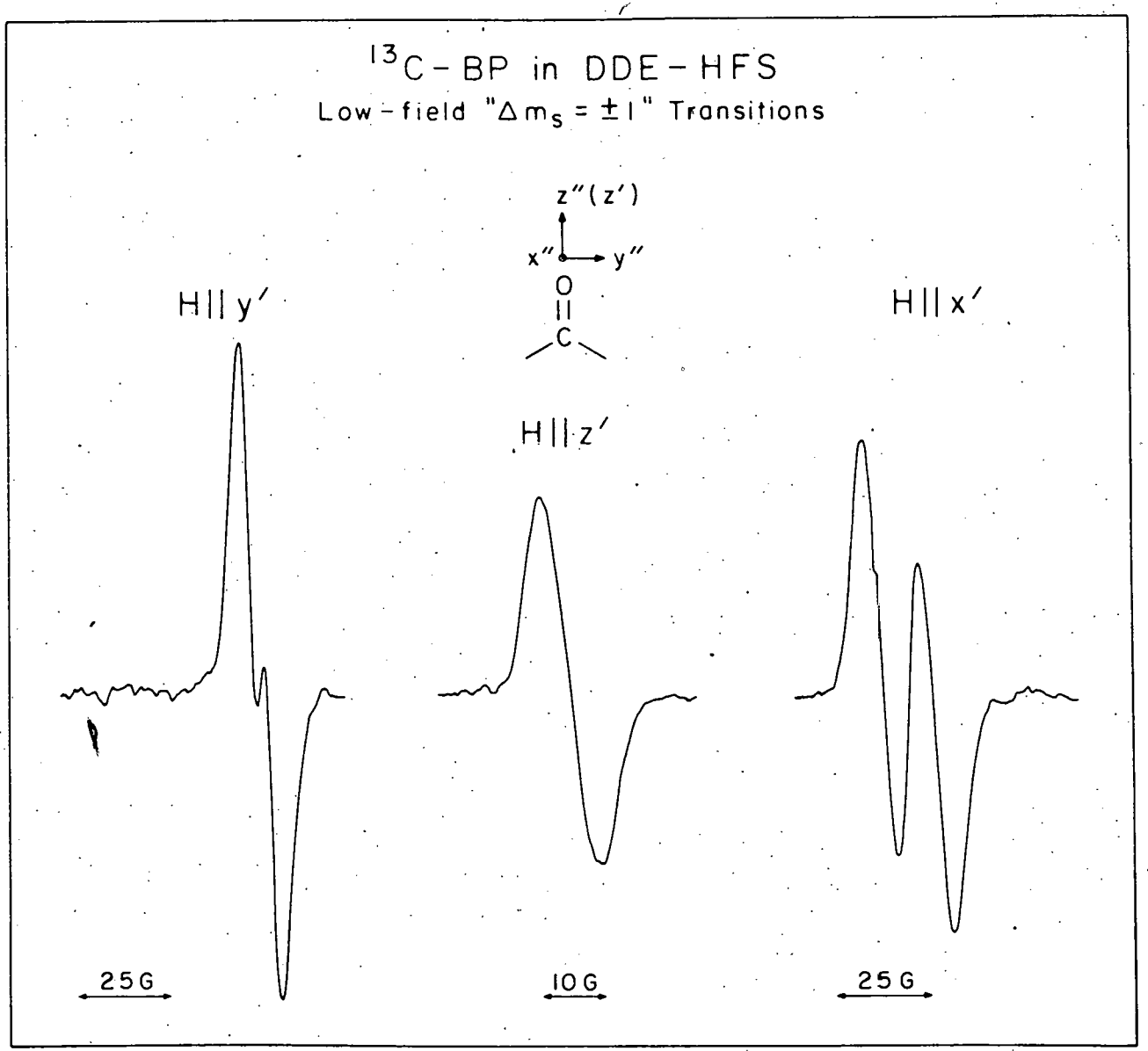
^{13}C-BP in DDE-HFS
Low-field "$\Delta m_s = \pm 1$" Transitions
z"(z')
x"
y"
O
C
H||y'
H||z'
H||x'
25G
10G
25G

lines of this pattern also disappeared rapidly as the microwave power was reduced.

The power sensitivity of the additional structure in the ^{12}C-BP ODMR spectra suggests that it is due to forbidden transitions involving simultaneous electron and nuclear (e.g., proton) spin flips. In contrast, the ^{13}C-BP doublet pattern was insensitive to power (although better resolution was obtained at low power) and the magnitude of the splitting was highly sensitive to orientation. Thus, it was concluded that the additional structure in the ^{13}C-BP ODMR spectra is due to allowed transitions of the type "$\Delta m_S = \pm 1$, $\Delta m_I = 0$" which are split by an electron-nuclear hyperfine interaction involving the ^{13}C ($I=\frac{1}{2}$) nucleus.

The spectra for the $\underline{H}||\underline{x}'$ and $\underline{y}'$ orientations shown in Fig. 17 were computer simulated using coupling constants of 14.5 ± 0.4 ($A_{x'}$) and 6.4 ± 0.2 G ($A_{y'}$), respectively. From the single line observed in the $\underline{H}||\underline{z}'$ orientation, a ^{13}C coupling constant of 6.0 ± 1 G ($A_{z'}$) was estimated using the linewidth observed in ^{12}C-BP at the same orientation and microwave power level. These values may then be used to obtain estimates of the principal values of the ^{13}C hyperfine tensor ($\underset{\sim}{A}^C$) in ^{13}C-BP.

It would seem reasonable to assume that the principal axes of $\underset{\sim}{A}^C$ ($\underline{x}''$, $\underline{y}''$, $\underline{z}''$), are directed along the p_x, p_y, and p_z orbitals of the carbonyl carbon as defined at the top of Fig. 17. With this assumption, these axes should be nearly coincident (± 2) with the $\underline{a}$, $\underline{b}$, and $\underline{c}$ crystal axes of DDE, respectively, if the ^{13}C-BP enters the host substitutionally. Thus, the ^{13}C coupling constant observed with $\underline{H}||\underline{z}'$ (6 G) corresponds to the $A_{z''z''}$ principal element of $\underset{\sim}{A}^C$; however, the coupling constants $A_{x'}$ and $A_{y'}$ are not principal values of $\underset{\sim}{A}^C$ since the principal axes $\underline{x}'$ and $\underline{y}'$ of $\underset{\sim}{D}$ do not lie along $\underline{a}$ and $\underline{b}$.

Figure 18 shows the angular dependence of the ^{13}C hyperfine splitting in the low-field "$\Delta m_S = \pm 1$" transition of one of the two magnetically-inequivalent molecules in the $\underline{ab}$ plane. The closed circles represent coupling constants which were obtained by computer simulation of observed spectra showing resolved splittings and are accurate to better than 1.0 G. The coupling constants indicated by open circles were obtained by computer simulation using the linewidths observed for ^{12}C-BP in the same orientations and are significantly less accurate (± 2 G). The major source of error is the inability to accurately account for the additional width due to the forbidden transitions mentioned previously since

Figure 18. Observed orientational dependence of the ^{13}C hyperfine splitting for the lowest triplet state of ^{13}C-BP in the ab crystallographic plane. The data plotted are for the low-field "$\Delta m_S = \pm 1$" ODMR transition. Solid circles represent coupling constants obtained by computer simulation of the experimental spectrum. Open circles represent estimates based on the difference in line-widths observed for ^{13}C-BP and ^{12}C-BP in identical orientations.

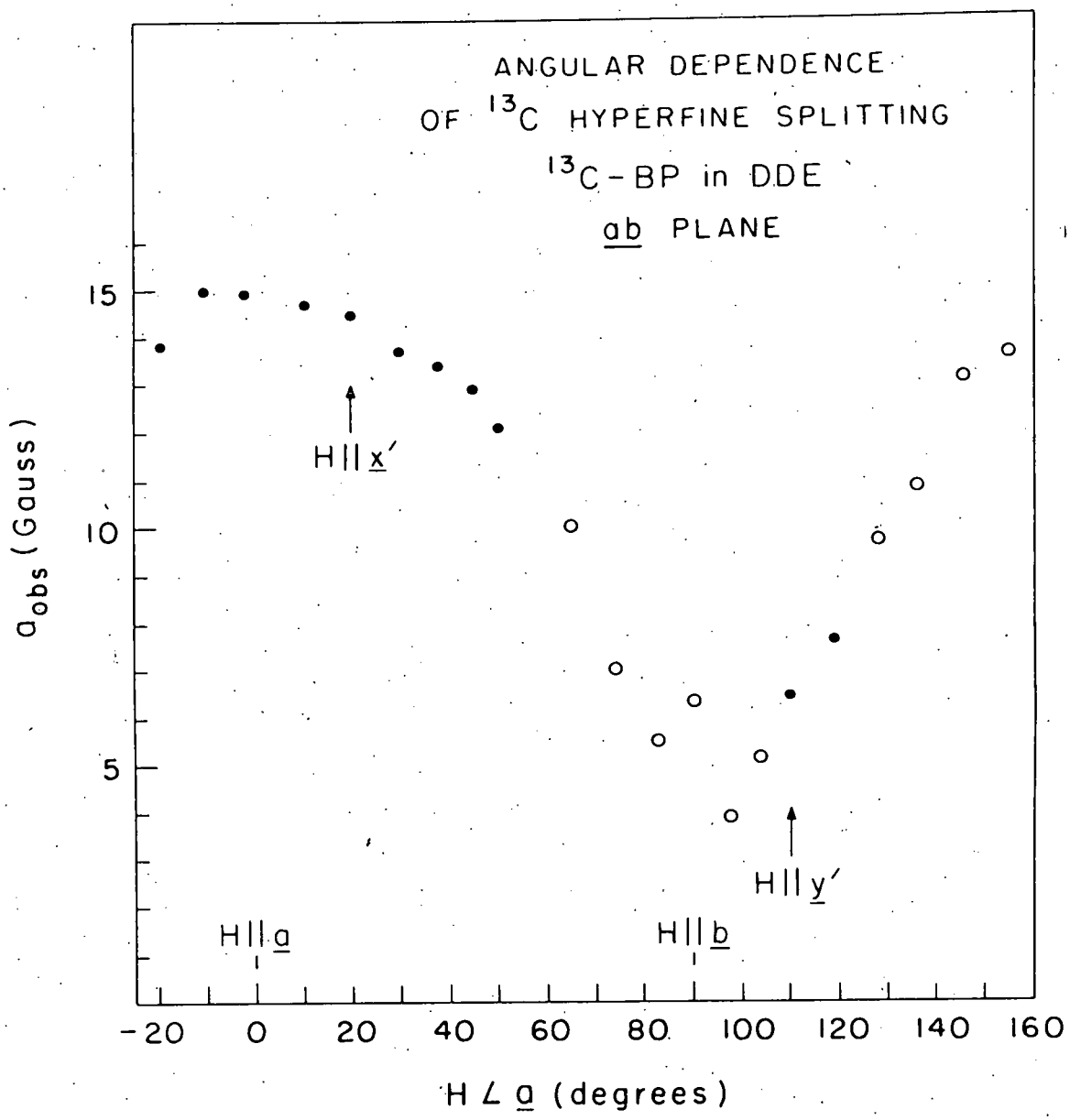
ANGULAR DEPENDENCE
OF ^{13}C HYPERFINE SPLITTING
^{13}C-BP in DDE
ab PLANE
15
10
5
a_{obs} (Gauss)
H || x′
H || y′
H || a
H || b
-20
0
20
40
60
80
100
120
140
160
H ∠ a (degrees)

they do tend to distort the lineshapes even at low power. However, Fig. 18 indicates that the extrema in the observed hyperfine splittings (~15 and ~4 G) occur near the a and b crystal axes, respectively. This is in agreement with axis system defined at the top of Fig. 17 and the crystal structure data (cf., Table IIA) and verifies the assumption that the benzophenones are incorporated substitutionally in the DDE crystal. Furthermore, it confirms that rotation of the $\underset{\sim}{D}$ tensor observed in the ab plane is intrinsic to the molecule and not due to a rotation of the molecule as a whole.

In order to account for the observed structure in the ODMR spectra of ^{13}C-BP, we consider the somewhat more general spin Hamiltonian

$$\mathcal{H}_S = \mathcal{H}_{ZF} + \mathcal{H}_Z + \mathcal{H}_{HF} + \mathcal{H}_Z' \qquad (49)$$

which takes into account the effects of the nuclear hyperfine interaction ($\mathcal{H}_{HF}$) and the nuclear Zeeman interaction ($\mathcal{H}_Z'$) in addition to those terms previously discussed. $\mathcal{H}_Z'$ is small in comparison to spectral resolution and is not considered further. The nuclear hyperfine Hamiltonian is of the form[16]

$$\mathcal{H}_{HF} = \underline{S} \cdot \underset{\sim}{A} \cdot \underline{I} \qquad (50)$$

which becomes, when referred to its principal axes,*

$$\mathcal{H}_{HF} = A_{xx}S_xI_x + A_{yy}S_yI_y + A_{zz}S_zI_z \qquad (51)$$

where A_{xx}, A_{yy}, and A_{zz} are the principal values of $\underset{\sim}{A}$ and contain contributions from both Fermi contact (isotropic) and dipole-dipole (anisotropic) interactions.

Since the hyperfine splittings observed in the ODMR spectra of ^{13}C-BP along principal axes of $\underset{\sim}{D}$ are more accurate than those observed for other orientations, these values were used to determine the principal values of $\underset{\sim}{A}^{C}$. It is also noted that in these orientations the effects of $\mathcal{H}_{ZF}$ on the magnitude of the hyperfine interaction are simplified. Recalling that since $\mathcal{H}_{ZF}$ and $\mathcal{H}_S$ are comparable in magnitude, the electron spins are not completely decoupled from the molecular framework. Thus, the electron spin states are not the high-field spin states $|+1\rangle$, $|0\rangle$, and $|-1\rangle$ but rather are (cf., Eq. (23))

---

*Since the principal axes of the ^{13}C hyperfine interaction (x", y", z") are observed to be coincident with those of the carbonyl group (x, y, z), the double-primed notation has been discarded.

$$|+\rangle = \cos\phi\ |+1\rangle - \sin\phi\ |-1\rangle$$
$$|0\rangle = |0\rangle$$
$$|-\rangle = \sin\phi\ |+1\rangle + \cos\phi\ |-1\rangle \qquad (52)$$

with, for example, $\tan 2\phi = (Y-X)/2g_{ZZ}\beta H$ for the orientation $\underline{H} \| \underline{z}'$. Thus, the average value of m_S in the states $|+1\rangle$ and $|-1\rangle$ is reduced from ± 1 to $\cos 2\phi$[6] and the observed hyperfine parameters are smaller by a factor of $\cos 2\phi$. Using the data in Tables IV and IX one finds the true ^{13}C hyperfine coupling constants to be

$$A_{x'} = 15.4 \text{ G},$$
$$A_{y'} = 6.8 \text{ G},$$

and

$$A_{z'} = A_{z\,z} = 6.0 \text{ G}.$$

It was considered desirable to carry out an exact diagonalization of the Hamiltonian given by Eq. (49); however, some approximations were made to simplify the calculation. Since $\mathcal{H}_{ZF}, \mathcal{H}_Z >> \mathcal{H}_{HF}, \mathcal{H}_{HF}$ was treated as a perturbation of the eigenvalues of

$$\mathcal{H}_S^o = \mathcal{H}_{ZF} + \mathcal{H}_Z \qquad (15)$$

and hyperfine terms which give rise to off-diagonal elements between the electron spin states were neglected. Since the

observed ^{13}C coupling constants were corrected for the actual expectation value of m_S, the electron spin states were assumed to be the strong-field states $|+1\rangle$, $|0\rangle$, and $|-1\rangle$ to simplify calculation of the matrix elements. Furthermore, only those elements of the Hamiltonian which were diagonal in S_z were considered. These approximations allow one to "avoid" the fact that the principal axes of $\mathcal{H}_S^o$ and $\mathcal{H}_{HF}$ are different.

Since we are particularly interested in the angular dependence in the xy hyperfine plane (x'y' plane of $\underset{\sim}{D}$), transformation of $\mathcal{H}_{HF}$ from its principal axis system by rotation about the z (=z') axis gives

$$\mathcal{H}'_{HF} = A_{xx}S_zI_z \cos^2\theta + (A_{xx}-A_{yy})S_zI_x \sin\theta\cos\theta + A_{yy}S_zI_z \sin^2\theta \tag{54}$$

where θ is the angle the field makes with the x axis of the hyperfine tensor. Diagonalization of $\mathcal{H}'_{HF}$ gives the effective hyperfine splitting

$$A^2_{eff} \approx A^2_{xx} \cos^2\theta + A^2_{yy} \sin^2\theta \tag{55}$$

for the xy plane of $\underset{\sim}{A}^C$. More rigorous calculations are planned in order to treat the effects of the ZF splitting on the hyperfine interaction for orientations in the xy plane. However, using this simplified expression, the principal values A_{xx} and A_{yy} can be estimated.

The observed orientational dependence of the ^{13}C hyperfine splitting fixes the value 0 for which A_x, and A_y, were observed. Applying Eq. (55) for the two corresponding orientations, the A_{xx} and A_{yy} principal elements of the ^{13}C hyperfine tensor were easily calculated. Thus, the diagonal form of $\underset{\sim}{A}^C$ is given by

$$\underset{\sim}{A}^C = \begin{bmatrix} A_{xx} & & \\ & A_{yy} & \\ & & A_{zz} \end{bmatrix} = \begin{bmatrix} 16.3 & & \\ & 4.1 & \\ & & 6.0 \end{bmatrix} \quad (56)$$

where the signs of the elements are assumed to be positive. Recalling that $\underset{\sim}{A}^C$ includes both isotropic and anisotropic contributions, it is of the form

$$\underset{\sim}{A}^C = a^C \cdot \underset{\sim}{1} + \underset{\sim}{T}^C \quad (57)$$

where a^C is the isotropic component and $\underset{\sim}{T}^C$ is the dipolar tensor of the hyperfine interaction. Since $\underset{\sim}{T}^C$ is traceless, $\underset{\sim}{A}^C$ readily reduces to

$$\underset{\sim}{A}^C = a^C \cdot \underset{\sim}{1} + \begin{bmatrix} t_{xx} & & \\ & t_{yy} & \\ & & t_{zz} \end{bmatrix} = 8.8 + \begin{bmatrix} 7.5 & & \\ & -4.7 & \\ & & -2.8 \end{bmatrix} \quad (58)$$

If unit spin density were present in the $\pi(p_x)$ orbital on the carbonyl carbon, one would expect the isotropic

component to be the order of 39 G.[87] The observed $a_{\approx}^{C} \approx 8.8$ G suggests that the π spin density (ρ_C^{π}) on the carbonyl carbon is of the order of 0.23. However, this value also reflects contributions from spin density on neighboring atoms which can only be determined if the signs and magnitudes of these spin densities are known. Thus, we turn to the anisotropic part of $\underset{\sim}{A}^{C}$ in order to obtain a second estimate of ρ_C^{π}.

As can be seen in Eq. (58), the experimentally observed ^{13}C dipolar tensor deviates somewhat from axial symmetry. Again, this reflects the presence of unpaired electron spin density on neighboring atoms and involves delocalization and σ-π polarization within the $\backslash C{=}O /$ fragment. Thus, the experimental tensor ($\underset{\sim}{T}^{C}$) can be considered as a sum of dipolar contributions of the form

$$\underset{\sim}{T}^{C} = \underset{\sim}{B}_C^{\pi_x} \rho_C^{\pi_x} + \underset{\sim}{B}_C^{\pi_y} \rho_C^{\pi_y} + \underset{\sim}{B}_O^{\pi} \rho_O^{\pi} + \underset{\sim}{B}_O^{n} \rho_O^{n} + \underset{\sim}{B}_{CO}^{\sigma} \rho_{CO}^{\sigma} + 2\underset{\sim}{B}_{C'}^{\pi} \rho_{C'}^{\pi} \quad (59)$$

Here, the first two terms are one-center interactions from electron spin density in the p_x and p_y orbitals of the carbonyl carbon. The remaining terms are two-center terms that take into account spin density on atomic centers which are adjacent to the carbonyl group. $\underset{\sim}{B}_O^{\pi} \rho_O^{\pi}$ and $\underset{\sim}{B}_{C'}^{\pi} \rho_{C'}^{\pi}$ represent contributions to $\underset{\sim}{T}^{C}$ from spin density in p_x orbitals of the oxygen and C_1,C_1' carbons of the phenyl rings, respectively. $\underset{\sim}{B}_O^{n} \rho_O^{n}$ represents contributions from electron spin

density in the $n(p_y)$ orbital on oxygen, and $\underset{\sim}{B}^{\sigma}_{CO}\rho^{\sigma}_{CO}$ includes the effect of $\sigma-\pi$ polarization of the C=O σ bond.

Considering first the one-center contributions to $\underset{\sim}{T}^{C}$, we note that spin density in the p_x and p_y orbitals should give rise to axially symmetric tensors of the form (2B,-B,-B) and (-B',2B',-B'), respectively. $\underset{\sim}{B}^{\pi x}_{C}\rho^{\pi x}_{C}$ most assuredly gives rise to the dominant element of $\underset{\sim}{T}^{C}$ as can be seen by examination of Eq. (58). Attempting to explain the deviation of $\underset{\sim}{T}^{C}$ from axial symmetry on the basis of the other one-center term, $\underset{\sim}{B}^{\pi y}_{C}\rho^{\pi y}_{C}$, is clearly inadequate. One notes in Eq. (58) that $|t_{yy}| > |t_{zz}|$. Any significant contribution from the term $\underset{\sim}{B}^{\pi y}_{C}\rho^{\pi y}_{C}$ should lead to the opposite relative magnitudes (i.e., $|t_{yy}| < |t_{zz}|$). Hence, we conclude that $\rho^{\pi y}_{C}\sim 0$.

We next examine the effects of the two-center terms in Eq. (59). It would be a formidable task to determine $\underset{\sim}{B}^{\pi x}_{C}\rho^{\pi x}_{C}$ even if the hyperfine tensors of all neighboring atoms were known. However, it is believed that the main source of the deviation of $\underset{\sim}{T}^{C}$ from axial symmetry is the spin density on the oxygen atom. If one assumes that the excitation is localized on the carbonyl group, then the spin density for the $^3(n,\pi^*)$ state will be in the π^* orbital consisting of both carbon and oxygen atomic orbitals, and in the n orbital localized on oxygen. As will be shown later, a significant

amount of π-electron spin density is delocalized onto the rings. Furthermore, since the ionization potential of oxygen is greater than carbon, simple MO theory predicts that the π* orbital will be mainly carbon in character. Indeed, calculations by Dixon[81] on the $^3(n,\pi^*)$ state of formaldehyde indicate that 67% of the π-orbital spin density is centered on carbon. Hence, we neglect the contribution from spin density in the p_x orbital on oxygen ($\underset{\sim}{B}_O^{\pi}\rho_O^{\pi}$) and consider only the effect of the additional term $\underset{\sim}{B}_O^{n}\rho_O^{n}$ in Eq. (59).

Since the dipolar interaction exhibits a $(3\cos^2\theta-1)/r^3$ † behavior, one can qualitatively predict neighboring atom contributions to $\underset{\sim}{T}^C$ by estimating the signs of this term in different regions of space.[88] One notes that the n orbital of oxygen is in a region where

$$(3\cos^2\theta-1) < 0 \text{ when } \underline{H}\,||\,\underline{x}",$$

and

$$(3\cos^2\theta-1) > 0 \text{ when } \underline{H}\,||\,\underline{z}".$$

When $\underline{H}\,||\,\underline{y}"$, the n orbital extends almost equally over positive and negative regions of $(3\cos^2\theta-1)$ and can be neglected for simplicity. Thus, considering only the additional term $\underset{\sim}{B}_O^{n}\rho_O^{n}$, the experimental dipolar tensor can be approximated as

---

† θ is the angle between the magnetic field and a line joining the two dipoles which are separated by a distance r.

$$\underset{\sim}{T}^{C} \approx \underset{\sim}{B}_{C}^{\pi x}\,\rho_{C}^{\pi x} + \underset{\sim}{B}_{O}^{n}\,\rho_{O}^{n}$$

$$\begin{bmatrix} 7.5 & & \\ & -4.7 & \\ & & -2.8 \end{bmatrix} \approx \begin{bmatrix} 2B & & \\ & -B & \\ & & -B \end{bmatrix} + \begin{bmatrix} -B_{O}^{n} & & \\ & 0 & \\ & & B_{O}^{n} \end{bmatrix} \qquad (60a)$$

which yields the ^{13}C anisotropic hyperfine tensor

$$\begin{bmatrix} 2B & & \\ & -B & \\ & & -B \end{bmatrix} \approx \begin{bmatrix} 9.4 & & \\ & -4.7 & \\ & & -4.7 \end{bmatrix} \qquad (60b)$$

A similar analysis of terms of the form $B_i^{\pi}\rho_i^{\pi}$ (i=O, C_1,C_1') shows that each can contribute to the observed deviation of $\underset{\sim}{T}^{C}$ from axial symmetry. To a first approximation, these contributions only affect the elements t_{yy}, t_{zz} and are of the form (O, $-B^{\pi}$,B^{π}). As a result, the 2B element of Eq.(60b) can be used to reliably estimate the spin density in the p_x orbital of the carbonyl carbon. The principal elements of $\underset{\sim}{B}_{C}^{\pi x}\rho_{C}^{\pi x}$ for a carbon atom bearing unit spin density are (65 G, -32.5 G, -32.5 G).[89] Comparing the 2B elements of the experimental and theoretical tensors, a value of $\rho_C^{\pi} \approx 0.14$ is obtained for the carbonyl carbon.

From the isotropic and anisotropic components of $\underset{\sim}{A}^{C}$, we estimate the π-orbital spin density on the carbonyl carbon to be of the order of 0.2, which is considerably smaller than

expected for an excitation localized on the C=O group. However, this result does support the conclusions of Chapter III. As can be seen, the analysis of the hyperfine interaction is serverely complicated by neighboring atom effects. The analysis of ^{17}O hyperfine interactions should be somewhat simplified since only one neighboring atom need be considered. Attempts to observe ^{17}O hyperfine structure in enriched samples have thus far been unsuccessful. The nature of the spin density distribution in the C=O group requires this information as well as an experimental determination of the spin densities on C_1 and C_1'.

B. 4,4'-DFBP in DDE

Hyperfine interactions involving ring atoms were also observed in the ODMR spectra of triplet benzophenones. For example, Fig. 19 shows some representative spectra taken in two (ZF) principal axis orientations of 4,4'-DFBP using field modulation techniques and low microwave power. In the $\underline{H} \| \underline{z}'$ orientation, a 1:2:1 pattern is observed with a splitting of 9 G which is consistent with a hyperfine interaction involving two equivalent fluorine nuclei. The relative intensities of the two lines in the spectrum denoted by an asterisks were found to be power dependent.

Figure 19. Observed ^{19}F hyperfine splittings in the lowest triplet state of 4,4'-DFBP. A splitting of 9 G is observed for the high-field "$\Delta m_S = \pm 1$" ODMR transition in the $\underline{H}||\underline{z}'$ orientation while an 18G splitting is observed for the low-field transition in the $\underline{H}||\underline{x}'$ orientation. The asterisks indicate forbidden transitions corresponding to simultaneous electron-nuclear spin flips.

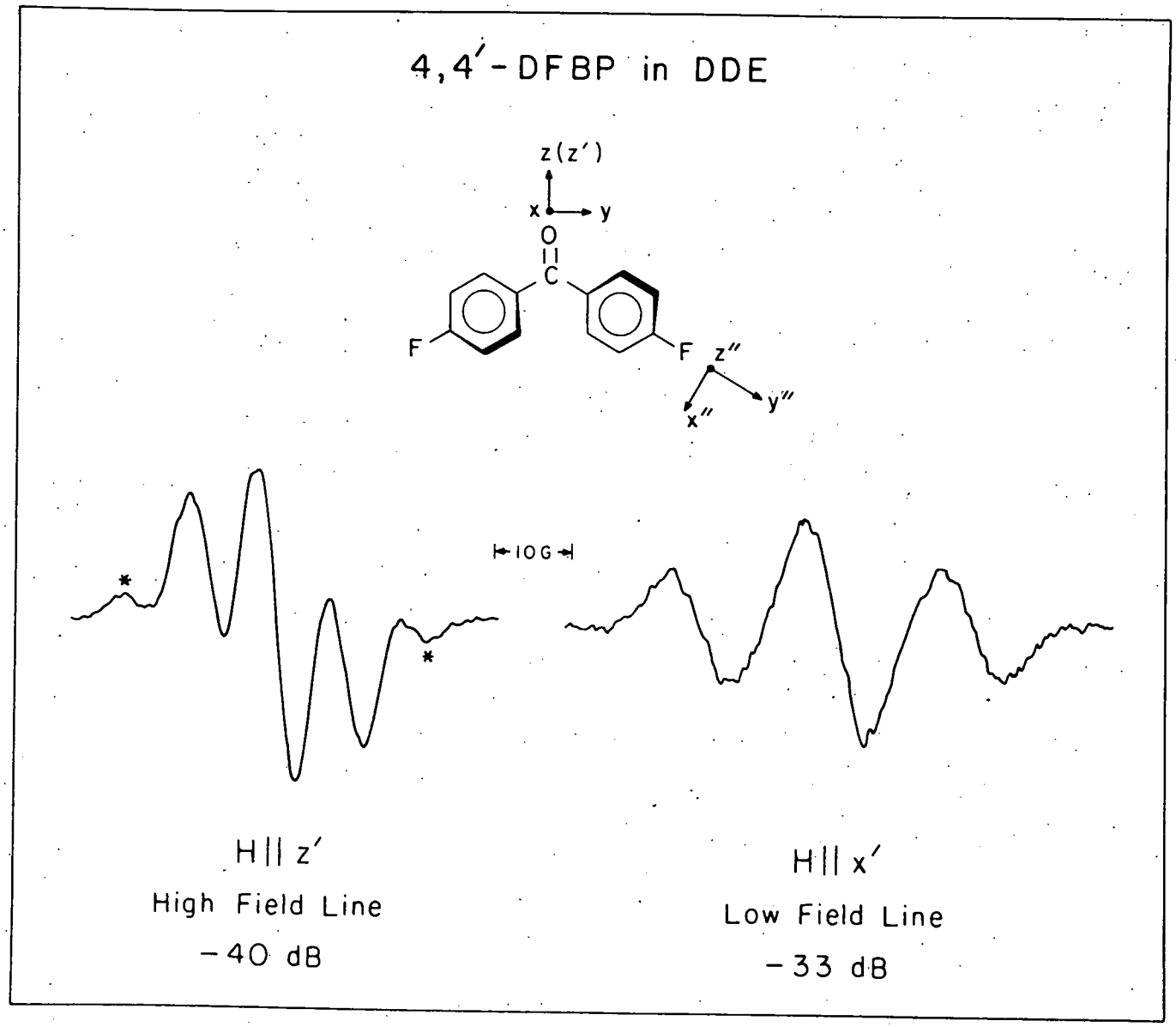
4,4′-DFBP in DDE
z(z′)
x
y
O
C
F
F
z″
y″
x″
10G
H || z′
High Field Line
−40 dB
H || x′
Low Field Line
−33 dB

Thus, these lines are probably forbidden transitions involving simultaneous electron and nuclear spin flips. Transitions of this type have been observed previously in the EPR spectra of triplet quinoxaline and an analysis of the intensities provided an estimate of spin densities even though first-order splittings were unresolved.[90] In the $\underline{H}||\underline{x}'$ orientation of 4,4'-DFBP, the low-field "$\Delta m_S = \pm 1$" transition exhibits a 1:2:1 pattern with a splitting of 18 G. Although a complete orientational study of the hyperfine splittings would be necessary to accurately determine the spin densities in the 4 and 4' ring positions, approximate values can be obtained from the splitting observed in the $\underline{H}||\underline{x}'$ ODMR spectrum.

As in the case of ^{13}C-BP, a nuclear hyperfine term (cf., Eq. (51)) must be included in the spin Hamiltonian which is diagonal in the $\underline{x}''$, $\underline{y}''$, $\underline{z}''$ coordinate system shown at the top of Figure 19. If one assumes that in the $\underline{H}||\underline{x}'$ orientation the field is also parallel to the $\underline{z}''$ axis of the hyperfine tensor, then the observed splitting of 18 G is approximately $A_{z''z''}$. Applying the cos 2ϕ correction (cf. p.111) for the average value of m_S in the states $|+1\rangle$ and $|-1\rangle$ at a magnetic field of 1929 G, the true hyperfine coupling constant is $A_{z''z''} \approx 19.5$ G.

In EPR studies of triplet fluoronaphthalenes, Mispelter et al.[91] derived the fluorine hyperfine tensor for a $\backslash C\text{-}F$ // fragment bearing unit spin density. These were shown to be related to the π spin density on the corresponding carbon atom in terms of an effective coupling tensor

$$\underset{\sim}{A}^{F}_{ii} = \underset{\sim}{B}^{F}_{eff}\ \rho_C^{\pi} \qquad (61)$$

where the principal values of $\underset{\sim}{B}^{F}_{eff}$ are

-24 G along the C-F bond (i=y"),

+193 G normal to fragment plane (i=z"),

-11 G normal to the other two directions (i=x"),

and the $\underset{\sim}{B}^{F}_{eff}$ values include both the isotropic and anisotropic components of the hyperfine splitting.[91] A simple ratio of $A_{z"z"} \approx 19.5$ G for 4,4'-DFBP and $B^{F}_{eff} = +193$ G gives $\rho_C^{\pi} \sim 0.1$ for the 4 and 4' carbon atoms of the phenyl rings. Further, it is clear from the signs and magnitudes of the principal values of $\underset{\sim}{B}^{F}_{eff}$ that $\rho_C^{\pi} \sim 0.1$ represents a lower limit to the spin density in these positions. Thus, this result confirms the conclusion that the triplet excitation is not localized on the carbonyl group in benzophenones and suggests that perhaps half of the π-orbital spin density is located on the phenyl rings.

C. 4,4'-DBBP in DDE

A striking power dependence was observed in the ODMR spectra of 4,4'-DBBP in all orientations. At low microwave power, only the electron spin transitions are observed; however at high microwave power each of these lines is flanked by a pair of satellites which are split symmetrically from the main peak. Figure 20A shows a representative scan of the low field "$\Delta m_S = \pm 1$" transition in the orientation $\underline{H} \| \underline{z}'$ using maximum microwave power (OdB $\sim$ 130 mW). In this case, as in other orientations, the field separation between the satellites is 190 G. Additional structure corresponding to 10 G separations is observed on both satellites when field modulation is employed. This is shown in the extreme left and right portions of Fig. 20B. At low power, when the satellites are unobservable, the electron spin transition (center, Fig. 20B) is observed to consist of three equally-spaced components separated by 10 G with approximate relative intensities 1:2:1. Comparison of the structure of the lower field satellite with that of the electron spin transition indicates each satellite is in fact composed of two transitions which exhibit similar structure to that observed in the main line.

Figure 20. Quadrupole and hyperfine structure observed in the low-field ODMR transition of 4,4'-DBBP in the $\underline{H} \parallel \underline{z}'$ orientation. (A) Electron spin transition and quadrupole satellites obtained by amplitude modulation of microwave power (OdB). (B) Higher resolution trace of (A) obtained by field modulation showing a 10 G bromine ($^{79}Br + ^{81}Br$) hyperfine splitting. The dashed lines indicate the centers of the ^{79}Br and ^{81}Br quadrupole satellites which are separated from the main line by 97 and 82 G, respectively.

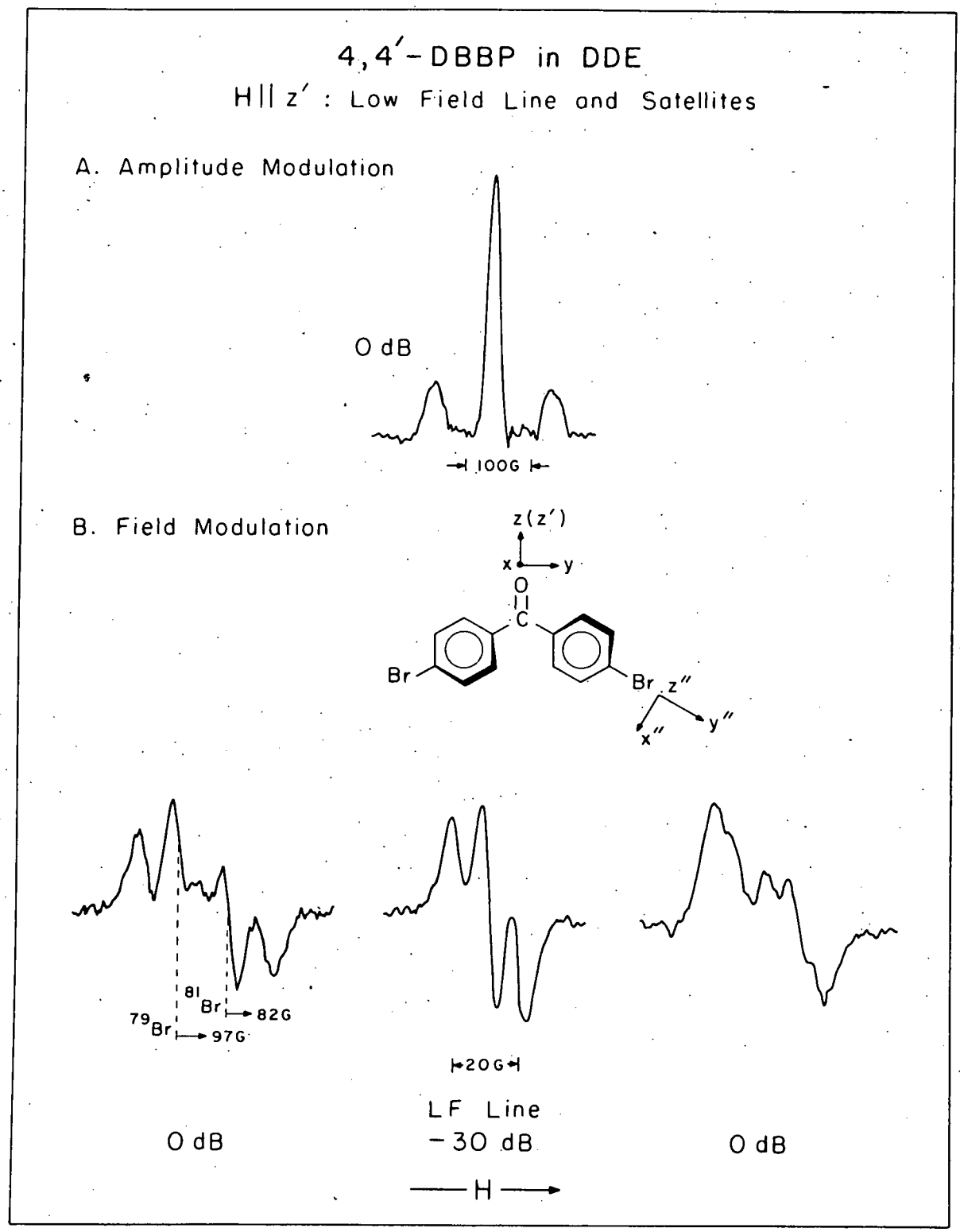
4,4′-DBBP in DDE
H || z′ : Low Field Line and Satellites
A. Amplitude Modulation
0 dB
100G
B. Field Modulation
z(z′)
x
y
O
C
Br
Br
z″
y″
x″
81Br
82G
79Br
97G
20G
LF Line
−30 dB
0 dB
0 dB
H

It is apparent that the spin Hamiltonian (Eq. (49)) used in the analysis of the ODMR spectrum of ^{13}C-BP and 4,4'-DFBP is insufficient to account for these observations. Thus, we must consider the more general spin Hamiltonian

$$\mathcal{H}_S = \mathcal{H}_{ZF} + \mathcal{H}_Z + \mathcal{H}_Q + \mathcal{H}_{HF} + \mathcal{H}'_Z \qquad (14)$$

for the additional features. First, one notes that each of the terms $\mathcal{H}_Q$, $\mathcal{H}_{HF}$, and $\mathcal{H}'_Z$; representing the nuclear quadrupole interaction, the nuclear hyperfine interaction, and the nuclear Zeeman interaction, respectively; depend on the nuclear quantum number m_I and the magnitude at the respective interaction constants. Both bromine isotopes (^{79}Br and ^{81}Br) have I=3/2 and possess large nuclear magnetic moments (2.0991 and 2.2626 $eh/2M_pc$, respectively) and quadrupole moments (0.34 x and 0.28 x 10^{-24} cm^2, respectively). In addition, both isotopes are present in approximately equal natural abundance. Hence, it seems reasonable that both $\mathcal{H}_Q$ and $\mathcal{H}_{HF}$ might contribute to the spectrum of 4,4'-DBBP. $\mathcal{H}'_Z$ would be small relative to the spectral resolution and thus was not considered further.

The Hamiltonian $\mathcal{H}_Q$ has the general form[92]

$$\mathcal{H}_Q = \underline{I} \cdot \underset{\sim}{P} \cdot \underline{I} \qquad (62a)$$

and when referred to its principal axes it becomes

$$\mathcal{H}_Q = P_{xx}I_x^2 + P_{yy}I_y^2 + P_{zz}I_z^2 \qquad (62b)$$

which is similar in form to that of the $\underset{\sim}{D}$ tensor (cf., Eq. (7)). Thus, by analogous reasoning, we can set $P_{xx}+P_{yy}+P_{zz}=0$, so that there are only two independent parameters. Then, one can transform Eq. (62b) into an expression analogous to Eq. (9):

$$\mathcal{H}_Q = P_{||}\left\{ I_z^2 - \frac{1}{3}I(I+1) + \frac{1}{3}\eta\,(I_x^2 - I_y^2)\right\} \qquad (62c)$$

where

$$P_{||} = \frac{3P_{zz}}{2} = \frac{3e^2qQ}{4I(2I-1)} \qquad (62d)$$

$$\eta = (P_{xx} - P_{yy})/P_{zz} \qquad (62e)$$

and where Q is the quadrupole moment. For $I = 3/2$, $P_{||} = e^2qQ/4$, and diagonalization of the matrix form of the Hamiltonian $\mathcal{H}_Q$ obtained using an appropriate nuclear spin basis set yields the eigenvalues

$$\begin{aligned} W_{\pm 3/2} &= \frac{e^2qQ}{4}\,(1 + \eta^2/3)^{1/2} \\ W_{\pm 1/2} &= -\frac{e^2qQ}{4}\,(1 + \eta^2/3)^{1/2} \end{aligned} \qquad (63)$$

Thus, each electron spin sublevel is split into two degenerate pairs, one pair with $m_I = \pm 3/2$ and the second with $m_I = \pm 1/2$. Each of the "$\Delta m_S = \pm 1$" transitions is therefore split into

four lines by the quadrupole interaction. Two are "allowed" transitions of the type "$\Delta m_I = 0$" which are degenerate in first order and are not affected by the quadrupole interaction. Two are "forbidden" with "$\Delta m_I \neq 0$" but are not degenerate and in first order are symmetrically displaced from the allowed transition by $\pm e^2qQ/2$.

The field positions indicated by the dashed lines on the lower field satellite in Fig. (20B) were assigned as "$\Delta m_I \neq 0$" transitions of the two bromine isotopes. The separations of these lines from the allowed transitions are 97 G for ^{79}Br and 82 G for ^{81}Br. Thus, assuming $\eta = 0$, the values of the nuclear quadrupole coupling constants (e^2qQ/h) of ^{79}Br and ^{81}Br in the lowest triplet state of 4,4'-DBBP are estimated to be 544 and 460 MHz, respectively. The ratio of the two is 1.182, in excellent agreement with the ratio of the respective quadrupole moments.

Next, we consider hyperfine interactions with the two bromines of 4,4'-DBBP as a possible source for the additional structure in the main line and its satellites. In the orientation $\underline{H} \| \underline{z}'$, the field is in an arbitrary, but equivalent, position with respect to the principal axes of the hyperfine tensor defined at the top of Fig. 20B when one considers the conrotatory displacement of the phenyl

rings. However, recalling that the ZF tensor axes of 4,4'-DBBP are rotated from the a and b crystallographic axes by only 9°, the approximation that the rings are coplanar with the carbonyl group should provide a reasonable simplification for estimating the magnitude of the hyperfine interaction. Using this approximation in the orientation $\underline{H}||\underline{z}'$, the field lies in the $\underline{x}''\underline{y}''$ plane and makes an angle of $\sim 60^\circ$ with each of the two C-Br fragments which are magnetically equivalent with a total spin of three. Hence, one predicts that a 7-line hyperfine pattern should be observed. However, only three are observed experimentally.

To see why this is the case, one must diagonalize the spin Hamiltonian consisting of $\mathcal{H}_Q$ and $\mathcal{H}_{HF}$. In a recent study of bromine hyperfine interactions in sym-tetrabromobenzene (TBB) in durene,[93,94] such calculations were carried out for various orientations of the magnetic field in the $\underline{x}''\underline{y}''$ plane. It was found that, at an angle of 60° with respect to the C-Br bond, the four hyperfine components of a single C-Br fragment collapse into two nearly degenerate pairs. Thus, the allowed transition of triplet 4,4'-DBBP, with two C-Br fragments, should exhibit two overlapping doublets with nearly equal spacing, yielding a 1:2:1 hyperfine pattern. This is consistent with the spectrum shown in Figure 20B.

The calculations[94] also show that the "forbidden" satellites should exhibit a two-line hyperfine pattern in all orientations of the C-Br fragment in this plane. Thus, both the ^{79}Br and ^{81}Br satellites of triplet 4,4'-DBBP should consist of a 1:2:1 pattern. Since the difference in field positions of the satellites of ^{79}Br and ^{81}Br (15 G) is somewhat larger than the observed hyperfine splitting (10 G), the center components are broadened and not well resolved. This effect is more prominent in the satellites on the high field side of the allowed transition since the magnitude of the hyperfine interaction is somewhat larger for these satellites than that for the satellites appearing on the low field side. The fact that the hyperfine structure appearing in the main line and satellites of 4,4'-DBBP are in good qualitative agreement with the TBB analysis indicates that spin densities determined using this orientational approximation should be reasonable estimates of the π spin density in the 4 and 4' ring positions. The agreement supports the conclusion that the rotation of the axes of the ZF tensor in the ab plane is accompanied by a change in conformation of the phenyl rings.

Estimates of the spin densities in the 4 and 4' ring positions of 4,4'-DBBP can also be determined from direct comparison with the results in triplet TBB. In TBB a 27 G* hyperfine splitting was observed for this orientation at a field of 2500 G corresponding to a spin density of 0.25 in the 1, 2, 4, and 5 ring positions. The 10 G* splitting observed in 4,4'-DBBP at 2146 G therefore indicates $\rho^{\pi} \sim 0.1$ in the 4 and 4' ring positions. These are in good agreement with those estimated from the hyperfine splittings observed in 4,4'-DFBP.

Considering the amount of spin density of the 4 and 4' ring positions, it is not surprising that heavy-atom substituents produce second-order SO contributions to the energies of the spin sublevels in the lowest triplet state of benzophenones. It is clear that the $^3(n,\pi^*)$ state cannot be considered in terms of a localized excitation. However, it is not yet clear whether such delocalization is an intrinsic property of an "n,π^*" state, or whether such states are better described by a linear combination of molecular orbitals which includes the group orbitals of the phenyl rings. The experimental ODMR results indicate that this class of excited state must be scrutinized more closely by theoreticians and experimentalists.

---

*Corrected for the average value of m_S in weak fields.

V. LEVEL ANTICROSSING AND CROSS-RELAXATION EFFECTS.

A. Principles of Level Crossing, Level Anticrossing, and Cross-Relaxation

1. Level Crossing

When two or more energy levels of an atomic or molecular system cross as a function of an external parameter, the physical properties of the system may change in the crossing region. Wood and Ellet[95] and Hanle[96] observed that the polarization and intensity of the resonance fluorescence of Hg vapor changed significantly when a magnetic field of 2 G was applied. This was explained in terms of a ZF level crossing (LC) (Hanle effect) of the three Zeeman components of the Hg $^3P_1$ state. The quantum mechanical explanation of the Hanle effect was later provided by Breit[97] who showed these changes were the result of coherent coupling of the Zeeman components by the time-dependent field of the exciting radiation. Since then LC effects have been observed in the presence of a magnetic field as well and have proved to be an important technique for studying the energies and lifetimes of atomic[98] and molecular[99] systems in the gas phase.

In the triplet state of benzophenone, a LC effect might be expected with the magnetic field aligned parallel the $\underline{x}'$ and $\underline{z}'$ axes of the fine-structure tensor (cf. Fig. 12). However, two complications arise that make this improbable. First, the von Neumann and Wigner non-crossing rule[100] states that two levels with the same symmetry are forbidden from crossing as a function of a single external parameter since a perturbation always exists which will lead to a mutual repulsion of the two states. If the molecular symmetry of triplet BP were accurately C_{2v}, then one would expect level crossings to occur since the two crossing levels ($|0\rangle$ and $|-1\rangle$ with $\underline{H}||\underline{x}'$, $|+1\rangle$ and $|0\rangle$ with $\underline{H}||\underline{z}'$) belong to different representations of the symmetry group, i.e.

$\underline{H}||\underline{x}'$

$$|+1\rangle \subset B_2;\ |0\rangle \subset B_1;\ |-1\rangle \subset B_2$$

$\underline{H}||\underline{z}'$

$$|+1\rangle \subset A_2;\ |0\rangle \subset A_1;\ |-1\rangle \subset A_2$$

However, it has been shown previously that the molecular symmetry of triplet BP is C_2; hence, the two crossing

levels transform identically:

$\underline{H} \| \underline{x}'$

$$|+1\rangle \subset B; \quad |0\rangle \subset B; \quad |-1\rangle \subset B$$

$\underline{H} \| \underline{z}'$

$$|+1\rangle \subset A; \quad |0\rangle \subset A; \quad |-1\rangle \subset A$$

Thus, because of the non-crossing rule, the level crossings in the $\underline{x}'$ and $\underline{z}'$ orientations become level anticrossings.

Even if the molecule in the crystal had C_{2v} symmetry, the crossing of the triplet sublevels would be very unlikely in an actual experiment since a small deviation in orientation will introduce a matrix element between the states which are involved in the crossing. For a crossing to occur, the energy differences between the two states must be comparable to or smaller than the average width of the states caused by radiative and non-radiative decay. Since the lifetimes of the triplet sublevels of benzophenone are of the order of msec,[53-55] the off-diagonal matrix elements introduced by misalignment must be less than 10^{-3} Hz. Such a situation would

occur only when the angle between the magnetic field and a principal axis is smaller than 10^{-5}degrees. Thus, it is highly unlikely that the interference effects associated with a level crossing could be observed in the phosphorescence from an organic crystal.

2. Level Anticrossing

When two states that are expected to cross are coupled by a perturbation, an anticrossing situation arises which may also lead to changes in the physical properties of the system in the level anticrossing (LAC) region. Nowhere is this more apparent than in LAC spectroscopy of gas phase systems,[101,102] where the signals observed are presumed to be the result of (incoherent) state mixing in an avoided crossing region. LAC effects have also been observed in the phosphorescence of triplets in organic crystals.[67,103-6] Why this is so can be seen by considering two states ϕ_a and ϕ_b which would cross as a function of magnetic field if the static perturbation $\mathcal{H}_{ab}$ that mixes them were absent. Application of perturbation theory including the static perturbation with matrix element

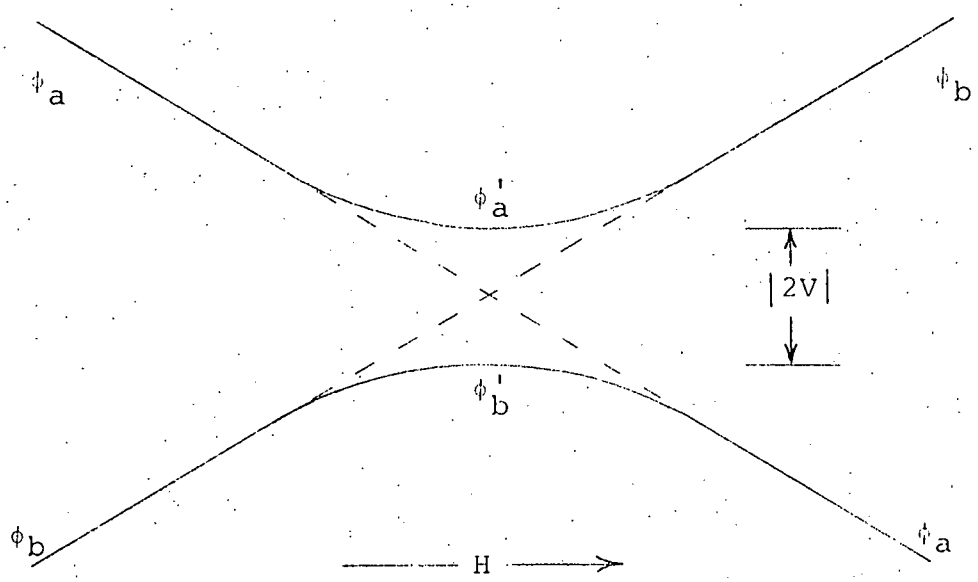

FIGURE 21. Energy level diagram for two states involved in an avoided crossing. Dashed lines indicate the case of a level crossing

$$V = \langle \phi_a | \mathcal{H}_{ab} | \phi_b \rangle \tag{64}$$

gives the eigenvalues $E_{a'}$, $E_{b'}$ (see Fig. 21):

$$E\begin{pmatrix} a' \\ b' \end{pmatrix} = \tfrac{1}{2}(E_a+E_b) \pm \tfrac{1}{2}\left[|2V|^2 + \delta^2\right]^{\frac{1}{2}} \tag{65a}$$

where

$$\delta = E_a - E_b \tag{65b}$$

With proper normalization one finds the eigenfunctions of the perturbed levels to be

$$\phi_{a'} = a\,\phi_a + b\,\phi_b \tag{66a}$$

$$\phi_{b'} = b\,\phi_a - a\,\phi_b \tag{66b}$$

where

$$a = \frac{\left[\left(|2V|^2 + \delta^2\right)^{\frac{1}{2}} - \delta\right]^{\frac{1}{2}}}{2\left(|2V|^2 + \delta^2\right)^{\frac{1}{2}}} \tag{66c}$$

and

$$b = \frac{\left[\left(|2V|^2 + \delta^2\right)^{\frac{1}{2}} + \delta\right]^{\frac{1}{2}}}{2\left(|2V|^2 + \delta^2\right)^{\frac{1}{2}}} \tag{66d}$$

For $\delta = 0$ one obtains

$$E_{a'} - E_{b'} = 2V \tag{67}$$

and $a = b = 1/\sqrt{2}$, that is, the perturbed states are 50:50 mixtures of the unperturbed states at the avoided crossing point. If $\delta >> |2V|$, b approaches 1 while a approaches 0, that is, $\phi_{a'} \rightarrow \phi_b$ and $\phi_{b'} \rightarrow \phi_a$.

We now consider the effect of this perturbation on the populating rates K_a and K_b, depopulating rates k_a and k_b, and radiative rates k_a^r and k_b^r of the unperturbed states ϕ_a and ϕ_b.* When there is no coupling between the states ϕ_a and ϕ_b ($\delta >> |2V|$), the steady-state populations are

$$N_{a'} \approx N_a = K_a/k_a \qquad N_{b'} \approx N_b = K_b/k_b \tag{68}$$

---

*Note that in practice these rates are the magnetic field dependent linear combinations of the corresponding ZF rates and can be calculated if the magnitude and direction of the magnetic field relative to the fine-structure axes are known [cf., Eqs. (32)].

The emission intensity is therefore

$$I = N_a k_a^r + N_b k_b^r = (K_a/k_a) k_a^r + (K_b/k_b) k_b^r \qquad (69)$$

However, in the region of the LAC ($\delta = 0$), where the stationary states are equal mixtures of ϕ_a and ϕ_b, the steady state populations of the perturbed states are

$$N_{a'} = N_{b'} = (K_a + K_b)/(k_a + k_b) \qquad (70)$$

and the emission intensity becomes

$$I' = \frac{K_a + K_b}{(k_a + k_b)} (k_a^r + k_b^r) \qquad (71)$$

Comparison of Eq. (69) and (71) shows that $I \neq I'$. Therefore, a change in the intensity of the emission will be observed at the LAC point.

Assuming that one could resolve the emission from the individual states, dramatic effects would occur in the region of the LAC due to the mixing of states. For example, if the intensity of emission from the unperturbed state ϕ_a was more intense than that from ϕ_b, one would expect to see a gradual decrease in the intensity of emission from ϕ_a and a gradual increase in the intensity from ϕ_b as the LAC region is approached. Furthermore, the two bands would move closer and closer to each other until at the LAC they would be

separated by $|2V|$. At this point $\delta = 0$ and the two transitions exhibit equal intensities. After passing through the LAC region, the two transitions would gradually return to their original relative intensities. Unfortunately, there are no optical methods of sufficient resolution to carry out such an experiment; however, as will be shown later, the ODMR technique provides a unique opportunity for observing such effects.

3. Cross-Relaxation

Thus far, LC and LAC effects have been discussed in terms of properties of the individual spin states of the individual molecules. In actuality, the magnetic interactions between the spins are very important and the system must be described as an ensemble in which each spin feels a local field due to the combined effects of every other spin. The most important effect of these additional interactions is that an additional broadening (beyond that due to the excited state lifetime) of the energy levels will be observed.

Consider a system composed of two identical spins. The precession of one spin about $\underline{H}_o$ produces an oscillating field perpendicular to $\underline{H}_o$ which can reorient the other spin.

This shortens the lifetime of the spins and therefore broadens the individual states owing to the Heisenberg uncertainty principle. This effect is called homogeneous broadening and in the case of the spin-spin interaction can be related to a spin-spin relaxation time T_2. Although spin-lattice relaxation also produces homogeneous width, the results presented earlier indicate T_1 to be longer than the excited state lifetimes (msec). T_2, on the other hand, is probably as short as microseconds [108] in the systems studied in this work. Thus, the width (~MHz) of the states is dominated by the spin-spin interaction. Again, level crossing effects should be absent since T_2 is considerably less than the phosphorescence lifetimes - spin diffusion occurs more rapidly than photon emission and destroys the phase coherence necessary for a level crossing effect. LAC effects, however, might still be observed since the width due to the spin-spin interaction can easily be less than the minimum separation of the two anticrossing states ($|2V|$).

The weakly interacting ensemble of identical spins can be described in a thermodynamic way. For example, two spins can exchange Zeeman energy through a flip-flop process in which one spin α is converted to β while, simultaneously, the second spin β becomes α in an energy-conserved process. In an ensemble of identical spins, the

flip-flop processes tend to bring the spin system into internal equilibrium in a time T_2. At equilibrium a spin temperature, T_S, can be defined by the relation[107]

$$N_\alpha/N_\beta = \exp \frac{E_\beta - E_\alpha}{kT_S} \tag{72}$$

where N_α and N_β are the populations, and E_α and E_β the energies of the α and β spin states, respectively. This relation only holds when $T_2 \ll T_1$, otherwise the spin system will come into thermal equilibrium with the lattice.

When a system consists of spins with $S > \frac{1}{2}$, more than two states result, and a spin temperature can be similarly defined for each pair of states. Consider two such pairs which at some external field are separated by different energies. The two separate spin systems can each be in internal equilibrium (separately) with two different spin temperatures, T_{S_1} and T_{S_2}, since there is no energy conserving process leading to direct contact between them. However, at some other magnetic field the energy separation of the two pairs may become equal within the widths of the states, and flip-flop processes can bring the two spin systems into equilibrium with each other at a common spin temperature. This process is

called cross-relaxation[109] and is responsible for the observation of steady-state electron-nuclear double resonance (ENDOR) transitions.

It is easily seen that cross-relaxation effects can change the steady-state populations of the spin components of a phosphorescent triplet and thereby affect the steady-state emission intensity. The elegant experiments of Veeman and van der Waals[67,105] showed that cross-relaxation leads to a change in the phosphorescence intensity at magnetic fields where the transition frequencies between the states $|0\rangle \rightarrow |+1\rangle$ and $|+1\rangle \rightarrow |-1\rangle$ are degenerate. Similar effects were also noted when the separation between triplet spin states was the same as the hydrogen atom (shown to be present in their crystals) nuclear spin state as well as typical free radical electron spin state separations.

B. LAC Spectra - Results and Interpretation

LAC spectra were obtained in the absence of microwave using field modulation after the $\underline{H} \| \underline{z}'$ and $\underline{H} \| \underline{x}'$ orientations were located by extremum behavior in ODMR experiments. The phosphorescence intensity of ^{12}C-BP in DDE crystal as a function of magnetic field at 1.6°K is shown in Fig. 22 in the orientation $\underline{H} \| \underline{z}'$ ($\phi=0$). The $\phi=0$ spectrum

Figure 22. Angular dependence of the H||z' LAC spectrum of ^{12}C-BP in DDE at 1.6°K. ϕ is the angle between the $\underline{z}'$ axis and the magnetic field axis.

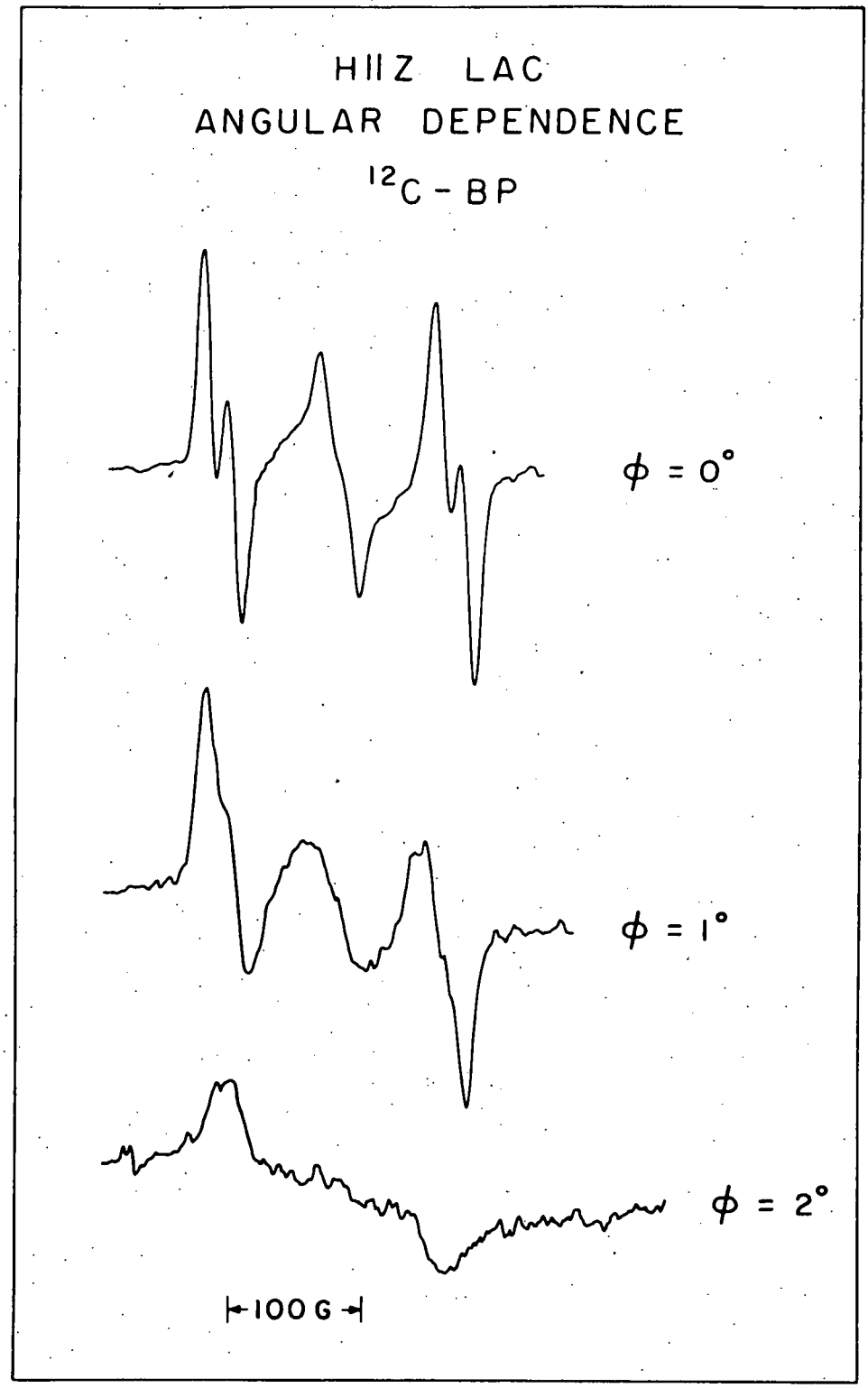
H∥Z LAC
ANGULAR DEPENDENCE
^{12}C - BP
$\phi = 0°$
$\phi = 1°$
$\phi = 2°$
100 G

was obtained by making fine adjustments of the crystal orientation so that the peak-to-peak width of the center line in the spectrum was minimized. One notices that small misorientations lead to a considerable increase in the width and that the center line broadens more rapidly than the satellites which flank it. This was true for all other LAC spectra except 4,4'-DBBP in DDE. The difference in orientational behavior of the center and satellite lines indicates that two different processes are responsible for the observed changes in phosphorescence intensity. The orientational sensitivity of the LAC spectra increased the accuracy of determining two of the three canonical orientations - $\underline{H}||\underline{x}'$ and $\underline{H}||\underline{z}'$. Of course, in the $\underline{H}||\underline{y}'$ orientation no LAC effect is expected (cf. Fig. 12) and none was observed. The LAC spectra for the $\underline{H}||\underline{z}'$ and $\underline{H}||\underline{x}'$ canonical orientations of all the systems studied are shown in Figs. 23 and 24, respectively.

Consider the LAC spectra of ^{12}C-BP in DDE. The positions of the center LAC lines in the two orientations were found to be at magnetic fields where two electron spin sublevels of the triplet state "cross". These field positions are easily calculated from the eigenvalue expressions given in Table VIII and the ZF parameters

Figure 23. $\underline{H}||\underline{z}'$ LAC spectra of benzophenones in DDE at 1.6°K.

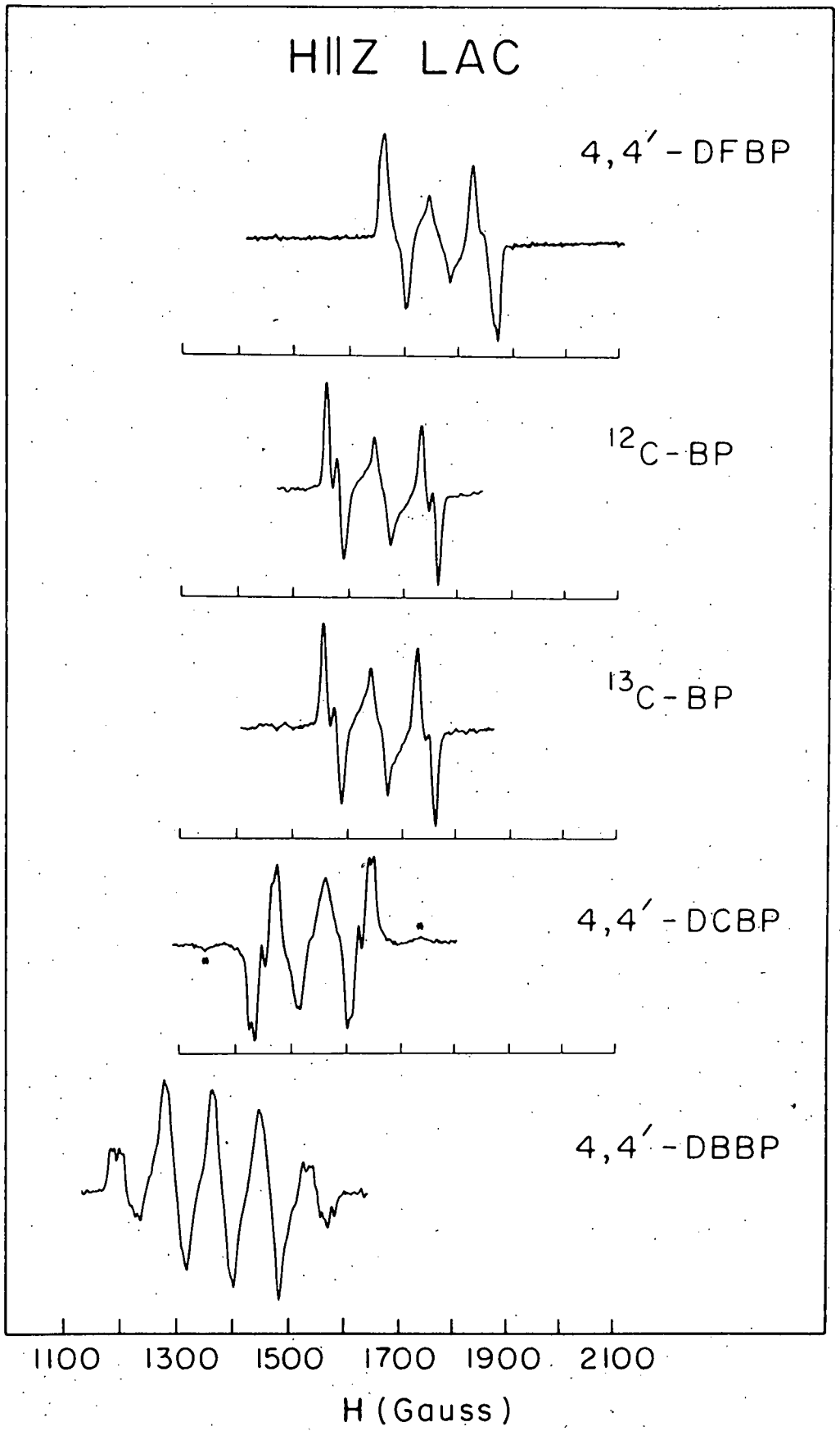
H||Z LAC
4,4′-DFBP
^{12}C-BP
^{13}C-BP
4,4′-DCBP
4,4′-DBBP
1100
1300
1500
1700
1900
2100
H (Gauss)

Figure 24. $\underline{H}||\underline{x}'$ LAC spectra of benzophenones in DDE at 1.6°K.

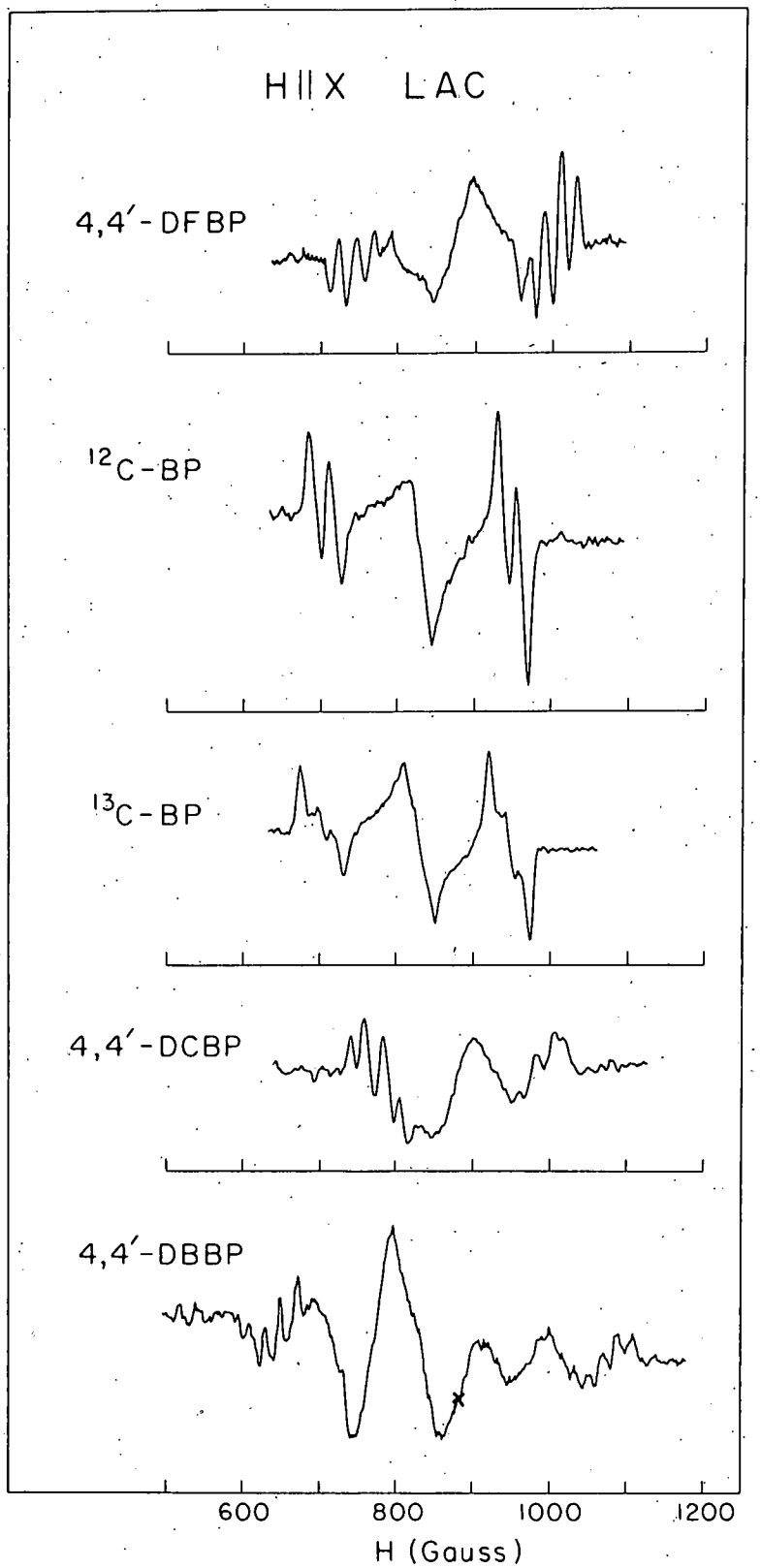
H||X LAC
4,4′-DFBP
^{12}C-BP
^{13}C-BP
4,4′-DCBP
4,4′-DBBP
600
800
1000
1200
H (Gauss)

(cf. Table IX) determined from the ODMR experiments. For example, in the $\underline{H}||\underline{z}'$ orientation, two levels are expected to cross when $W_o=W_+$ and the field position for this crossing is found to be

$$H_C^z = \frac{hc}{g_{zz}\beta}\left[(Z-X)(Z-Y)\right]^{\frac{1}{2}} \tag{73}$$

where X, Y, and Z are in cm^{-1} and H_C in Gauss. Similarly, in the $\underline{H}||\underline{x}'$ orientation,

$$H_C^x = \frac{hc}{g_{xx}\beta}\left[(X-Y)(X-Z)\right]^{\frac{1}{2}}. \tag{74}$$

The agreement between the crossing fields H_C calculated from the ZF parameters and the observed positions of the LAC lines for ^{12}C-BP and other molecules is excellent (see Table XI). Because of this agreement, it appears reasonable that the center lines are indeed LAC in nature; however, a more dramatic proof is found in the ODMR experiments to be discussed later. The width of the LAC signals can be used to determine the magnitude ($|2V|$) of the perturbation leading to the LAC, provided the radiative and total decay rate constants are known.[101] However, the ODMR experiments to be discussed later provide a direct method for obtaining $|2V|$ which requires no knowledge of the decay properties.

TABLE XI: LAC Line field positions and widths in Gauss

System	Expt'l $\underline{H} \| \underline{z}'$	Width	Calc[a] $\underline{H} \| \underline{z}'$	Expt'l $\underline{H} \| \underline{x}'$	Width	Calc[b] $\underline{H} \| \underline{x}'$
neat 4,4'-DCBP	1523	43	1523	——	——	954
4,4'-DCBP/DDE	1535	44	1537	887	47	888
^{13}C-BP/DDE	1657	34	1656	832	39	832
^{12}C-BP/DDE	1662	30	1659	835	28	833
4,4'-DFBP/DDE	1767	40	1764	874	50	877
4,4'-DBBP/DDE	1357	47	1358	(887)	53	880

[a]Calculated from Eq. 73.

[b]Calculated from Eq. 74.

The satellites which exhibit a doublet structure and flank the ^{12}C-BP LAC line symmetrically in both $\underline{H}||\underline{z}'$ and $\underline{H}||\underline{x}'$ orientations are more difficult to interpret. The center-to-center separations of the satellites are found to be 178 G with $\underline{H}||\underline{z}'$ and 242 G with $\underline{H}||\underline{x}'$ and these are much too large to be caused by LAC of hyperfine components. Nearly the same separations were found in the corresponding orientations for the other systems studied, but additional structure is observed in these satellites as shown in Figs. 23 and 24 . Considering the ^{12}C-BP LAC spectrum in the $\underline{H}||\underline{z}'$ orientation, the observed field positions of the satellites including the doublings were found to be 1562, 1575, 1742, and 1762 G. Using the eigenvalue expressions of Table VIII and the ZF parameters of Table IX, the separation between the $|+1\rangle$ and $|0\rangle$ spin levels at these fields were calculated to be 271, 235, 232 and 274 MHz,* respectively. Thus, these signals correspond to cross-relaxation between the triplet state electron spin system and two other spin systems with frequency separations of about 273 MHz and 233 MHz. The nuclear quadrupole coupling constants (e^2qQ) of

---

*Since the error in field measurements is $\pm$3 G, the frequency separations calculated for this and other systems are probably accurate to $\pm$15 MHz.

Br in the DDE ground state were found to be 556 MHz (^{79}Br) and 464 MHz (^{81}Br) by Hooper and Bray[110] which correspond to NQR transitions at 278 MHz and 232 MHz, respectively. Thus, the cross-relaxation process responsible for the satellites in the LAC spectrum appears to be between spin systems of the guest and host. In the $\underline{H}||\underline{x}'$ orientation of ^{12}C-BP, even though the separation of the satellites is larger, the same type of analysis supports this interpretation. The difference in energy of the $|0\rangle$ and $|-1\rangle$ states with $\underline{H}||\underline{x}'$ at the fields where the satellite lines are observed match the values of $\frac{1}{2}e^2qQ$ for ^{79}Br and ^{81}Br of the host, as can be seen in Table XII. Similar analyses of ^{13}C-BP, 4,4'-DFBP, and 4,4'-DCBP in DDE based on the center position of the satellites were also in good agreement with the average value of $\frac{1}{2}e^2qQ$ for the two bromine isotopes. These values are also listed in Table XII.

The fact that the triplet electron spin system is weakly coupled to the bromine nuclear spin system of the host was also evidenced in the ODMR spectra of benzophenones which contain no nuclei with $I \geq 1$. On several occasions, weak power-dependent satellites were observed on the high field and low field sides of the ODMR signal. These were separated from the ODMR line by approximately 95 G and were roughly a

TABLE XII: LAC Satellite Positions and Energy Separation of Electron Levels Involved in the Anticrossing

Molecule	H||z' Satellite Position(Gauss)	$\|W_o-W_+\|$ (MHz)[a]	H||x' Satellite Position(Gauss)	$\|W_o-W_-\|$ (MHz)[a]	Assignment[b]
^{12}C-BP	1562,1762	271,274	693,960	280,275	^{79}Br(DDE)
	1575,1742	235,232	718,943	230,234	^{81}Br(DDE)
^{13}C-BP	1564,1744	256,247	707,949	251,252	½[^{79}Br(DDE)+^{81}Br(DDE)]
4,4'-DFBP	1668,1855	253,254	750,997	255,256	½[^{79}Br(DDE)+^{81}Br(DDE)]
4,4'-DFBP	1446,1627	252,252	771,992	254,238	[^{79}Br(DDE)+^{81}Br(DDE)]
4,4'-DBBP	1271,1444	241,240	775,979	241,236	two-spin cross-relaxation[c]
	1182,1530	488,479	663,1071	486,460	three-spin crcss-relaxation[c]

[a] Calculated from the eigenvalue expressions in Table VIII and ZF parameters in Table IX.

[b] ^{81}Br(DDE) = ½e^{2}qQ = 232 MHz[110]

^{79}Br(DDE) = ½e^{2}qQ = 278 MHz[110]

[c] See test, p. 160.

factor of 70 less intense than the allowed signal. By comparison with observations made in the 4,4'-DBBP/DDE system (Chapter IV), it is clear that a quadrupole interaction involving the bromine nuclei of the DDE host is necessary to explain these satellites. Similar guest-host interactions have been observed in high-field[111] and ZF[112] ODMR studies of other triplet state systems. Thus, it is concluded that the ODMR and LAC satellites observed in the benzophenones are the result of a transferred hyperfine interaction which results from the overlap of the triplet wavefunction of excited benzophenones with the ground state wavefunction of adjacent DDE molecules.

Thus far, the major cross-relaxation and LAC effects have been readily explained in terms of the triplet electron spins only. However, as was shown in Chapter IV, guest molecule hyperfine and quadrupole interactions are present which split the electron spin sublevels of the triplet. It is therefore quite reasonable that these interactions contribute to the additional structure observed in the cross relaxation lines which appear as satellites of the LAC lines. The knowledge of the magnitude of hyperfine splittings determined in the ODMR experiment can be used to show that this is probably the case. For example, consider

the cross-relaxation lines in the $\underline{H} \| \underline{x}'$ LAC spectrum of ^{13}C-BP in DDE shown in Fig. 24 . It is seen that these lines have a triplet structure when compared to the LAC spectrum of ^{12}C-BP in the same orientation. The major difference between the two molecules is the presence of an $I=\frac{1}{2}$ nuclear spin in ^{13}C-BP. The hyperfine interaction resulting from this $I=\frac{1}{2}$ nucleus produces no splitting of the $|0\rangle$ electron spin state; however, it does split the $|-1\rangle$ sublevel into two components differing in energy by the magnitude of the hyperfine coupling constant. In the $\underline{H} \| \underline{x}'$ orientation, this was measured to be 14.5 G (41 MHz) in the ODMR spectrum. Correcting this coupling constant for the fact that the electron spins are not quantized along the field axis at the position in field where the satellites are observed, one obtains a coupling constant of ~37 MHz.* One would expect cross-relaxation between each of these states and the ^{79}Br and ^{81}Br nuclear quadrupole states of the DDE host. As a result, the cross-relaxation signals due to ^{79}Br and ^{81}Br will each be split into two components and one would expect to see a doublet of doublets.

---

*This correction involves the ratio of $\cos 2\phi$ for the field at which the ODMR hfs was measured and the field at which the LAC satellite is observed. $\cos 2\phi$ is defined by the relationship:

$$\tan 2\phi = \frac{Z-Y}{2g_{xx}\beta H}$$

where all variables have been previously defined.

However, the difference between the resonance frequencies of the ^{79}Br and ^{81}Br quadrupole transitions is about 46 MHz; that is, slightly larger than the hyperfine splitting. Thus, one observes three lines in the LAC satellites. These are not in the intensity ratio of 1:2:1 because of the slight difference between the hyperfine coupling constant and the difference between the two quadrupole resonance frequencies. The field positions and assignments of these lines are given in Table XIIIA, and a schematic representation of the cross-relaxation is shown in Fig. 25A. The solid (dashed) arrows represent values of $|W_o-W_-|$ that are resonant with the ^{79}Br (^{81}Br) quadrupole resonance frequency of the DDE host. The $\underline{H}||\underline{z}'$ LAC spectrum of ^{13}C-BP (Fig. 23) shows no additional structure on the cross-relaxation satellites since the magnitude of the hyperfine splitting in this orientation is very small.

A similar analysis of the $\underline{H}||\underline{x}'$ LAC spectrum of 4,4'-DFBP (Fig. 24) supports the argument that hyperfine interaction is responsible for the additional structure observed in the cross-relaxation lines. In this case, the hyperfine interaction of the two fluorines ($I=\frac{1}{2}$) split the $|-1\rangle$ electron spin state into three electron-nuclear components with a coupling constant of 45 MHz (corrected for the field position of the satellites). The hyperfine splitting is now

Table XIII: Assignment of structure appearing on LAC Satellites in the Orientation $\underline{H}||\underline{x}'$

Satellite Position (Gauss)	$\lvert W_o - W_- \rvert$ (MHz)[a]	Assignment[b]
A. ^{13}C-BP		
678	306	^{79}Br(DDE) + a_C
707	251	^{79}Br(DDE)-a_C, ^{81}Br(DDE)+a_C
734	198	^{81}Br(DDE) - a_C
921	190	^{81}Br(DDE) + a_C
946	245	^{81}Br(DDE)-a_C, ^{79}Br(DDE)+a_C
973	305	^{79}Br(DDE) + a_C
B. 4,4'-DFBP		
718	316	^{79}Br(DDE) + a_F
739	276	^{79}Br(DDE), ^{81}Br(DDE) + a_F
762	232	^{81}Br(DDE), ^{79}Br(DDE) - a_F
784	185	^{81}Br(DDE) - a_F
963	181	^{81}Br(DDE) + a_F
981	222	^{81}Br(DDE), ^{79}Br(DDE) + a_F
1003	268	^{79}Br(DDE), ^{81}Br(DDE) - a_F
1023	312	^{79}Br(DDE) - a_F
C. 4,4'-DCBP		
742	314	^{79}Br(DDE) + ^{35}Cl
758	281	^{79}Br(DDE), ^{81}Br(DDE)+^{35}Cl
782	230	^{81}Br(DDE), ^{79}Br(DDE)-^{35}Cl
804	183	^{81}Br(DDE) - ^{35}Cl
967	180	^{81}Br(DDE) + ^{35}Cl
986	224	^{81}Br(DDE), ^{79}Br(DDE)+^{35}Cl
1004	266	^{79}Br(DDE), ^{81}Br(DDE)-^{35}Cl
1019	301	^{79}Br(DDE)-^{35}Cl

[a] Calculated from the eigenvalue expressions in Table VIII and the ZF parameters in Table IX.

[b] ^{81}Br(DDE) = ½ e^2qQ = 232 MHz[110] a_C = 37 MHz (see text p. 151)

^{79}Br(DDE) = ½ e^2qQ = 278 MHz[110] a_F = 45 MHz (see test p. 152)

^{35}Cl = ½ e^2qQ ∿ 35-40 MHz (typical value from ref. 110).

Figure 25. Cross-relaxation interpretation of the LAC satellites observed in ^{13}C-BP and 4,4'-DFBP. Solid (dashed) arrows indicate field positions of coincidences with ^{79}Br (^{81}Br) quadrupole resonance frequencies of DDE.

A ^{13}C-BP in DDE

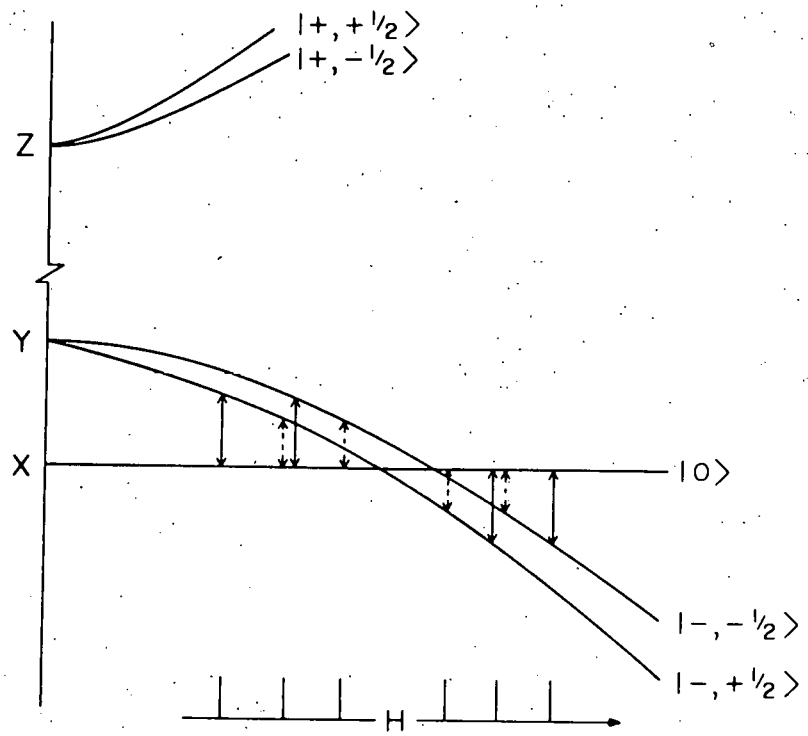

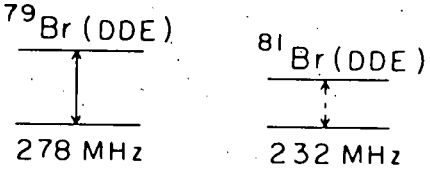

B 4,4′-DFBP in DDE

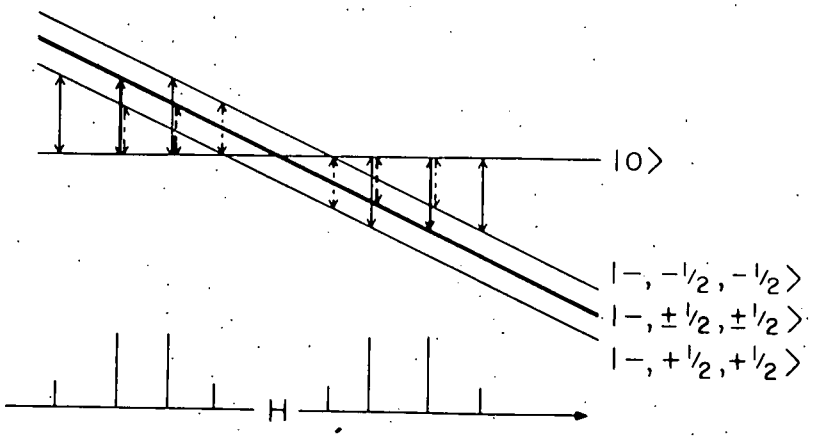

essentially equal to the difference between the ^{79}Br and ^{81}Br quadrupole resonance frequencies, and the schematic representation shown in Fig. 25B indicates that each cross-relaxation line should exhibit a 1:3:3:1 pattern. Indeed, this is found to be the case experimentally, and the assignments are listed in Table XIIIB. However, problems do arise in the interpretation of the $\underline{H}||\underline{z}'$ and $\underline{H}||\underline{x}'$ LAC spectra of 4,4'-DCBP in DDE. Using the above analysis, one finds that a 30-40 MHz interaction is responsible for the additional structure, and no evidence of this interaction was observed in the ODMR experiments. Since 30-40 MHz is typical of ^{35}Cl, ^{37}Cl quadrupole frequencies in aromatic molecules,[110] it seems probable that this interaction is a dominant factor in the observed structure in the cross-relaxation lines. The assignments listed in Table XIIIC are based on the effect of a ^{35}Cl quadrupole interaction on the electron spin sublevels. The situation is much more complex than the assignments given since now the $|0\rangle$, $|+1\rangle$ and $|-1\rangle$ electron spin states are split by the quadrupole interaction. In addition, the effects of chlorine hyperfine have been totally neglected and are probably important. Nonetheless, there appears to be ample evidence to suggest that the satellites in the LAC spectra <u>are</u> due to cross-relaxation and that the additional structure is introduced by nuclear perturbations of the triplet electron states.

Before discussing the LAC spectra of 4,4'-DBBP in DDE, which are in some respects different from those just analyzed, some remarks must be made about the appearance of the LAC spectra. First, the cross-relaxation lines exhibit the effects of hyperfine interaction while no such effects were observed in the LAC lines. One might expect that in a LAC situation additional structure should be present due to the anticrossing of individual hyperfine components. Some of the LAC lines did show shoulders but no structure was resolvable. There are two possible reasons for this. If the interaction coupling the two electron spin states ($|V|$) is larger than the hyperfine or quadrupole splittings, the additional structure will be washed out. Also, as the states mix at the expected crossing, the $|0\rangle$ spin state will no longer have a spin expectation value of zero. The $|0\rangle$ state will itself be split by the hyperfine interaction. In addition, as the separation between the electron spin states approaches the magnitude of the hyperfine interaction, cross-relaxation between the electron and nuclear spins is likely to occur. All of these effects combined will tend to increase the width of a given component and decrease the probability of resolving additional structure.

By comparing Figs. 23 and 24, one notes that the $\underline{H}||\underline{x}'$ cross-relaxation lines are considerably better resolved than those observed in the $\underline{H}||\underline{z}$ orientation. Of course, different magnitudes of the hyperfine interaction, such as in ^{13}C-BP, do affect the resolution. However, in ^{12}C-BP where hyperfine is not important, the resolution of the ^{79}Br and ^{81}Br cross-relaxation signals is considerably better in the $\underline{H}||\underline{x}'$ orientation. The reasons for this also explain why the satellite separations in the two orientations differ, even though the energy separation between electron spin states is the same at these fields. First, Table IX shows that $g_{xx} < g_{zz}$ and the slope of the energy level perturbed by the presence of a magnetic field is less in the $\underline{H}||\underline{x}'$ orientation. Secondly, the $\underline{H}||\underline{x}'$ LAC occurs at lower fields than the $\underline{H}||\underline{z}'$ LAC. Thus, in the $\underline{H}||\underline{x}'$ orientation the Zeeman effect has not decoupled the electron spin from the molecular framework to the same extent as in the $\underline{H}||\underline{z}'$ orientation. As a result, the effective g-values at the lower fields are considerably less than those given in Table IX. Therefore, the change in energy of the Zeeman levels per unit increment of magnetic field is also less in the $\underline{H}||\underline{x}'$ orientation. This leads to better frequency resolution in a cross-relaxation sense in this orientation and the satellites are displaced from the LAC line by a greater amount.

The LAC spectra of triplet 4,4'-DBBP are unique in several respects and can be interpreted equally well in terms of a LAC or cross-relaxation picture. Consider the results with $\underline{H}||\underline{z}'$. The LAC spectrum consists of five main lines at 1182, 1271, 1357, 1444, and 1530 G, with the outside pair showing some evidence of additional structure. In the LAC picture, we consider what interactions could lead to a splitting of the electron spin sublevels. The ODMR spectra of triplet 4,4'-DBBP exhibit quadrupole satellites which can be fit with values of $e^2qQ/2$ of 272 and 230 MHz for ^{79}Br and ^{81}Br, respectively. Hence, each of the electron spin states is split by the quadrupole interaction with four states having m_I values $|\pm 3/2,\pm 3/2\rangle$, $|\pm 3/2,\pm 1/2\rangle$, $|\pm 1/2,\pm 3/2\rangle$, and $|\pm 1/2,\pm 1/2\rangle$ for the two nuclei. To a reasonable approximation, the states $|\pm 3/2,\pm 1/2\rangle$ and $|\pm 1/2,\pm 3/2\rangle$ can be considered degenerate. Figure 26A shows the resulting energy level diagram in the vicinity of the LAC with $\underline{H}||\underline{z}'$. At the magnetic field H_C^z, anticrossings occur between electron spin states with the same nuclear spin functions. The other crossings are between electron spin states with different nuclear spin functions which become anticrossings due to the effect of hyperfine interactions. By considering the number of states involved at each LAC field, one predicts a five-line spectrum with relative intensities of 1:4:6:4:1.

Figure 26. Possible interpretations of LAC satellites of 4,4'-DBBP in DDE. (A) LAC picture showing anticrossings of 4,4'-DBBP nuclear states split by the quadrupole interaction. (B) Cross-relaxation picture: arrows indicate coincidences between electron spin and nuclear spin state energy separations. Both possibilities probably contribute to the observed spectrum.

4,4′ - DBBP in DDE

A LAC Picture

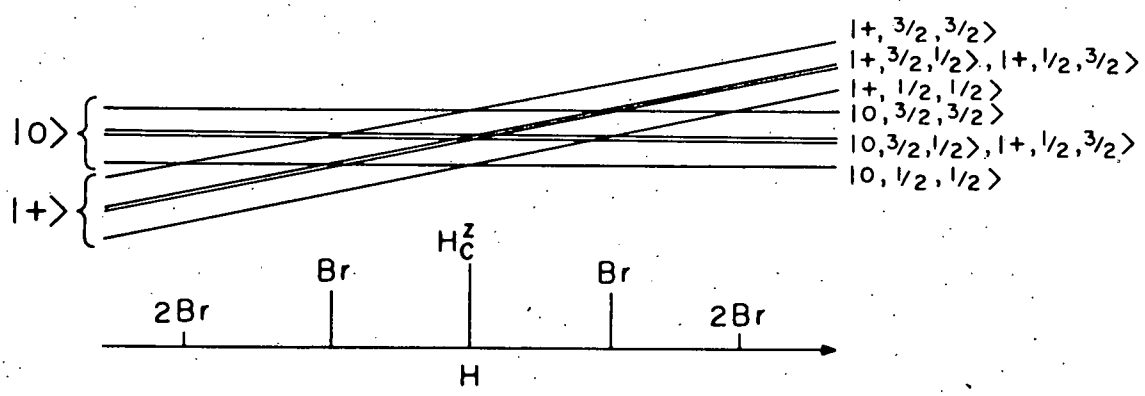

B Cross-Relaxation Picture

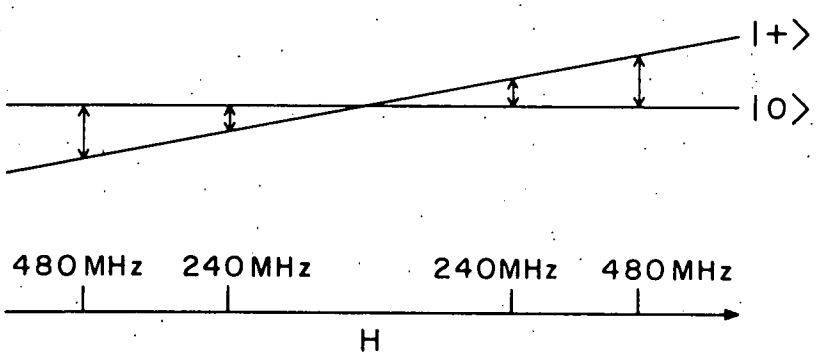

Experimentally, five lines are observed but their relative intensities are more nearly 1:2:2:2:1.

Since the quadrupole coupling constants of 4,4'-DBBP determined in Chapter IV are the same as those of DDE (within experimental error), it not surprising that cross-relaxation occurs at the same fields as the Br and 2 Br LAC lines shown in Fig. 26B. At the magnetic fields where these lines occur, the splitting between the $|0\rangle$ and $|+1\rangle$ triplet sublevels is equal to the splitting of the two nuclear spin states of a single Br or a Br pair. Thus, the lines labeled Br and 2Br gain additional intensity from two-spin cross-relaxation and three-spin cross-relaxation processes, respectively. The two-spin cross-relaxation involves an electron spin of the triplet and a ^{81}Br (or ^{79}Br) spin of the DDE host. The three-spin cross-relaxation involves, for example, the electron spin and ^{81}Br (^{79}Br) nuclear spin of the triplet along with a ^{81}Br(^{79}Br) nuclear spin of the host. This can be seen by studying Fig. 26A. Cross-relaxation can provide additional intensity to the 2 Br and Br LAC lines and the 1:2:2:2:1 pattern observed experimentally is not surprising. The assignments based on cross-relaxation are presented in Table XII.

In the H||x' orientation, the results are more complicated and not completely understood. The spectrum shown in Fig. 24 was obtained by orienting the crystal in an ODMR experiment. Since the two molecules in the unit cell are inequivalent by only 18° in the ab plane, a quadrupole satellite of the molecule not in the canonical orientation is strongly overlapped with the allowed ODMR transition of the molecule in H||x' canonical orientation. The LAC spectrum with H||x' (Fig. 24) shows five main lines; however, the high-field components have very diminished intensity. Rotation of the crystal away from the a axis of the crystal caused the whole LAC spectrum to disappear. Rotation toward the a axis produced shifts in the positions of the LAC lines, and the high-field components gained intensity while the low-field components diminished in intensity. This could be caused by some long-range coupling between the triplet states of the two molecules since their ODMR spectra become overlapped significantly during such a rotation. The field position marked by an "X" in the H||x' LAC spectrum was chosen as the origin of the LAC spectrum based on the position calculated from the ZF parameters. The assignments presented in Table XII were made in accord with this choice.

The results and interpretations have been presented here in rather qualitative but, nonetheless, convincing manner. More detailed accounts can be found in the elegant treatise by Veeman.[67] In summary, these spectra can be used to obtain valuable information concerning the magnetic properties of the phosphorescent triplet state. The ZF parameters can be obtained from the known LAC fields using Eqs. (73) and (74) along with the X + Y + Z = 0 condition. In addition, the cross-relaxation signals in favorable cases can be used as a probe for the hyperfine splittings in triplet state systems.

C. Level Anticrossing Effects in ODMR Spectroscopy

In the experiments just described, the detailed behavior of the two anticrossing levels and their wavefunctions in the region of close approach is not exposed, and measurements of the interaction coupling the two states are limited to indirect estimates based on the observed LAC linewidths. The orientation dependence of the ODMR spectrum of ^{13}C-BP (Fig. 6) indicated that LAC effects could be observed in the ODMR spectra. The curves due to the "$\Delta m_S = 2$" and "$\Delta m_S = \pm 1$" resonances in the orientational dependence were not observed

to cross in the low field region; however, the final assignment indicated that the "$\Delta m_S = 2$" and LF "$\Delta m_S = \pm 1$" transitions had switched identities at the $\underline{H} \| \underline{z}'$ orientation. It is also noted that at the operating frequency of this experiment the two ODMR transitions in question occur at fields below the LAC field. Stimulated by these observations, an investigation of the ODMR properties of triplet states in the vicinity of such avoided crossings was begun. The results have shown that it is possible, using ODMR methods, to directly (a) observe the mixing and mutual repulsion of a pair of Zeeman energy levels of a phosphorescent triplet state as the magnetic field is tuned through an avoided crossing region and (b) measure the magnitude of the interaction coupling the two states.

The Zeeman energy level diagram calculated from the ODMR data (Table IX) on triplet ^{13}C-BP for fields up to 3kG along the $\underline{z}'$ axis is shown in Fig. 27. The states are labeled by their high-field quantum numbers $|m_S\rangle = |+1\rangle$, $|0\rangle$, and $|-1\rangle$. On the basis of these calculations, it is predicted that the $|+1\rangle$ and $|0\rangle$ spin sublevels will cross at a field of $H_c^z = 1657$ G, where the separation between the two degenerate sublevels and the $|-1\rangle$ sublevel is $\nu_c^z = 9.388$ GHz. Consequently, if the ODMR experiment is carried out at a microwave frequency (ν_o) different from ν_c^z, two transitions will be

Figure 27. Calculated Zeeman energy level diagram of the lowest triplet state of ^{13}C-BP in the orientation $\underline{H}||\underline{z}'$. Transitions indicated by A and F refer to the "$\Delta m_S = \pm 1$" and "$\Delta m_S = 2$" transitions at different microwave frequencies, respectively. ν_C^z corresponds to the frequency where both are expected to be degenerate.

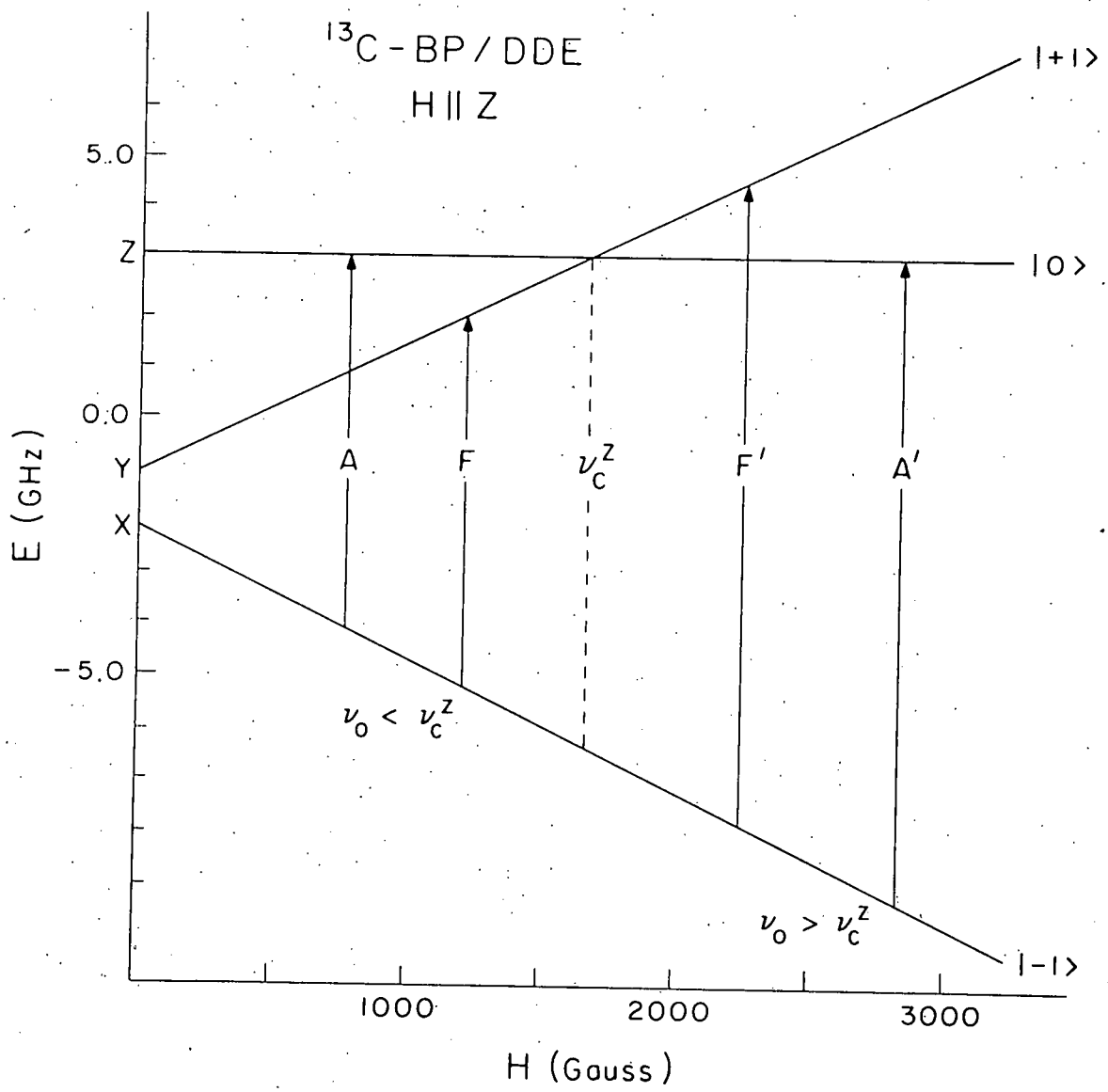
^{13}C - BP / DDE
H || Z
|+1>
|0>
|-1>
5.0
Z
0.0
Y
X
-5.0
E (GHz)
A
F
ν_c^Z
F'
A'
$\nu_0 < \nu_c^Z$
$\nu_0 > \nu_c^Z$
1000
2000
3000
H (Gauss)

observed in the vicinity of H_c^z. If $\nu_o < \nu_c^z$, then the "allowed" transition of the type "$\Delta m_S = \pm 1$", labeled A in Fig. 27 will occur on the low-field side of the "forbidden", "$\Delta m_S = \pm 2$", transition (F in Fig. 27) and both lines will be observed at fields below H_c^z. If $\nu_o > \nu_c^z$, the field positions of the two lines (A' and F') will be reversed and both transitions will lie at fields above H_c^z. On the other hand, if $\nu_o = \nu_c^z$, Fig. 27 predicts that the two transitions will collapse into a single line, centered at H_c^z.*

Figure 28 illustrates the results of several ODMR experiments on triplet ^{13}C-BP in the orientation $\underline{H} \| \underline{z}'$. At frequencies below ν_c^z (e.g., ν_o = 9.162 GHz), both microwave transitions occur at fields below H_c^z, and the less intense forbidden line (F) appears on the high-field side of the more intense allowed one (A). At frequencies above ν_c^z (e.g., ν_o = 9.723 GHz), both transitions occur above H_c^z and the weak forbidden line (F') is on the low-field side of the allowed one (A'). These observations are in complete accord with the predictions of Fig. 27. However, at $\nu_o = \nu_c^z$ (i.e., ν_o = 9.388 GHz), two lines are observed in the ODMR spectrum rather

---

*We neglect, of course, the high-field "$\Delta m_S = \pm 1$" transition which is observed at fields greater than 3 kG in all cases.

Figure 28. ODMR Spectra of triplet ^{13}C-BP in DDE in the vicinity of the level anticrossing (H_C^z) at different microwave frequencies. The magnetic field ($\underline{H}||\underline{z}'$) increases from left to right.

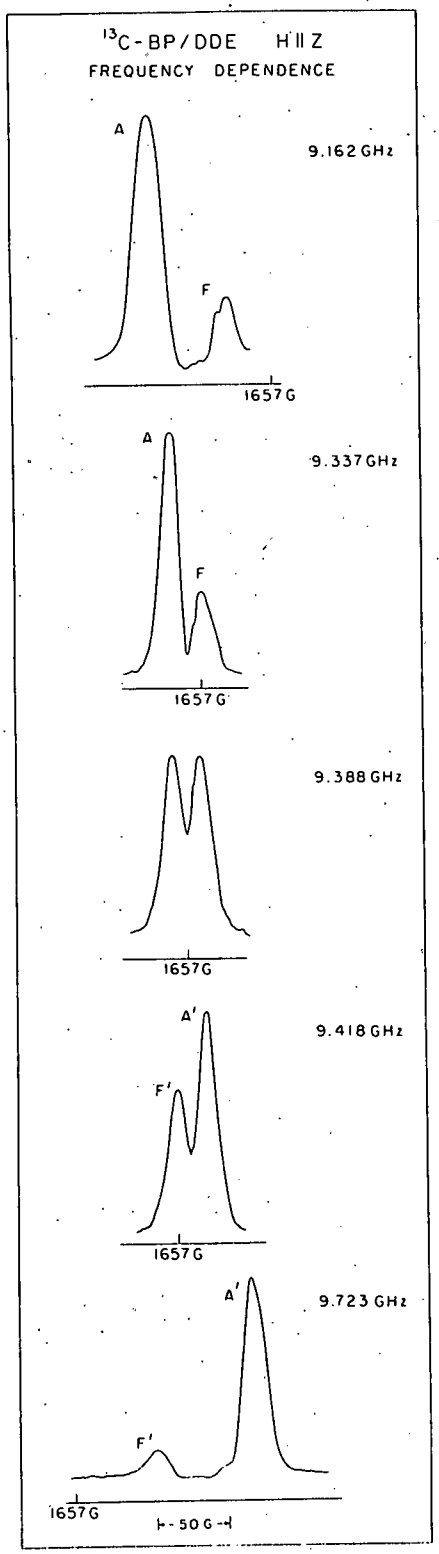
^{13}C-BP/DDE H∥Z
FREQUENCY DEPENDENCE
A
F
9.162 GHz
1657G
A
F
9.337 GHz
1657G
9.388 GHz
1657G
A'
F'
9.418 GHz
1657G
A'
F'
9.723 GHz
1657G
50G

than the expected one, and these are split symmetrically about H_c^z with a separation of 19 G. Moreover, it is also found that the intensity of the forbidden line increases relative to that of the allowed one as ν_o approaches ν_c^z, and that the two lines are equally intense at $\nu_o = \nu_c^z$. These observations are clearly not in agreement with the predictions of Fig. 27.

The explanation for the above behavior is, of course, that the $|+1\rangle$ and $|0\rangle$ sublevels are prevented from crossing at H_c^z by the presence of a small static interaction which couples the two states. To demonstrate this explicitly, a plot summarizing the results of ODMR experiments on triplet ^{13}C-BP at frequencies below, at, and above ν_c^z is shown in Fig. 29. The points are the observed relative positions of the two microwave transitions in the vicinity of H_c^z. Since both transitions originate in the $|-1\rangle$ sublevel, these points also establish experimentally the relative energies (in gauss) of the two upper sublevels. These are compared with the predicted relative energies of the upper sublevels in the absence of a perturbing interaction which are shown as dashed lines in Fig. 29. Immediately apparent from this plot is the increasing deviation of the "$|+1\rangle$" and "$|0\rangle$" sublevels from their predicted positions as ν_o approaches

Figure 29. Relative positions of the (low-field) "$\Delta m_S = \pm 1$" and "$\Delta m_S = 2$" transitions of triplet ^{13}C-BP as a function of microwave frequency. The solid circles are experimental line positions; the solid curves and dashed lines are the calculated positions in the presence and absence of a perturbing interaction, respectively. V is the matrix element of this interaction.

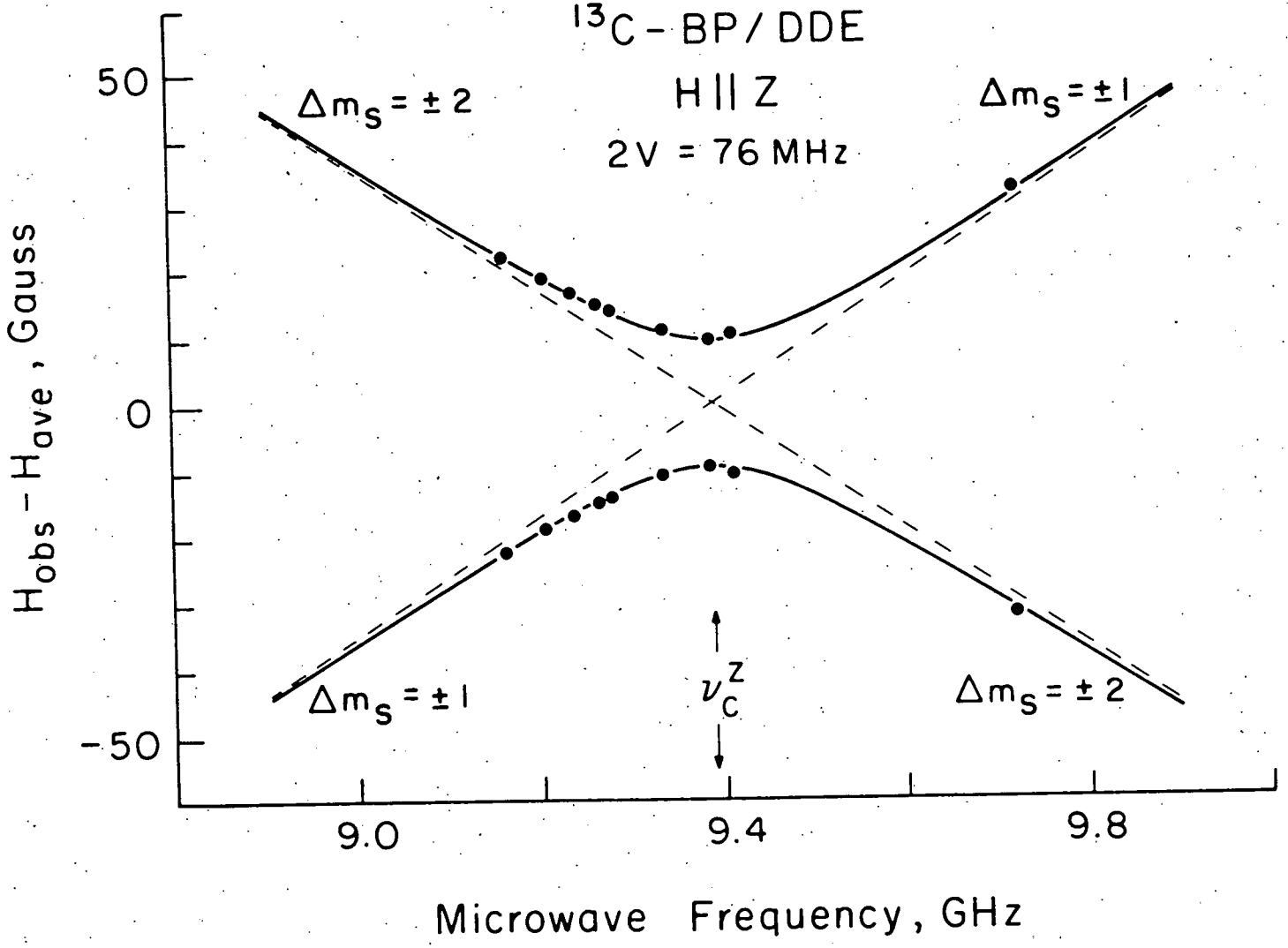
^{13}C - BP / DDE
H || Z
2V = 76 MHz
$\Delta m_s = \pm 2$
$\Delta m_s = \pm 1$
$\Delta m_s = \pm 1$
$\Delta m_s = \pm 2$
ν_C^Z
50
0
-50
$H_{obs} - H_{ave}$, Gauss
9.0
9.4
9.8
Microwave Frequency, GHz

ν_c^z, and their mutual repulsion where the two unperturbed levels cross. Furthermore, since the two transitions interchange their identities at $\nu_o = \nu_c^z$, it is also clear that the wavefunctions of the perturbed levels are <u>equal</u> mixtures of the states $|+1\rangle$ and $|0\rangle$ at the avoided crossing point. Thus, the variable frequency ODMR data provide a rather unique <u>experimental</u> example of the effect of a static perturbation on the energies and wavefunctions of a pair of coupled energy levels.

Two methods may be used to determine the magnitude of the interaction which is responsible for the observed level anticrossing in triplet ^{13}C-BP. In the first, which is indirect, the spin Hamiltonian was modified to include a small variable off-diagonal element V between the states $|+1\rangle$ and $|0\rangle$, and diagonalized. The eigenvectors which diagonalize $\mathcal{H}_{ZF} + \mathcal{H}_Z$ were chosen as the basis set to simplify the calculation and V was treated as a static perturbation. The final eigenvalues and eigenvectors were similar in form to Eqs. 65 and 66. The eigenvalue expressions were then used to calculate the field positions of the two microwave transitions (see Appendix II). The magnitude of the static perturbation was adjusted in these calculations until a fit between the observed and calculated

field positions in the vicinity of H_c^z was obtained. This yielded a value of $|V| = 38$ MHz, where $|2V| = 76$ MHz is the separation of the upper sublevels at the avoided crossing point. The resulting calculated positions of the two transitions as a function of microwave frequency in the presence of the perturbation are shown as solid curves in Fig. 29 . The agreement between theory and experiment is seen to be excellent.

The magnitude of V may also be measured <u>directly</u> using the variable frequency ODMR technique. In this case, allowing the coolant level to drop provided sufficient tunability of cavity frequency although variable frequency cavities are generally preferred. The method is illustrated in Fig. 28 . At $\nu_o = 9.337$ GHz the forbidden transition (F), which originates in the $|-1\rangle$ sublevel and terminates in the <u>lower</u> sublevel of the perturbed pair, is observed at 1657 G (<u>i.e.</u>, at H_c^z). At $\nu_o = 9.418$ GHz, the forbidden transition (F') again is observed at H_c^z and originates in the $|-1\rangle$ sublevel, but now terminates in the <u>upper</u> sublevel of the perturbed pair. Since the forbidden transition is observed at the same field strength in both experiments, the absolute energy of the $|-1\rangle$ sublevel is the same in both cases. Hence, the separation of the perturbed sublevels

at the avoided crossing point is simply the difference in the microwave frequencies of the two experiments, or $2|V| = 81$ MHz. Thus, $|V| = 40.5$ MHz, which is in good agreement with the value obtained by the more indirect method. An entirely equivalent method for determining $2|V|$ directly is to measure the separation of the two transitions in a swept frequency/fixed field experiment at H_c^z. It should also be noted that small shifts in the energy of the $|-1\rangle$ sublevel, which might occur at H_c^z, will not affect the measured value of $2|V|$ in either method.

It is known from the ODMR experiments that the symmetry of triplet ^{13}C-BP in the DDE crystal is C_2. As a result, the $|+1\rangle$ and $|0\rangle$ states in the orientation $\underline{H} \| \underline{z}'$ belong to the same irreducible representations of the symmetry group of the molecule plus field, and therefore are forbidden to cross because of the "non-crossing" rule.[100] However, as noted previously, it is unlikely that the two states would cross even in highly "symmetrical" systems since they are likely to be coupled in some order of perturbation and thus possess common symmetry properties. In solid state systems, primary emphasis has been placed on the role of off-diagonal elements of the Zeeman interaction which occur due to slight misalignments of the crystal relative to the applied field.[67,105]

Indeed, we find that the magnitude of V is strongly dependent on crystal orientation, increasing to ~70 MHz when the field is rotated by 1^{o} away from $\underline{H}||\underline{z}'$. However, we also find that there exists in triplet ^{13}C-BP a minimum value of $|V|$ (30 MHz), and that this value is different for different molecules in the same host. For example, for ^{12}C-BP in DDE, $|V| \lesssim 23$ MHz with $\underline{H}||\underline{z}'$. Thus, it is possible that other interactions (_e.g._, off-diagonal hyperfine and crystal field terms) are responsible for the observed anticrossing in ^{13}C-BP, and that the minimum value of the interaction parameter is a characteristic property of the system (guest + host).

Since the static perturbation mixes the two upper states in the vicinity of H_c^z, their radiative and radiationless properties also become mixed. As mentioned previously, this allows the direct observation of LAC spectra as changes in phosphorescence in the vicinity of H_c^z and H_c^x. This mixing effect is also apparent in the relative intensities of the two ODMR transitions in the vicinity of H_c^z shown in Fig. 28. One notes that, at $\nu_o = {}^{z}_{c}$, the two transitions are equally intense indicating that the $|+1\rangle$ and $|0\rangle$ states, as well as their photophysical properties, are equal mixtures of each other. This is in agreement with the theoretical predictions outlined previously. The _direct_ observation of such mixing

in these experiments confirms the interpretation that the LAC spectra arise from avoided crossings,[67,105] and shows that these LAC effects must arise from coupling through a static perturbation rather than the time-dependent field of a level crossing experiment.

APPENDIX I

Computer program for obtaining magnetic parameters of the lowest triplet state from observed positions of "$\Delta m_S = \pm 1$" ODMR transitions.

```
C     TMPP.F4  09-DEC-73
CXXXXXXXXXXXXXXXXXXXXXXXXXXXXXXXXXXXXXXXXXXXXXXXXXXXXXXXXXXXXXXXXXX
C
C                  TRIPLET MAGNETIC PARAMETERS PROGRAM
C                    APPLIES TO LEVEL ORDERING:
C                            T>0>M>B
C
C       1)CALCULATES ZF-PARAMETERS AND G-VALUES FROM "G=2"
C         STATIONARY FIELD POSITIONS WHEN NO MAGNETIC PAR-
C         AMETERS ARE KNOWN USING AN ITERATIVE PROCESS.
C       2)CALCULATES G-VALUES FROM KNOWN ZF-PARAMETERS AND
C         "G=2" STATIONARY FIELD POSITIONS.
C       3)CALCULATES "G=2" AND "G=4" STATIONARY FIELD POS-
C         ITIONS WHEN ZF-PARAMETERS AND G-VALUES ARE KNOWN.
CXXXXXXXXXXXXXXXXXXXXXXXXXXXXXXXXXXXXXXXXXXXXXXXXXXXXXXXXXXXXXXXXXX
C****WHAT IS KNOWN?
9      FORMAT(/ ' ARE ZF-PARAMETERS KNOWN? YES(M=1),NO(M=0)',$)
       WRITE(6,9)
10     FORMAT(I)
       READ(5,10)M
       IF(M.EQ.0)GO TO 1125
11     FORMAT(/ ' ARE G-VALUES KNOWN? YES(N=1),NO(N=0)',$)
       WRITE(6,11)
       READ(5,10)N
       IF(N.EQ.0)GO TO 110
C****ZF-PARAMETERS AND G-VALUES ARE BOTH KNOWN
12     FORMAT(/ ' INPUT T,M,B IN CM-1'/)
       WRITE(6,12)
13     FORMAT(F)
       READ(5,13)T,AM,B
14     FORMAT(/ ' INPUT GT,GM,GB'/)
       WRITE(6,14)
       READ(5,13)GT,GM,GB
15     FORMAT(/ ' INPUT FREQUENCIES HVT,HVM,HVB IN GHZ'/)
       WRITE(6,15)
       READ(5,13)HVT,HVM,HVB
        H=3.33586*0.01
        HVT=HVT*H
        HVM=HVM*H
        HVB=HVB*H
        BB=4.66882*0.01
       GO TO 200
C****G-VALUES UNKNOWN,ZF-PARAMETERS AND "G=2" FIELDS KNOWN
C     INPUT FOR CALCULATING G-VALUES
110    WRITE(6,12)
111    FORMAT(F)
       READ(5,111)T,AM,B
112    FORMAT( ' INPUT FIELD POSITION,KG,AND FREQUENCY,GHZ.')
1125   WRITE(6,112)
113    FORMAT(/ ' FIELD ALONG T-AXIS')
       WRITE(6,113)
114    FORMAT(/ '  G=4 LINE,LOWFIELD,HIGHFIELD,FREQUENCY'/)
       WRITE(6,114)
       READ(5,111)H3T,HLT,HHT,HVT
115    FORMAT(/ ' FIELD ALONG M-AXIS')
       WRITE(6,115)
       WRITE(6,114)
       READ(5,111)H3M,HLM,HHM,HVM
116    FORMAT(/ ' FIELD ALONG B-AXIS')
       WRITE(6,116)
```

```
      WRITE(6,114)
      READ(5,111)HBB,HLB,HHB,HVB
C     CALCULATION OF G-VALUES
      H=3,33586*0,01
      HVT=HVT*H
      HVM=HVM*H
      HVB=HVB*H
      BB= 4,66882*0,01
      IF(M,EQ,0)GO TO 168
      GT1=((2,*HVT**2,+4,5*T*T)-(AM-B)**2,/2,)
      GT2=GT1/(BB*BB*(HLT**2,+HHT**2,))
      GT=SQRT(GT2)
      TMB=(T-B)**2,
      GM1=(2,*HVM*HVM+4,5*AM*AM)-TMB/2,
      GM2=GM1/(BB*BB*(HHM**2,+HLM**2,))
      GM=SQRT(GM2)
      TMM=(T-AM)**2,
      GB1=(2,*HVB*HVB+4,5*B*B)-TMM/2,
      GB2=GB1/(BB*BB*(HLB**2,+HHB**2,))
      GB=SQRT(GB2)
117   FORMAT(/ 1X,F12,6,' GT',F12,6,' GM',F12,6,' GB')
      WRITE(6,117)GT,GM,GB
      GO TO 200
C****ITERATION OF KNOWN STATIONARY FIELDS FOR MAGNETIC PARAMETERS
C     INITIAL ESTIMATES OF PARAMETERS,CONVERGENCE TOLERANCE
168   ITMAX=100
      T=0,1
      AM=-0,0
      B=-0,1
      GT=2,0023
      GM=2,0023
      GB=2,0023
      TOL=0,0000001
      IT=1
C     BEGIN ITERATION
169   GMM=GM
      AMM=AM
      GBB=GB
      BBB=B
      TT=T
      GTT=GT
      TMB=(T-B)**2,
      GM1=(2,*HVM*HVM+4,5*AM*AM)-TMB/2,
      GM2=GM1/(BB*BB*(HHM**2,+HLM**2,))
      GM=SQRT(GM2)
      AM1=SQRT(TMB/4,+(GM*BB*HLM)**2,)
      AM2=SQRT(TMB/4,+(GM*BB*HHM)**2,)
      AM=(AM1-AM2)/3,
      TMM=(T-AM)**2,
      GB1=(2,*HVB*HVB+4,5*B*B)-TMM/2,
      GB2=GB1/(BB*BB*(HLB**2,+HHB**2,))
      GB=SQRT(GB2)
      B1=SQRT(TMM/4,+(GB*BB*HLB)**2,)
      B2=SQRT(TMM/4,+(GB*BB*HHB)**2,)
      B=(B1-B2)/3,
      GT1=((2,*HVT**2,+4,5*T*T)-(AM-B)**2,/2,)
      GT2=GT1/(BB*BB*(HLT**2,+HHT**2,))
      GT=SQRT(GT2)
      T1=SQRT((AM-B)**2,/4,+(GT*BB*HHT)**2,)
      T2=SQRT((AM-B)**2,/4,+(GT*BB*HLT)**2,)
```

```
      T=(T1-T2)/3.
C#    T=-(AM+B)
C#    AM=-(T+B)
C#    B=-(AM+T)
      TR=T+AM+B
      DGM=ABS(GM-GMM)
      DAM=ABS(AM-AMM)
      DGB=ABS(GB-GBB)
      DB=ABS(B-BBB)
      DT=ABS(T-TT)
      DGT=ABS(GT-GTT)
      IT=IT+1
     IF(IT.GE.ITMAX)GO TO 170
     IF(DGM.GT.TOL)GO TO 169
     IF(DAM.GT.TOL)GO TO 169
     IF(DGB.GT.TOL)GO TO 169
     IF(DB.GT.TOL)GO TO 169
     IF(DT.GT.TOL)GO TO 169
     IF(DGT.GT.TOL)GO TO 169
170   WRITE(6,171)IT
171   FORMAT(/ ' NUMBER OF ITERATIONS IS' I4)
172   FORMAT(/ '  T,M,B,TRACE IN CM-1 UNITS'/)
      WRITE(6,172)
173   FORMAT(/ 1X,F12.6,' T',F12.6,' M',F12.6,' B',
     +F12.6,' TRACE')
      WRITE(6,173)T,AM,B,TR
      WRITE(6,117)GT,GM,GB
C****CALCULATION OF RESONANT FIELDS
200    TH1=SQRT((HVT-3.*T/2.)**2.-((AM-B)/2.)**2.)
       TH1=TH1/(GT*BB)
       TH2=SQRT((HVT+3.*T/2.)**2.-((AM-B)/2.)**2.)
       TH2=TH2/(GT*BB)
       TH3=SQRT((HVT/2.)**2.-((AM-B)/2.)**2.)
       TH3=TH3/(GT*BB)
      WRITE(6,113)
201   FORMAT(/1X,F12.6,' G4 FIELD',1X,F12.6,' LOW-FIELD',
     +1X,F12.6,' HIGH-FIELD')
      WRITE(6,201)TH3,TH1,TH2
       FH1=SQRT((HVM+3.*AM/2.)**2.-(T-B)**2./4.)
       FH1=FH1/(GM*BB)
       FH2=SQRT((HVM-3.*AM/2.)**2.-(T-B)**2./4.)
       FH2=FH2/(GM*BB)
       FH3=SQRT((HVM/2.)**2.-((T-B)/2.)**2.)
       FH3=FH3/(GM*BB)
      WRITE(6,115)
      WRITE(6,201)FH3,FH1,FH2
       BH1=SQRT((HVB+3.*B/2.)**2.-(T-AM)**2./4.)
       BH1=BH1/(GB*BB)
       BH2=SQRT((HVB-3.*B/2.)**2.-(T-AM)**2./4.)
       BH2=BH2/(GB*BB)
       BH3=SQRT((HVB/2.)**2.-(T-AM)**2./4.)
       BH3=BH3/(GB*BB)
      WRITE(6,116)
      WRITE(6,201)BH3,BH1,BH2
      CALL EXIT
      END
```

APPENDIX II

Computer program for calculating separation of "$\Delta m_S = \pm 1$" (low-field) and "$\Delta m_S = 2$" ODMR transitions for the $\underline{H} \| \underline{z}'$ orientation as a function of microwave frequency and magnitude of the perturbation between the state $|+1\rangle$ and $|0\rangle$.

```
C     LACP.F4  7-JUNE-74
      REAL NU,NV
      DIMENSION HORZ(400),VERT1(400),VERT2(400)
      COMMON/H1/XSYM,XLABEL(10),YSYM,YLABEL(10)
      COMMON/H2/XL,XU,XI,XSPAN
      COMMON/H3/YL,YU,YI,YSPAN
      COMMON/H4/XORIG,XMARG,XLONG,YORIG,YMARG,YLONG
      COMMON/H5/SLOPE,CEPT
      DATA XSYM/.16/,YSYM/.16/,SYM/.08/
      DATA XORIG/.2/,YORIG/.2/,XLONG/7./,YLONG/5./
      DATA XMARG/2./,YMARG/2./
      INP=2
1     FORMAT(/ ' INPUT T,M,B IN CM-1 AND GT'/)
      WRITE(6,1)
2     FORMAT(5F)
      CALL IFILE(INP,'JAY','INP')
      READ(INP,2)T,AM,B,GT
3     FORMAT(/ ' INPUT INTERACTION ENERGY,2V,IN MHZ'/)
      WRITE(6,3)
      READ(5,2)V
4     FORMAT(/ ' INPUT INITIAL,FINAL FREQUENCIES AND INCREMENT,GHZ'/)
      WRITE(6,4)
      READ(INP,2)NU,NV,VINC
5     FORMAT(/ ' INPUT LAC-FIELD IN GAUSS'/)
      WRITE(6,5)
      READ(INP,2)HLAC
       HT=HLAC
       HM=HLAC
       VMIN=1.E+20
       NN=0
       HMIN=VMIN
       VMAX=-VMIN
       HMAX=-HMIN
       V=V/29979.3
       H=3.33586*0.01
6      HV=NU*H
       BB=4.66882E-5
       ITMAX=100
       TOL=0.0001
       IT=1
7      HTT=HT
       HMM=HM
       BT=SQRT((AM-B)**2./4.+(GT*BB*HT)**2.)
       BM=SQRT((AM-B)**2./4.+(GT*BB*HM)**2.)
       DT=1.5*T-BT
       DM=1.5*T-BM
       PT1=SQRT(V**2.+DT**2.)
       PT=PT1/3.
       PM1=SQRT(V**2.+DM**2.)
       PM=PM1/3.
       R=2.*HV/3.-T/2.
       RT=(R-PT)**2.
       RM=(R+PM)**2.
       HT1=SQRT(RT-(AM-B)**2./4.)
       HT=HT1/(GT*BB)
       HM1=SQRT(RM-(AM-B)**2./4.)
       HM=HM1/(GT*BB)
       DTT=ABS(HT-HTT)
       DTM=ABS(HM-HMM)
       IT=IT+1
```

```
      IF(IT.GE.ITMAX)GO TO 8
      IF(DTT.GT.TOL)GO TO 7
      IF(DTM.GT.TOL)GO TO 7
      GO TO 10
8     WRITE(22,9)IT
9     FORMAT(/ ' ITERATION LIMIT EXCEEDED,NO,OF IT,=' I4)
10     H1=HT-(HT+HM)/2.
       H2=HM-(HT+HM)/2.
       AX=9*(R-BT)**2.
       AY=9*(R-BM)**2.
       VVX=SQRT(AX-DT**2.)
       VVY=SQRT(AY-DM**2.)
       VV1=VVX*29979.3
       VV2=VVY*29979.3
11    FORMAT(/ 1X,F12.6,' NU,GHZ',F12.3,' 2V(T),MHZ',
     +F12.3,' 2V(M),MHZ')
      WRITE(22,11)NU,VV1,VV2
12    FORMAT(/ 1X,F12.2,' LF,GAUSS',1X,F12.2,' G4,GAUSS')
      WRITE(22,12)HT,HM
13    FORMAT(/ 1X,F12.2,' LF-(LF+G4)/2',1X,F12.2,' G4-(LF+G4)/2')
      WRITE(22,13)H1,H2
       NN=NN+1
       HORZ(NN)=NU
       VERT1(NN)=H1
       VERT2(NN)=H2
       VMIN=AMIN1(VMIN,H1,H2)
       VMAX=AMAX1(VMAX,H1,H2)
       HMIN=AMIN1(HMIN,NU)
       HMAX=AMAX1(HMAX,NU)
       NU=NU+VINC
      IF(NU.LE.NV)GO TO 6
C--CALCOMP PLOT
      XPAGE=1.+2.*XMARG+XLONG
      YPAGE=12.
      PLOTN=0.
      CALL PCHECK(PLOTN,6,XPAGE,YPAGE)
      CALL CORNER(XORIG,YORIG,XPAGE,YPAGE,3.)
      YL=-60.
      YU=+60.
      YI=10.
      XL=8.8
      XU=10.0
       XI=.2
      IP=3
      XSPAN=XU-XL
      YSPAN=YU-YL
      XM=XMARG+XORIG
      YM=YMARG+YORIG
      DO 200 I=1,NN
      XX=XM+XLONG*(HORZ(I)-XL)/XSPAN
      YY=YM+YLONG*(VERT1(I)-YL)/YSPAN
      CALL PLOT(XX,YY,IP)
  200 IP=2
      IP=3
       DO 210 I=1,NN
      XX=XM+XLONG*(HORZ(I)-XL)/XSPAN
      YY=YM+YLONG*(VERT2(I)-YL)/YSPAN
      CALL PLOT(XX,YY,IP)
  210 IP=2
C--READ ACTUAL DATA AND PLOT
```

```
      CALL IFILE(1,'JAY','ACT')
      READ(1,1000)XLABEL,YLABEL
 1000 FORMAT(1X,10A5)
      NN=0
      DO 230 I=1,99
      READ(1,1001)HORZ(I),VERT1(I),VERT2(I)
 1001 FORMAT(3F)
      IF(HORZ(I).LE.0.)GO TO 240
  230 NN=NN+1
  240 CALL HPLOT(HORZ,VERT1,NN,1,1,3,SYM)
      CALL HPLOT(HORZ,VERT2,NN,1,1,1,SYM)
      PLOTN=-PLOTN
      CALL PCHECK(PLOTN,6,XPAGE,YPAGE)
      CALL EXIT
      END
```

REFERENCES

1. J. Dewar, Proc. Roy. Soc. (London), 36, 164 (1880).

2. E. Wiedman, Ann. Phys., 34, 446 (1888).

3. G. N. Lewis, D. Lipkin and T. T. Magel, J. Am. Chem. Soc., 63, 3005 (1941).

4. G. N. Lewis and M. Kasha, J. Am. Chem. Soc., 66, 2100 (1944); 67, 944 (1945).

5. G. N. Lewis, M. Calvin and M. Kasha, J. Chem. Phys., 17, 804 (1949).

6. D. F. Evans, Nature, 176,777 (1955).

7. C. A. Hutchison, Jr. and B. W. Mangum, J. Chem. Phys., 29, 952 (1958); 32, 1261 (1960).

8. A. B. Zahlan (Editor), The Triplet State, Beirut Symposium 1967 (Cambridge University Press, 1967).

9. S. P. McGlynn, J. Azumi and M.Kinoshita, Molecular Spectroscopy of the Triplet State (Prentice Hall, Englewood Cliffs, N. J., 1969).

10. S. K. Lower and M. A. El-Sayed, Chem. Revs., 66, 199 (1966).

11. J. B. Birks, Photophysics of Aromatic Molecules (Wiley-Interscience, New York, 1970).

12. There are important exceptions to these "rules". See reference 11, Chapter 4.

13. J. G. Calvert and J. N. Pitts, Photochemistry (J. Wiley and Sons, Inc., New York, 1966).

14. C. J. Ballhausen, Introduction to Ligand Field Theory (McGraw-Hill, New York, 1962).

15. S. A. Boorstein and M. Gouterman, J. Chem. Phys., 39, 2443 (1963).

16. A. Carrington and A. D. McLachlan, Introduction to Magnetic Resonance (Harper and Row, New York, 1967).

17. E. Wasserman, A. M. Trozzolo, W. A. Yager and R. W. Murray, J. Chem. Phys., 40, 2408 (1964).

18. M. S. deGroot and J. H. van der Waals, Mol. Phys., 6, 545 (1963).

19. M. S. deGroot, I. A. M. Hesselmann and J. H. van der Waals, Mol. Phys., 13, 583 (1967); 16, 45 (1969); J. H. van der Waals, A. M. D. Berghuis and M. S. deGroot, Mol. Phys., 21, 497 (1971); J. van Egmond, D. M. Burland and J. H. van der Waals, Chem. Phys. Letters, 12, 206 (1971).

20. R. W. Brandon, R. E. Gerkin and C. A. Hutchison, Jr., J. Chem. Phys., 37, 447 (1962).

21. J. Brossel and A. Kastler, Compt. Rend., 229, 1213 (1949).

22. J. Brossel and F. Bitter, Phys. Rev., 86, 308 (1952).

23. S. Geschwind, R. J. Collins and A. L. Schawlow, Phys. Rev. Letters, 3, 544 (1959).

24. D. S. McClure, J. Chem. Phys., 17, 665 (1949); 20, 682 (1952).

25. M. A. El-Sayed, J. Chem. Phys., 41, 2462 (1964).

26. M. S. deGroot, I. A. M. Hesselmann and J. H. van der Waals, Mol. Phys., 12, 259 (1967).

27. M. Sharnoff, J. Chem. Phys., 46, 3263 (1967).

28. A. L. Kwiram, Chem. Phys. Letters, 1, 272 (1967).

29. J. Schmidt, I. A. M. Hesselmann, M. S. deGroot and J. H. van der Waals, Chem. Phys. Letters, 1, 434 (1967).

30. M. A. El-Sayed, Accounts of Chem. Res., 4, 23 (1971); in MTP International Review of Science, Vol. III, ed. D. A. Ramsay (University Park Press, Baltimore, 1972), p. 119; in Excited States, Vol. I, ed. E. C. Lim (Academic Press, New York, 1974), p. 35; in Creation and Detection of the Excited State, Vol. II, ed. A. A. Lamola (Marcel Dekker, Inc., New York, 1974).

31. A. L. Kwiram, in MTP International Review of Science, Vol. IV, ed. C. A. McDowell (University Park Press, Baltimore, 1974).

32. J. Schmidt and J. H. van der Waals, Chem. Phys. Letters, 2, 640 (1968); 3, 546 (1969).

33. D. S. Tinti, M. A. El-Sayed, A. H. Maki and C. B. Harris, Chem. Phys. Letters, 3, 343 (1969).

34. G. Ciamician and P. Silber, Ber., 33, 2911 (1900); 34, 1541 (1901).

35. G. S. Hammond, W. R. Moore, W. P. Baker, R. P. Foss, N. J. Turro and A. Fischer, J. Am. Chem. Soc., 81, 6334 (1959); 83, 2789, 2795, 4674 (1961).

36. J. N. Pitts, Jr., R. L. Letsinger, R. P. Taylor, J. M. Patterson, G. Recktenwald and R. B. Martin, J. Am. Chem. Soc., 81, 1068 (1958). G. Porter and F. Wilkinson, Trans. Faraday Soc., 57, 1686 (1961).

37. A. N. Terenin and V. I. Ermolaev, Trans. Faraday Soc., 52, 1042 (1956).

38. H. L. J. Bäckstrom and K. Sandros, Acta. Chem. Scand., 12, 823 (1958); 14, 48 (1960).

39. G. S. Hammond, N. J. Turro and A. Fischer, J. Am. Chem. Soc., 83, 4674 (1961).

40. W. Kirmse, Carbene Chemistry (Academic Press, New York, 1964).

41. K. R. Kopecky, G. S. Hammond and P. A. Leermakers, J. Am. Chem. Soc., 84, 1015 (1962).

42. D. S. McClure, J. Chem. Phys., 17, 665 (1949); 20, 682 (1952).

43. D. S. McClure and P. L. Hanst, J. Chem. Phys., 23, 1772 (1955).

44. Y. Kanda, H. Kaseda and T. Matamura, Spectrochimica Acta, 20, 1387 (1964).

45. R. Shimada and L. Goodman, J. Chem. Phys., 43, 2027 (1965).

46. S. Dym, R. M. Hochstrasser and M. Schafer, J. Chem. Phys., 48, 646 (1968).

47. R. M. Hochstrasser, T. -S. Lin, J. Chem. Phys. 49, 4929 (1968).

48. S. Dym and R. M. Hochstrasser, J. Chem. Phys., 51, 2458 (1969).

49. M. Sharnoff, J. Chem. Phys., 51, 451 (1969).

50. M. Sharnoff, Symp. Faraday Soc., 3, 137 (1969).

51. M. Sharnoff and E. B. Iturbe, Phys. Rev. Letters, 27, 576 (1971).

52. M. Sharnoff, Chem. Phys. Letters, 17, 355 (1972).

53. I. Y. Chan and J. Schmidt, Symp. Faraday Soc., 3, 156 (1969).

54. C. J. Winscom and A. H. Maki, Chem. Phys. Letters, 12, 264 (1971).

55. A. L. Shain and M. Sharnoff, J. Chem. Phys., 59, 2335 (1973).

56. R. M. Hochstrasser, G. W. Scott and A. H. Zewail, J. Chem. Phys., 58, 393 (1973).

57. P. J. Wagner, M. J. May, A. Huag and D. R. Graber, J. Am. Chem. Soc., 92, 5269 (1970).

58. W. A. Case and D. R. Kearns, J. Chem. Phys., 52, 2175 (1970).

59. R. J. Zwarlich and L. Goodman, Chem. Phys. Letters, 7, 609 (1970); M. Koyanagi, R. Zwarlich and L. Goodman, Chem. Phys. Letters, 9, 74 (1970); J. Chem. Phys., 56, 3044 (1972). M. Koyanagi and L. Goodman, Chem. Phys. Letters, 9, 636 (1971); J. Chem. Phys., 55, 2959; 57, 1809 (1972); Molec. Photochem., 4, 369 (1972).

60. A. M. Nishimura and D. S. Tinti, Chem. Phys. Letters, 13, 278 (1972).

61. T. H. Cheng and N. Hirota, J. Chem. Phys., 56, 5019 (1972); Chem. Phys. Letters, 13, 194; 14, 415 (1972); Mol. Phys., 27, 281 (1974); S. W. Mao and N. Hirota, Mol. Phys., 27, 309 (1974).

62. M. Batley and R. Bramley, Chem. Phys. Letters, 15, 337 (1972).

63. H. Hayashi and S. Nagakura, Mol. Phys., 24, 801 (1972); Chem. Phys. Letters, 18, 63 (1973).

64. J. Toussaint, Bull. Soc. Roy. Liege,17, 10 (1948).

65. J. Toussaint, Bull. Soc. Roy. Liege, 15, 86 (1946).

66. D. A. Antheunis, J. Schmidt and J. H. van der Waals, Chem. Phys. Letters, 6, 255 (1970).

67. W. S. Veeman, Ph.D. Thesis, University of Leiden, the Netherlands (1972).

68. We wish to thank Professor D. E. Wood of the University of Connecticut for use of MAGNSPEC and many minutes of computer time.

69. A. W. Hornig and J. S. Hyde, Mol. Phys., 6, 33 (1968).

70. C. R. Chen, J. A. Mucha and D. W. Pratt, Chem. Phys. Letters, 15, 73 (1972).

71. M. A. El-Sayed, J. Chem. Phys., 54, 680 (1971).

72. J. H. van der Waals and M. S. deGroot, in: The Triplet State, ed. A. B. Zahlan (Cambridge Univ. Press, London, 1967) p.101.

73. J. H. van der Waals and M. S. de Groot, Mol. Phys., 2, 333 (1959).

74. R. M. Hochstrasser and J. W. Michaluk, J. Mol. Spec., 42, 197 (1972).

75. Evidence for the temperature dependence of detrapping rate constants in shallow trap systems has been obtained. See H. Port and H. C. Wolf, in The Triplet State, ed. A. B. Zahlan (Cambridge Univ. Press, 1967), p. 393; G. A. George and G. C. Morris, J. Chem. Phys., 54, 815 (1971); and references contained therein.

76. D. L. Dexter, J. Chem. Phys., 21, 836 (1953).

77. H. F. Hameka, in The Triplet State, ed. A. B. Zahlan (Cambridge Univ. Press, 1967), p. 1.

78. H. F. Hameka, J. Chem. Phys., 37, 328 (1962).

79. S. J. Fogel and H. F. Hameka, J. Chem. Phys., 42, 132 (1965); W. R. Hall and H. F. Hameka, ibid., 58, 226 (1973).

80. J. W. McIver, Jr. and H. F. Hameka, J. Chem. Phys., 45, 767 (1966); 46, 825 (1967).

81. W. R. Raynes, J. Chem. Phys., 41, 3020 (1964); R. N. Dixon, Mol. Phys., 13, 77 (1967).

82. C. R. Jones, F. Pappano, A. H. Maki and D. R. Kearns, Chem. Phys. Letters, 13, 521 (1972); C. R. Jones, A. H. Maki and D. R. Kearns, J. Chem. Phys., 59, 873 (1973).

83. J. J. Hopfield, Phys. Rev., 37, 160 (1931).

84. H. Sternlicht, J. Chem. Phys., 38, 2316 (1963).

85. G. Kothandaraman, H. J. Yue and D. W. Pratt, to be published.

86. R. Hoffmann and J. R. Swenson, J. Phys. Chem., 74, 415 (1970).

87. R. W. Fessenden and R. H. Schuler, J. Chem. Phys., 43, 2704 (1965).

88. H. M. McConnell and J. Strathdee, Mol. Phys., 2, 129 (1959).

89. J. R. Morton,,Chem. Rev., 64, 453 (1964).

90. J. S. Vincent and A. H. Maki, J. Chem. Phys., 39, 3088 (1963).

91. J. Mispelter, J. -Ph. Grivet and J. -M. Lhoste, Mol. Phys., 21, 999 (1971).

92. A. Abragam and B. Bleaney, Electron Paramagnetic Resonance of Transition Ions (Clarendon Press, Oxford, 1970).

93. C. R. Chen, H. J. Yue and D. W. Pratt, Chem. Phys. Letters, 20, 339 (1973).

94. H. J. Yue, Ph.D. Thesis, University of Pittsburgh, Pittsburgh, Pa. (1974).

95. R. W. Wood and A. Ellet, Proc. Roy. Soc., 103 (1923).

96. W. Hanle, Z. Physik, 30, 93 (1924).

97. G. Breit, Rev. Mod. Phys., 5, 91 (1933).

98. F. D. Colegrove, P. A. Franken, R. R. Lewis and R. H. Sands, Phys. Rev. Letters, 3, 420 (1959).

99. K. R. German, R. N. Zare and D. R. Crosley, J. Chem. Phys., 54, 4039 (1971).

100. I. von Neumann and E. Wigner, Z. Phys., 30, 467 (1929).

101. T. G. Eck, L. L. Foldy and H. Wieder, Phys. Rev. Letters, 10, 239 (1963); H. Wieder and T. G. Eck, Phys. Rev., 153, 103 (1967).

102. For a recent review, see D. H. Levy, in Advances in Magnetic Resonance, Vol. VI, ed. J. S. Waugh (Academic Press, New York, 1973), p. 1.

103. L. T. Cheng and A. L. Kwiram, Chem. Phys. Letters, 4, 457 (1964).

104. H. Sixl and M. Schwoerer, Chem. Phys. Letters, 6, 21 (1970).

105. W. S. Veeman and J. H. van der Waals, Chem. Phys. Letters, 7, 65 (1970).

106. H. Veenvliet and D. A. Wiersema, J. Chem. Phys., 60, 704 (1974).

107. A. Abragam, The Principles of Nuclear Magnetism, (Clarendon Press, Oxford, 1967), Chapter 5.

108. J. Schmidt, Chem. Phys. Letters, 14, 411 (1972).

109. N. Bloembergen, S. Shapiro, P. S. Pershan and J. O. Artman, Phys. Rev., 114, 445 (1959).

110. H. O. Hooper and B. J. Bray, J. Chem. Phys., 33, 334 (1960).

111. G. Kothandaraman, H. J. Yue and D. W. Pratt, J. Chem. Phys., 60, 3605 (1974).

112. M. D. Fayer, C. B. Harris and D. A. Yuen, J. Chem. Phys., 53, 4719 (1970).

ACKNOWLEDGEMENTS

I express my sincerest appreciation to my research director, Professor David W. Pratt, for his constant encouragement, assistance, and thoughtful advice throughout the course of this work. Many thanks to my confrères Mr. Henry F. Walter, Dr. Gopalan Kothandaraman, and Dr. Henry Yue for their valuable discussions and helpful cooperation. I am very grateful to Mrs. Barbara Hunt, who so diligently typed the thesis to its present form.

Finally, I gratefully acknowledge the Department of Health, Education, and Welfare, the National Science Foundation, and the Atomic Energy Commission for most valuable "moral" support. This work was supported by USAEC Contract No. AT-(11-1)-3435.